INNOVATIVE APPROACHES IN ENGINEERING

GECE AKADEMİ

Kitap Adı	**: Innovative Approaches in Engineering**
İmtiyaz Sahibi/Publisher	**:** Gece Kitaplığı
Genel Yayın Yönetmeni/Editor in Chief	**:** Doç. Dr. Atilla ATİK
Proje Koordinatörü/Project Coordinator	**:** Ethem BİLİCİ
Kapak&İç Tasarım/Cover&Interior Design	**:** Özge ERGENEL
Sosyal Medya/Social Media	**:** Arzu ÇUHACIOĞLU
Yayına Hazırlama	**:** Gece Akademi Dizgi Birimi
Sertifika/Certificate No	**:** 34559
ISBN	: 978-605-288-802-5

Editör/Editors

Prof. Dr. Tayyar Güngör

Doç. Dr. Gülden BAŞYİĞİT KILIÇ

Doç. Dr. Ahmet Uyumaz

Dr. Öğr. Üyesi Sertaç GÖRGÜLÜ

GECE AKADEMİ

Gece Publishing
ABD Adres/ USA Address: 387 Park Avenue South, 5th Floor, New York, 10016, USA
Telefon/Phone: +1 347 355 10 70

Gece Kitaplığı
Türkiye Adres/Turkey Address: Kızılay Mah. Fevzi Çakmak 1. Sokak Ümit Apt. No: 22/A Çankaya/Ankara/TR
Telefon/Phone: +90 312 431 34 84 - +90 555 888 24 26

web: www.gecekitapligi.com —www.gecekitap.com
e-mail: geceakademi@gmail.com

INNOVATIVE APPROACHES IN ENGINEERING

GECE AKADEMİ

CONTENTS

CHAPTER 1

CALCIUM PHOSPHATE COATING OF TI6AL4V ALLOYS IN ALANIN - ALANINE SODIUM SALT ENVIRONMENT WITH BIOMIMETIC METHOD AND OBSERVING OF MECHANICAL PROPERTIES

İbrahim AYDIN[1] , Muhammed Enes ÇAĞLAYAN[2]

1. Introduction

The most important feature of hydroxyapatite (HA) is its showing excellent biocompatibility with the body. Newly developed cells within the structure thereof ensure hydroxyapatite grow into these pores and allow the penetration of tissues into biomaterials. Furthermore, these pores within the hydroxyapatite act as a channel system in the new environment in which the bone will develops and ensure the access of blood and other important body fluids to the bone tissue. The bone tissue finding the suitable environment for development firstly develops fibrovascular tissue on the HA implant. Then mature lamellar on this tissue form new bone tissues [1].

There are various methods relating to HA coating processes on metallic biomaterial as base material such as plasma spray, electrophoretic coating, succesive ionic layer adsorbtion and reaction (SILAR) method, sol – gel and biomimetic [2]. Biomimetics is a term denoting all human-made materials, instruments and systems made by humans imitating the systems in the nature. The surfaces of base materials activated by various chemicals are coated by synthetic body fluid (SBF) prepared in the laboratory courses through precipitation by virtue of this method utilized by us in our study. Making the coating by synthetic body fluid environment ensures obtaining biomaterials fully compatible with the body [3]. Kokubo et al., have performed the HA coating on various biomaterials in SBF for the first time in this field [4]. Tas, has made some changes on the values of SBF prepared by Kokubo et al. and obtained the SBF which he claims to be closer to the ion concentration of blood plasma [5]. Sepahvandi et al. have obtained ion values fairly similar to SBF which prepared by Kokubo et al. in their study [6]. Faure et al., have not been able to obtain most of the values of blood plasma in their study [7]. Li et al., have not been able to obtain the desired degree of Ca2+ and HPO42- ions, Xiaobo et al., have not been able to obtain the desired degree of HCO3- ions [8, 9]. Following a new idea, Pasinli et al., have obtained all ions in the blood plasma for the first time [10]. The study worked out by Aydın, has been used same compound and has been obtained a successfully coating [2]. The data of these studies have shown in Table 1. All of the values in blood plasma in

1 Manisa Vocational School Correspondence
2 ManisaCelal Bayar University

Alanin-Alanine sodium salt buffer environment have been obtained successfully in this study.

Table 1.Ionic concentration of synthetic body fluid and human blood plasma [3]

Ion	Cl^-	HCO_3^-	K^+	Mg^{2+}	Ca^{2+}	HPO_4^{2-}	SO_4^{2-}	Cl^-
Kokubu et al. (MM)	142	147.8	4.2	5	1.5	2.5	1	0.5
Taş (mm)	142	125	27	5	1.5	2.5	1	0.5
Sepahvandi et al. (MM)	142	147.8	4.2	5	1.5	2.5	1	0.5
Faure et al. (MM)	154.56	120.5	44	5.37	0.8	1.82	1	0.8
Li et al. (MM)	142	103	27	5	1.5	6	2.4	0.5
Xiaobo et al. (MM)	142	103	10	5	1.5	2.5	1	0.5
Pasinli et al. (MM)	142	103	27	5	1.5	2.5	1	0.5
Aydın (MM)	142	103	27	5	1.5	2.5	1	0.5
Human Blood Plasma (mM)	142	103	27	5	1.5	2.5	1	0.5

2. Materials and Methods

2.1. Choosing the implant materials

Ti6Al4V alloy, which is frequently preferred in medical applications due to the high biocompatibility thereof, has been utilized in this study in which we performed the calcium phosphate coating process on metallic coating. The chemical composition of the Ti6Al4V alloy used is shown in Table 2 while the mechanical properties thereof are shown in Table 3.

Table 2. Chemical composition of Ti6Al4V alloy [2-3]

Ti	N	C	H	Fe	O	Al	V	Other
Remainder	0.05	0.08	0.0125	0.25	0.13	5.5-6.5	3.5-4.5	0.1-0.4

Table 3. Mechanical properties of Ti6Al4V alloy [3]

Tensile Strength (MPa)	Tensile Strength (MPa)	Elongation Rate (%)	Shrink Rate (%)
883	960	13	50

2.2 Preparation of the Coating

In the study, in order to clean surfaces of Ti6Al4V alloy that preferred base material, materials have been first sandpapered and then they were washed first with pure water and then with acetone. The materials that were washed with pure water again, have been waited in ultrasonic bathroom; in this way cleaning of surfaces of materials have been completed. In order to increase of chemical

bonding trends, materials have been waited at 40 °C for 1 day in the 100 mL 5M NaOH + 0.5 mL %35 H_2O_2 solution. Then materials were washed with pure water again and they have been left to dry at 60 °C for 24 hours. After being dried, it was waited for 1 hour at 600 °C and then cooled in room temperature for apatite nucleation on surface. With the completion of this process, materials have been waited in SBF (2L) those values of inorganic salts shown in Table 4. SBF that actualized coating has been prepared with the temperature at 37 °C and pH value at ~7.4. Then the materials went under the process of rinsing with waiting periods of 24, 48, 72, and 96 hours at 37 °C and the coating process with biomimetric method was realized. After the completion of process, the materials were washed with pure water and dried at 60 °C for 24 hours.

Table 4. Inorganic salts in simulated body fluid (SBF) (Total Volume = 2 L) [11]

Chemical matter	Amount (mg)
KCl	746.0
NaCl	10519.2
$Na_2HPO_4.2H_2O$	356.0
Na_2SO_4	142.0
$NaHCO_3$	4536.6
NA - Glycinate	4313.4
$CaCl_2.2H_2O$	735.2
$MgCl_2.6H_2O$	610.0
Alanin (89.99 g / L) 1M	

2.3. Preparation of Simulated Body Liquid

0,5 L of purified water and the salts in the first six rows of Table 4 were added by weighing into a 3L beaker to prepare 2L of synthetic body fluid equivalent to blood plasma ionic strength. Magnetic bar was placed into a magnetic stirrer and a pH electrode was immersed into the solution and the heating and mixing process began. At this stage previously prepared 1 M alanine solution (2-amino propionic acid) was slowly added and pH value was reduced to 7.5 at 37 ° C and pure water with a volume of 2L was added to the mixture and salts specified in Table 4, 7 and 8 were also added. The pH of the mixture was reduced to 7.4 by again adding M 1 alanine to the stirred solution. Then the mixture was transferred to a 2L volumetric flask and its volume was determined exactly as 2L and the required SBF was made ready for HA coating.

3. Results

3.1. Ultra Microhardness (Indentation) Tests

The tests for identifying microhardness and modulus of elasticity of coatings were conducted with IBIS Nanoindentation System DME-DS 95 Series AFM in Application Center for Electronic Materials (EMUM) in DokuzEylül University, Turkey. The indentation process using Berkovich tip under 2 mN load and at an indentation depth of 2 μm was performed. The measurement of each sample realized as per waiting periods of 24, 48, 72 and 96 hours in SBF were repeated

nine times and the average of results obtained was taken. Because of compatible to test device, square Ti6Al4V alloy in size 10x10x1,2 mm has been used as base material. Average indentation depth under maximum load (ht) and Vickers hardness (GPa) and modulus of elasticity (GPa) have been shown in Figure 1. and Figure 2a-b. As the values on the Fig. 1. are reviewed, it is seen that the average indentation depth (ht) increase depending on the waiting period in synthetic body fluid. It is seen in the Fig. 2a-b. that the values of Vickers hardness and modulus of elasticity decrease depending on the period of retention in SBF.

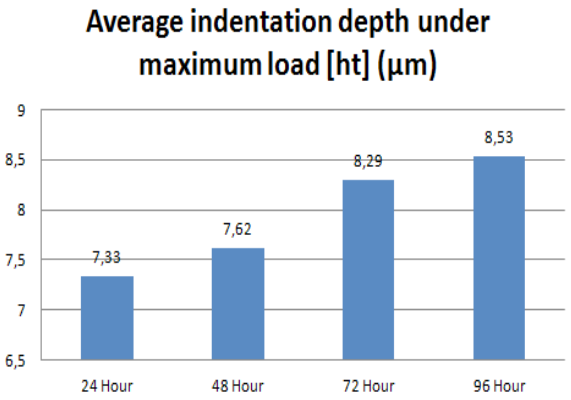

Figure 1. Average indentation depths formed under a load of 2 mN applied on hydroxyapatite coating surface [3]

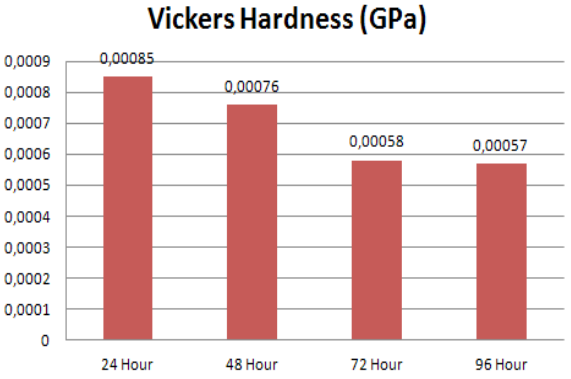

(a)

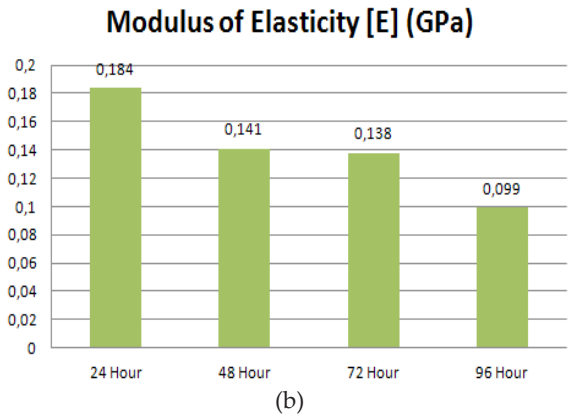

(b)

Figure 2. Change of Vickers hardness (a) and modulus of elasticity values of hydroxyapatite coating surface (b) [3].

Mechanical properties of human bones are different from each other. Change of modulus of elasticity values of human different bones are shown in Table 5. Reviewing the data in Fig 2a-b. and Table 5. obtained, it is seen that the values which is close to mechanics of bone was obtained.

Table 4. Inorganic salts in simulated body fluid (SBF) (Total Volume = 2 L) [12]

Bone Type	ModulusofElasticity	References
CorticalBone	7 – 30 GPa	Bonfield, 1984 [12]
CancellousBone	0.05 – 0.5 GPa	Audekerekeand Martens, 1984 [13]
ArticularCartilage	0.001- 0.01 GPa	Kempson, 1982 [14]
TendonBone	1 GPa	Butler et al, 1984 [15]

3.2. Scratch Tests

Scratch test for measure performances of fastening surface of coating layer were conducted with IBIS Nanoindentation System DME-DS 95 Series AFM in Application Center for Electronic Materials (EMUM) in Dokuz Eylül University, Turkey. The main purpose of device is ultra microhardness (indentation) test. But scratch tests are realized on same device with apparatus changes. Test was realized 100.00 μm/s and under 1-30 mN load. The measurement of each sample realized as per waiting periods of 24, 48, 72 and 96 hours in SBF were repeated three times and the average of results obtained was taken. The results of test are shown in Figure 3a. – Figure 3d. and the average of results are taken in Fig. 4.

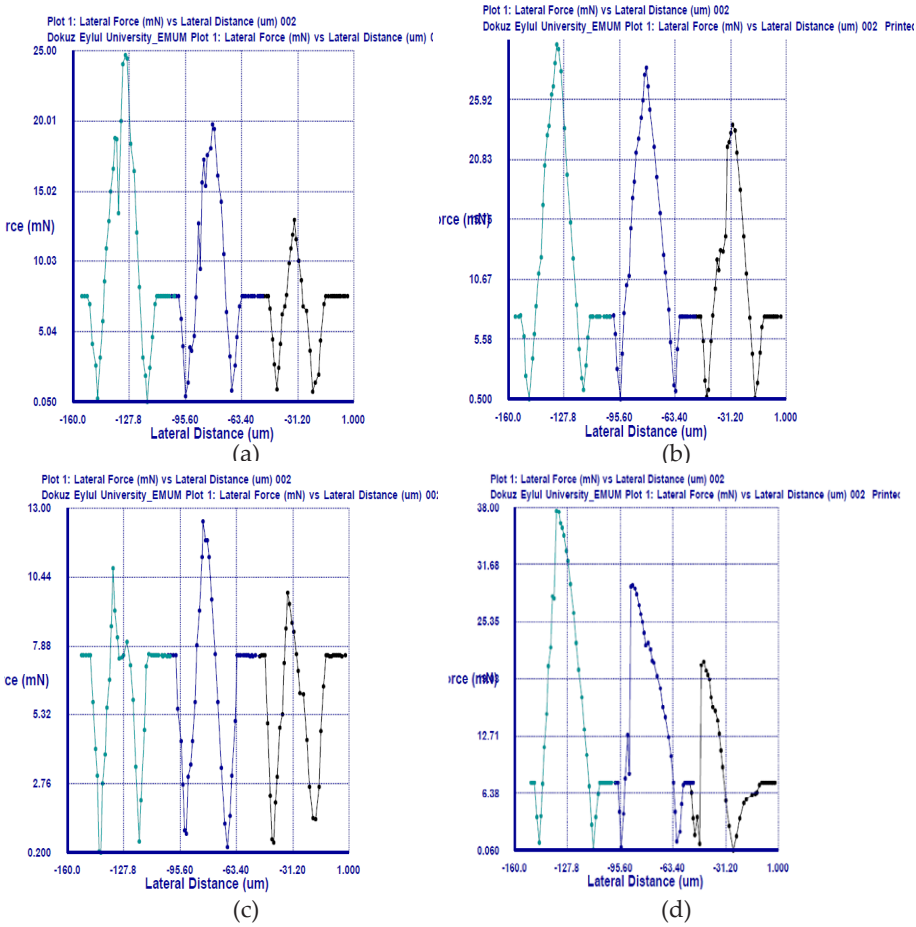

Figure 3. The critical load average values of the coatings kept in SBF for a) 24 hours b) 48 hours c) 72 hours d) 96 hours critical load values held [12].

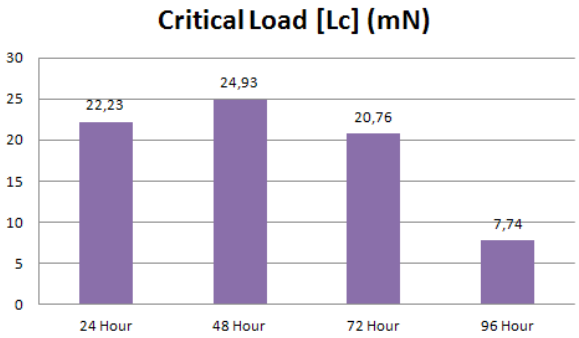

Figure 4. Average values of calcium phosphate coating critical loads depending on the waiting periods in synthetic body fluid [3].

The critical load values of coatings 24, 48, 72 and 96 hour which prepared by Aydın in citric acid- sodium citrate tampon system for the first time in the world, were obtained respectively 39.2 N, 54.79 N, 8.85 N and 8.69 N [11]. Kui et al. have reported critical loads between 390 – 478 mN on their study [16]. Xiang et al. have reported on their study they have measured critical load values 27.85 mN and 68.74 mN [17]. Dunstan et al. and Pasinli et al. have stated that critical load values of coatings respectively 2, 4 N and 8 mN [18, 10].In this study, critical loads of coating which have been obtained depending on waiting periods 24, 48, 72 and 96 hours in SBF, were measured 22.23 mN, 24.93 mN, 20.76 mN ve 7.74 mN. When results are reviewed, it is seen that the most high value of critic load and the best adhesion strength have been obtained in 48 hour with 24.93 mN.

3.3. Calculations of Fracture Toughness

Vickers indentation method was used for calculation of fracture toughness values. In this method, the pyramid diamond tip of hardness tester is applied on the surface of coating with a certain amount of load. At the end of this process, the mark on the surface of the material that was subjected to the load and the cracks on the corners. The size of the mark between the diagonals of the mark and size of the crack were measured and fracture toughness was calculated by the Equation (1) with P: applied load E: modulus of elasticity, H: Vickers hardness and c: size of the crack. The value α in the equation was assumed to be 0.016 in accordance with the literature [3, 11, 19].

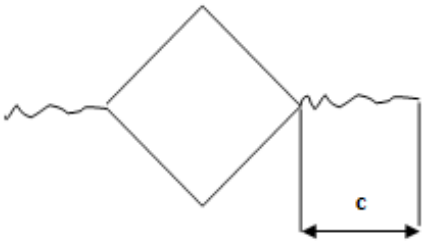

Figure 5. The crack distance which has occurred in the coating (c).

$$K_{1c} = \propto \left(\frac{E}{H}\right)^{0,5} \left(\frac{P}{c^{1,5}}\right) \quad (1)$$

0.245 N load were applied on coating surface with HVS-1000 Digital Display Microhardness Tester in Ege University, Ege Vocational High School. The result obtained from process, cracks were obtained like Figure 5 and size of the cracks (c) were measured. Fracture toughness was calculated by the Equation (1) with size of the cracks (c) and fracture toughness values which calculated have been expressed in Figure 6.

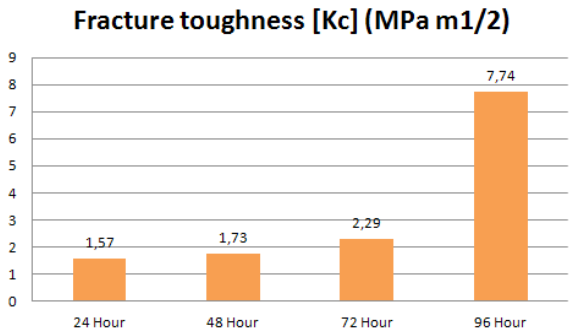

Figure 6. Fracture toughness values of calcium phosphate coatings created by retention in synthetic body fluid for different periods [3].

Zhang et al., reported that the fracture toughness values of coatings between ~ 0.12 – 0.31 MPa m1/2 [20], Marcelo et al., reported that the fracture toughness value of coating 1.18 MPa m1/2 [21], Tsui et al., reported that the fracture toughness values of coatings 0.23 – 1.20 MPa m1/2 [22], Li et al., expressed that fracture toughness values of coatings between 0.49 – 0.67 MPa m1/2 [23], Mohammadi et al. calculated fracture toughness values between 0.99 – 1.27 MPa m1/2 [24] and Bharati et al., reported that the fracture toughness value of coating 0.74 MPa m1/2 [25]. Aydın reported that the fracture toughness values of coatings between 1.98 – 2.075 MPa m1/2 on his study which prepared in citric acid- sodium citrate tampon system for the first time in the world [19]. Bonfield expressed that fracture toughness values of different areas of cortical bones between 2 - 12 MPa m1/2 [12]. As the values on the Fig. 6 and literature are reviewed, it is seen that good fracture toughness values of coatings have been obtained. At the same time, fracture toughness values which close to bone have been obtained take into consideration the study of Bonfield.

4. Conclusion

Result of this study, synthetic body fluid solution has been prepared in Alanin - Alanine Sodium salt environment which does not show any toxic effect on human body for the first time in literature by using biomimetic method and calcium phosphate coating processes have been realized. As mechanics tests are reviewed, it is seen that all coatings which produced in SBF are compatible with mechanics values of bone. Additionally, successful fracture toughness values have been obtained take into consideration the literature. All of the values in blood plasma obtained by Pasinli et al. and Aydin for the first time in literature have also been realized in this tampon system. Result of this study; take a new step on implant production in biocompatible environment with calcium phosphate coating.

REFERENCES

1. 1. İ. Aydın, A. Pasinli, H. Çetinel: Investigation of fracture toughness calcium phosphate coating on Ti6Al4V material, Electronic Journal of Machine Technology Vol: 7, No: 3, (2010) 69-75

2. 2. İ. Aydın, H. Çetinel, A. Pasinli, M. Yüksel: Preparation of hydroxyapatite coating by using citric acid sodium citrate buffer system in the biomimetic procedure, Materials Testing 10 (2013), pp 782-788 DOI:10.3139/120.110501

3. 3. M. E. Çağlayan: Hydroxyapatite coating of Ti6Al4V alloys in alanin - alanine sodium salt environment with biomimetic method and observing of some features, M.Sc. Thesis, Celal Bayar University, Turkey, (2016)

4. 4. T. Kokubo, H. M. Kim, F. Miyaji, H. Takadama, T. Miyazaki: Ceramic - metal and ceramicpolymer composites prepared by a biomimetic process, Comp. Part A: Applied Science and Manufacture 30 (1999), 405-409

5. 5. A. C. Taş, S. B. Bhaduri: Rapid coating of Ti6Al4V at room temperature with a cacium phosphate solution similar to 10 x SBF, Journal of Europen Ceramic Society (1999), 2573- 2579

6. 6. A. Sepahvandi, F. Moztarzadeh, M. Mozafari, M. Ghaffari, N. Raee; Photoluminescence in the characterization and early detection of biomimetic bone-like apatite formation on the surface of alkaline-treated titanium implant, State of the Art Biointerfaces 86 (2011), pp. 390 - 396

7. 7. J. Faure, A. Balamurugan, H. Benhayoune, P. Torres, G. Balossier,J. M. Ferreira: Morphological and chemical characterization of biomimetic bone like apatite formation on Ti6Al4V titanium alloy, Materials Science and Engineering. C 29 (2009), pp. 1252 - 1257

8. 8. P. J. Li: Biomimetic nano-apatite coating capable of promoting bone ingrowth, Journal of Biomedical Materials Research 6A (1) (2003) pp. 79 - 85

9. 9. C. Xiaobo, L. Yuncang, D. H. Peter, W. Cui'e: Microstructures and bond strengths of the calcium phosphate coatings formed on titanium from different simulated body fluids, Materials Science and Engineering C 29 (2009), pp. 165 - 171

10. 10. A. Pasinli, M. Yüksel, E. Çelik, S. Şener, C. A. Taş: A new approach in biomimetic synthesis of calcium phosphate coatings using lactic acid-Na lactate buffered body fluid solution, Acta Biomaterialia 6 (2010), pp. 2282 - 2288

11. 11. Aydin I., Caglayan M. E., Pasinli A. :Hydroxyapatite coating of Ti6A14V alloys in alanin - alanine sodium salt environment with biomimetic method" Celal Bayar University Journal of Science, 2016.

12. 12. W. Bonfield: Elasticity and Viscoelasticity of Cortical Bone, G.W. Hasting, P. Ducheyne (Eds.): Natural and Living Biomaterials, CRC Press, Boca Raton, Florida, USA (1984), pp. 43 - 60

13. 13. V. R. Audekereke, M. Martens: Mechanical Properties of Cancellous Bone, G. W. Hasting, P. Ducheyne (Eds.): Natural and Living Biomaterials CRC Press, Boca Raton, Florida, USA (1984) pp. 89 - 98

14. 14. G. E. Kempson: Relationship between the tensile properties of articular cartilage from the human knee and age, Annals of the Rheumatic Diseases 41 (1982), 508 -511 DOI:10.1136/ard.41.5.508

15. 15. D. L. Butler, E. S. Grood, F. R. Noyes, R. F. Zernicke, K. Bracket: Effects of structure and strain measurement techniques on the material properties of young human tendons

and fascia, Journal of Biomechanics, 17 (1984), pp. 579 – 596 DOI:10.1016/0021-9290(84)90090-3

16. 16. K. Cheng, C. Ren, W. Weng, P. Du, G. Shen, G.Han, S. Zhang: Bonding strength of fluoridated hydroxyapatite coatings: A comparative study on pull out and scratch analysis, Thin Solid Films 517 (2009), pp. 5361 – 5364 DOI:10.1016/j.tsf.2009.03.122
17. 17. G. Xiang, L. Yang, R. Fuzeng, L. Xiong: Integrity and zeta potential of fluoridated hydroxyapatite nanothick coatings for biomedical applications, Journal of the Mechanical Behavior of Biomedical Materials 4 (2011) pp. 1046 – 1056 DOI:10.1016/j.jmbbm.2011.03.013
18. 18. D. Barnes, S. Johnson, R. Snell, S. Best: Using scratch testing to measure the adhesion strength of calcium phosphate coatings applied to poly(carbonate urethane) substrates, Journal of the Mechanical Behavior of Biomedical Materials 6 (2012) pp. 128 – 138 DOI:10.1016/j.jmbbm.2011.10.010
19. 19. İ. Aydın, H. Çetinel, A. Pasinli, M. Yüksel: Fracturing and adhesion behavior of hydroxyapatite formed by a citric acid and sodium citrate buffer system, Materials Testing, 58 (2016) 2, pp 1 - 6 DOI:10.3139/120.110826
20. 20. S. Zhang, Y. S. Wang, X. T. Zeng, K. A. Khor, W. Weng, D. E. Sun: Evaluation of adhesion strength and toughness of fluoridated hydroxyapatite coatings, Thin Solid Films 516 (2008), pp. 5162–5167 DOI:10.1016/j.tsf.2007.07.063
21. 21. M. H. P. da. Silva, A. F. Lemos., José, M da. F. Ferreira, J. D. Santos: Mechanical characterization of porous glass reinforced hydroxyapatite ceramics – bonelike, Materials Research 6 (2003), No. 3, pp. 321 – 325 DOI:10.1590/S1516-14392003000300004
22. 22. Y. C. Tsui, C. Doyle, T. W. Clyne: Plasma sprayed hydroxyapatite coatings on titanium substrates - Part 2: optimization of coating properties, Biomaterials 19 (1998), pp. 2031-2043 DOI:10.1016/S0142-9612(98)00104-5
23. 23. F. Li, Q. L. Feng, F. Z. Cui, H. D. Li, H. Schubert: A simple biomimetic method for calcium phosphate coating, Surface & Coating Technology, 154 (2002) 88 – 93 DOI:10.1016/S0257-8972(01)01710-8
24. 24. Z. Mohammadi, A. A. Ziaei-Moayyed, S. M. Mesgar: Adhesive and cohesive properties by indentation method of plasma-sprayed hydroxyapatite coatings, Applied Surface Science 253 (2003) pp. 4960 – 4965 DOI:10.1016/j.apsusc.2006.11.002
25. 25. S. Bharati, C. Soundrapandian, D. Basu,S. Data: Studies on a novel bioactive glass and composite coating with hydroxyapatite on titanium based alloys: Effect of γ-sterilization on coating, Journal of the European Ceramic Society 29 (2009), pp. 2527–2535 DOI:10.1016/j.jeurceramsoc.2009.02.013

CHAPTER 2

INVESTIGATION OF FRACTURING AND ADHESION PROPERTIES OF HACOATING OF TI6AL4V ALLOYS IN GLYCOLIC ACID - SODIUM GLYCOLATE ENVIRONMENT PRODUCED BY USING BIOMIMETIC METHOD

İbrahim AYDİN[1] , Ferdi ENGİN[2]

1. Introduction

Hydroxyapatite (HAp) [$Ca_{10}(PO_4)_6OH_2$] is a material of choice for various biomedical applications such as orthopedic, dentistry, anti-microbial and drug delivery, because of its similarity of composition to mineral phase of the bone, excellent biocompatibility, and ability to promote cellular functions and expression and osteoconductivity [1].The material surface is coated with hydroxyapatite (HA) ceramics, which forms the inorganic structure of the bone for providing superficial compatibility by increasing the corrosion resistance of selected metallic biomaterials for implantation and increasing the surface activity to such an extent that it can bind to the tissues it contacts [2].

There are various methods relating to hydroxyapatite (HA) coating processes on metallic biomaterial as base material such as sol – gel, biomimetic, electrophoretic coating, PVD (physical vapour deposition), CVD (chemical vapour deposition), plasma spray, HVOF (high velocity oxygen fuel thermal spray process), in situ [3]. In this study, biomimetic method was preferred because of can be applied to all types of implants cause their prices are advantageous, they can be easily produced, they have a thin and durable bioactive plate, the structures have spores, and they do not change the morphology of the surface. Synthetic body fluid (SBF) which harmony with all ions in the blood plasma was used in this method [4, 5].

HA coating on various biomaterials in SBF has been performed by Kokubo et al. for the first time in this field [6]. Taş, has made some changes on the values of SBF prepared by Kokubo et al. and obtained the SBF which he claims to be closer to the ion concentration of blood plasma [7]. In the studies conducted by Sepahvandi, Faure, Li and Xiaobo together with the colleagues, blood plasma values could be derived in specifications inside SBF environment [8 - 11]. But the values that were exactly the same as blood plasma values could be realised for the first time by Pasinli et al. [12]. In his PhD thesis, Aydın has used citric acid - sodium citrate tampon system for the first time in

1 Manisa Vocational School Correspondence
2 ManisaCelal Bayar University

the literature and he has prepared a SBF solution that is equivalent to ionic values in blood plasma and more successful results were obtained [2]. In addition to these studies carried out in SBF with ionic values compatible with human blood plasma, successful HA coatings were also obtained in studies performed by Aydın et al. in alanin – alanine sodium salt and aminoacetic acid - sodium aminoacetate buffer systems [13, 14]. The SBF ion values of studies which HA coating on metallic biomaterial as base material have shown in Table 1.

Table 1. Human blood plasma and ion concentration of simulated body fluid (SBF) [2, 3]

Ion	Cl^-	HCO_3^-	K^+	Mg^{2+}	Ca^{2+}	HPO_4^{2-}	SO_4^{2-}	Cl^-
Kokubu et al. (MM)	142	147.8	4.2	5	1.5	2.5	1	0.5
Taş (mm)	142	125	27	5	1.5	2.5	1	0.5
Sepahvandi et al. (MM)	142	147.8	4,2	5	1.5	2.5	1	0.5
Faure et al. (MM)	154.56	120.5	44	5.37	0.8	1.82	1	0.8
Li et al. (MM)	142	103	27	5	1.5	6	2.4	0.5
Xiaobo et al. (MM)	142	103	10	5	1.5	2.5	1	0.5
Pasinli et al. (MM)	142	103	27	5	1.5	2.5	1	0.5
Aydın (MM)	142	103	27	5	1.5	2.5	1	0.5
TheValues of Study	142	103	27	5	1.5	2.5	1	0.5
Human Blood Plasma (mM)	142	103	27	5	1.5	2.5	1	0.5

In this study, SBF that is completely harmonious with the human blood plasma has been prepared, HA coating has been produced in glycolic acid - sodium glycolate environment and the related evaluations have been made.

2. Materials and Methods

2.1. Selection of Implant Material

Titanium and its alloys are today being used at surgical splints, dental implants, prosthesis joint, vascular stents and binders, partial prosthesis and crown-bridges. To improve the mechanical properties of the implant material, it is made of metal, such as aluminum, vanadium and iron [2]. In this study, Ti6Al4V alloy obtained by using aluminum and vanadium metals together with titanium as base material was used. The chemical composition of the alloy is indicated in Table 2, the mechanical features in Table 3 [5].

Table 2.Chemical composition of Ti6Al4V alloy [2]

Ti	N	C	H	Fe	O	Al	V	Other
Remainder	0.05	0.08	0.0125	0.25	0.13	5.5-6.5	3.5-4.5	0.1-0.4

Table 3. Mechanical properties of Ti6Al4V alloy [2]

Tensile Strength (MPa)	Tensile Strength (MPa)	Elongation Rate (%)	Shrink Rate (%)
883	960	13	50

2.2 Preparation of the Coating

As the first step of the work, sterilization of Ti6Al4V alloy shown in Table 2. and Table 3. is provided. In order to clean surfaces of Ti6Al4V alloy materials have been first sandpapered and then they were washed first with pure water. Then, samples immersed in acetone to dissolve the oil particles in the surface, were washed again with distilled water and left in the ultrasonic bath for about 20 minutes. In order to increase of chemical bonding trends, materials have been waited at 40 ºC for 1 day in the 100 mL 5M NaOH + 0.5 mL %35 H_2O_2 solution. Then materials were washed with pure water again and they have been left to dry at 60 ºC for 24 hours. The materials are converted ready for thermal treatment by wrapping these with aluminum folio in order to prevent an air contact after they dried. . Then the materials are placed into an oven and kept for 1 hour at a temperature of 600 ºC and left for cooling down at room temperature. With the completion of this process, the synthetic body fluid solution (2L) shown in Table 4. was obtained with the temperature at 37 ºC and pH value at ~7.4. Then the materials went under the process of rinsing with waiting periods of 24, 48, 72, and 96 hours at 37 ºC and the coating process with biomimetic method was realised. After the completion of process, the materials were washed with pure water and dried at 60 ºC for 24 hours. Various mechanical and metallographic tests have been applied to the samples which have been coated after this series of operations [5, 15].

Table 4. Inorganic salts in simulated body fluid (Total Volume = 2 L) [5, 15]

	Inorganic Salts	(mg / 2L)
1	*KCl*	746.0
2	*NaCl*	10519.2
3	$Na_2HPO_4 2H_2O$	356.0
4	Na_2SO_4	142.0
5	$NaHCO_3$	4536.6
6	*Na – Glikolat (>%97)*	4446.8
7	$CaCl_2 \cdot 2H_2O$	735.2
8	$MgCl_2 \cdot 6H_2O$	610.0
	glycolic acid (76.818 g/L)1 M	

2.3. Preparation of Simulated Body Fluid

1.5 L of purified water and the salts in the first six rows of Table 4 were added by weighing into a 3L beaker to prepare 2L of synthetic body fluid equivalent to blood plasma ionic strength. Magnetic bar was placed into a magnetic stirrer and a pH electrode was immersed into the solution and the heating and mixing process began. At this stage previously prepared 1 M glycolic acid solution (hydroxy acetic acid) was slowly added and pH value was reduced to ~8 at 37 ° C and pure water with a volume of 2L was added to the mixture and salts specified in Table 4, 7 and 8 were also added. The pH of the mixture was reduced to 7.4 by again adding M 1 glycolic acid to the stirred solution. Then the mixture was transferred to a 2L volumetric flask and its volume was determined exactly as 2L and the required SBF was made ready for HA coating [5].

2.4. Test Methods

The tests for identifying microhardness and modulus of elasticity of coatings were conducted with IBIS Nanoindentation System DME-DS 95 Series AFM in Application Center for Electronic Materials (EMUM) in DokuzEylul University, Turkey. The indentation process using Berkovich tip under 2 mN load and at an indentation depth of 2 μm was performed.

Scratch test for measure performances of fastening surface of coating layer were conducted with IBIS Nanoindentation System DME-DS 95 Series AFM in Application Center for Electronic Materials (EMUM) in DokuzEylül University, Turkey. The main purpose of device is ultra microhardness (indentation) test. But scratch tests are realized on same device with apparatus changes. Test was realized 100.00 μm/s and under 1-30 mN load.

Calculation of fracture toughness values of coatings prepared by using glycolic acid – sodium glycolate buffer system for the first time in the literature was carried out with HVS-1000 Digital Display Microhardness Tester in Ege University, Ege Vocational High School. Vickers indentation method was used for calculation of fracture toughness values. The application of the indentation test is shown in Figure 1. The pyramid diamond tip of hardness tester is applied on the surface of coating with 0.245 N loads. The result obtained from process, cracks were obtained and size of the cracks (c) were measured and fracture toughness was calculated by the Equation (1) with size of the cracks (c).

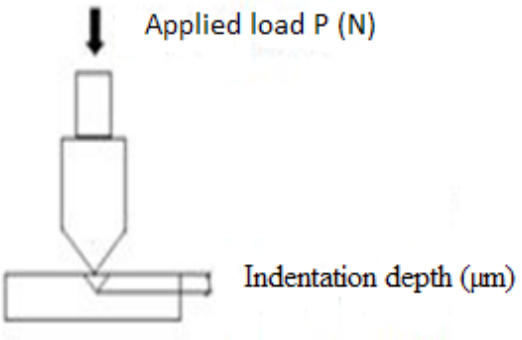

(a)

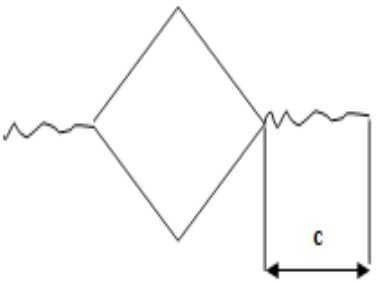

(b)

Figure 1. Practice of the Vickers indentation process a) load applied on the coating (P) b) the mark that formed on the coating surface (c)

$$K_{1c} = \propto \left(\frac{E}{H}\right)^{0,5} \left(\frac{P}{c^{1,5}}\right) \quad (1)$$

size of the mark between the diagonals of the mark and size of the crack were measured and fracture toughness was calculated by the Equation (1) with P: applied load E: modulus of elasticity, H: Vickers hardness and c: size of the crack. The value α in the equation was assumed to be 0.016 in accordance with the literature [5].

3. Results

3.1. Ultra Microhardness (Indentation) Tests

The measurement of each sample realized as per waiting periods of 24, 48, 72 and 96 hours in SBF were repeated nine times and the average of results obtained was taken. Average indentation depth under maximum load (ht) and Vickers hardness (GPa) and modulus of elasticity (GPa) have been shown in Table 5. and Table6.

Table 5. Average indentation depths formed under a load of 2 mN applied on hydroxyapatite coating surface [5]

Average Sinking Depths In Maximum Load [ht] (μm)	
24 hours	1.26
48 Hours	1.33
72 Hours	3.17
96 Hours	3.84

As the values on the Table 5. are reviewed, it is seen that the average indentation depth (ht) increase depending on the waiting period in synthetic body fluid.

Table 6. Change of Vickers hardness and modulus of elasticity values of hydroxyapatite coating surface [5]

HA Coating Period (Hours)	Vickers Hardness [H] (GPa)	Elasticity Module [E] (GPa)
24 hours	0.2123	9.72
48 Hours	0.1517	6.08
72 Hours	0.0105	2.03
96 Hours	0.0046	1.24

It is seen in the Table 6. that the values of Vickers hardness and modulus of elasticity decrease depending on the period of retention in SBF. Change of modulus of elasticity values of human different bones are shown in Table 7.

Table 7. Change of Vickers hardness and modulus of elasticity values of hydroxyapatite coating surface [5]

Bone Type	Modulus of Elasticity	References
Cortical Bone	7 – 30 GPa	Bonfield, 1984 [16]
Cancellous Bone	0.05 – 0.5 GPa	Audekereke and Martens, 1984 [17]
Articular Cartilage	0.001- 0.01 GPa	Kempson, 1982 [18]
Tendon Bone	1 GPa	Butler et al, 1984 [19]

Reviewing the data in Table 6. and Table 7. obtained, it is seen that the values which is close to mechanics of bone was obtained.

3.2. Scratch Tests

The measurement of each sample realized as per waiting periods of 24, 48, 72 and 96 hours in SBF were repeated three times and the average of results obtained was taken. The results of test are shown in Figure 2a. – Figure 2d. and the average of results are taken in Table 8.

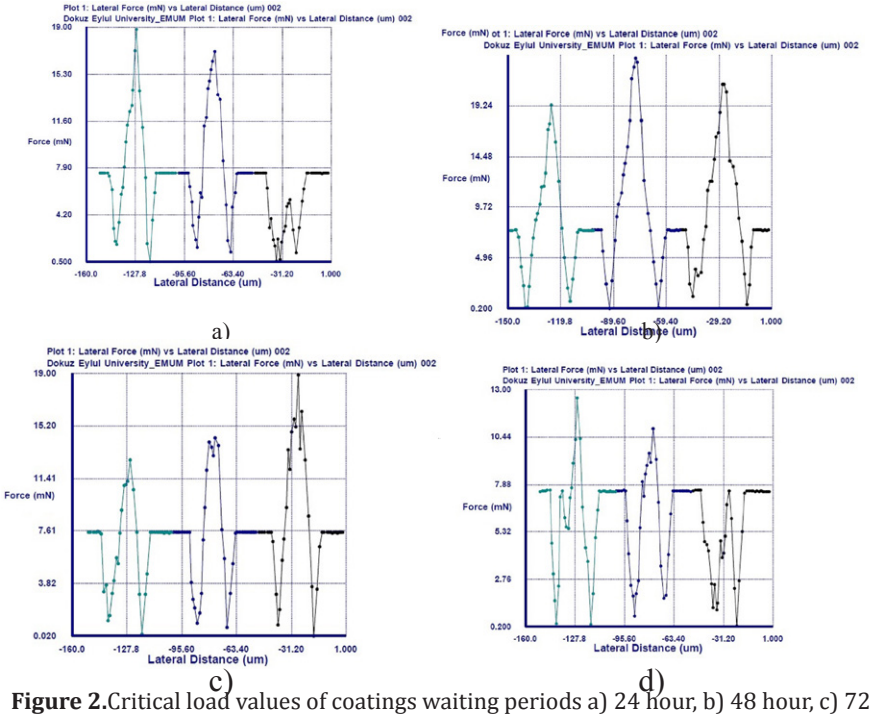

Figure 2. Critical load values of coatings waiting periods a) 24 hour, b) 48 hour, c) 72 hour and d) 96 hour in synthetic body fluid [5].

Table 8. Average values of hydroxyapatite coating critical loads depending on the waiting periods in synthetic body fluid [5].

Critical Load [Lc] (mN)	
24 hours	17.79
48 Hours	21.04
72 Hours	14.44
96 Hours	9.82

Kui et al. have achieved successful HA coatings with their work and have reported critical loads between 390 – 478 mN on their study [20]. Xiang et al. have reported on their study they have measured critical load values 27.85 mN and 68.74 mN [21]. Dunstan et al. have stated that critical load values of coatings 2.4 N [22]. HA coating was realized at 37 °C and pH = 7.4 by using lactic acid / Na - lactate buffer system by Pasinli et al. at an environment which is fully compatible with human blood plasma and they have stated that critical load values of coatings 8 mN [12]. After this work the critical load values of coatings 24, 48, 72 and 96 hour in citric acid- sodium citrate tampon system for the first time, were obtained respectively 39.2 N, 54.79 N, 8.85 N and 8.69 N [23]. In his M.Sc. thesis, Çağlayan has used in the alanin – alanine sodium salt buffer environment and he has measured the critical loads of the coatings obtained at the same waiting times as 22.23 mN, 24.93 mN, 20.76 mN and 7.74 mN, respectively [24]. In another study carried out by Kırman, aminoacetic acid - sodium aminoacetate buffer system has been used and the critical loads of the coatings have been measured 29.42 mN, 37.12 mN, 34.05 mN and 19.04 mN, respectively [3]. When results are reviewed, it is seen that the most high value of critic load and the best adhesion strength have been obtained in 48 hour with 21.04 mN.

3.3. Calculations of Fracture Toughness

Fracture toughness were obtained from process with Equation (1). The values of fracture toughness have been expressed in Table 9.

Table 9. Fracture toughness values of hydroxyapatite coatings created by retention in synthetic body fluid for different periods [5]

Fracture toughness [K_c] (MPa $m^{1/2}$)	
24 hours	1.62
48 Hours	1.84
72 Hours	1.87
96 Hours	2.19

In the literature, when looking at the surface fracture toughness values of the hydroxyapatite coating, Aydın et al. the fracture toughness of the coatings obtained by the activation of NaOH + H_2O_2 was found between 2.075 – 1.97 MPa m1/2 [23]. Zhang et al. have calculated the fracture toughness of the coatings approximately ~ 0.12 – 0.31 MPa $m^{1/2}$ [25]. Tsui et al., reported that the fracture toughness values of coatings 0.23 – 1.20 MPa $m^{1/2}$ [26], Marcelo et al., reported that the fracture toughness value of coating 1.18 MPa $m^{1/2}$ [27], Mohammadi et al. calculated fracture toughness values between 0.99 – 1.27 MPa $m^{1/2}$ [28], Li et al., expressed that fracture toughness values of coatings between 0.49 – 0.67 MPa m1/2 [10] and Bharati et al., reported that the fracture toughness value of coating 0.74 MPa m1/2 [29]. Çağlayan, were found the fracture toughness values 1.57, 1.73, 2.29 and 2.31 respectively at 24, 48, 72 and 96 hour waiting times in the HA coating in the alanin – alanine sodium salt buffer environment [24]. Kırman, calculated the fracture toughness

values in the aminoacetic acid - sodium aminoacetate buffer environment as 1.02, 1.25, 1.35 and 2.51, respectively, at the same waiting periods [3]. Bonfield expressed that fracture toughness values of different areas of cortical bones between 2 - 12 MPa $m^{1/2}$ [17]. When the results of this study are examined, it is seen that successful fracture toughness values are obtained according to the literature.

4. Conclusion

In this study, the mechanical properties of the HA coating which was produced using the glycolic acid sodium glycolate buffer system were investigated. When the results obtained from the mechanical tests are examined, it has been found that the produced coatings give successful results when compared with the literary data. It appears that the coatings are compatible with the mechanical properties of the bone. Based on the results of this study, biomaterials were obtained which are applicable to the industry.

References

1. Gayathri B., Muthukumarasamy N., Velauthapillai D., Santhosh S.B., Asokan V.," Magnesium incorporated hydroxyapatite nanoparticles: Preparation, characterization, antibacterial and larvicidal activity". Arabian Journal of Chemistry (2017), http://dx.doi.org/10.1016/j.arabjc.2016.05.010

2. Aydın İ., "An investigation of fracture and wear behavior of HA coatings deposited onto Ti6Al4V alloys in a new environment", PhD Thesis, Celal Bayar University, Institute of Science, 2013.

3. Kırman M., "Coating Ti6Al4V alloy by hydroxyapatite through biomimetic method using aminoacetic acid - sodium aminoacetate buffer system and examination of features of the coating", M.Sc. Thesis, Celal Bayar University, Institute of Science, 2016.

4. Pasinli A., Aksoy R. S., "Hydroxyapatite for artificial bone applications", Biotechnology Magazine, 1: pp. 41-51, 2010.

5. Engin, F. "Observing of mechanical features of hydroxyapatite coating using glycolic acid - sodium glycolate buffer system", M.Sc. Thesis, Celal Bayar University, Institute of Science, 2017.

6. Kokubo, T., Kim, H. M., Miyaji, F., Takadama, H., Miyazaki, T. Ceramic–metal and ceramic–polymer composites prepared by a biomimetic process. Composites Part A: Applied Science and Manufacturing. 1999, 30, 405–409.

7. Taş A. C. Synthesis of biomimetic Ca-hydroxyapatite powders at 37ºC in synthetic body fluids. Biomaterials. 2000, 21, 1429 - 1438.

8. Sepahvandi, A., Moztarzadeh, F., Mozafari, M., Ghaffari, M., Raee, N., 2011. Photoluminescence in the characterization and early detection of biomimetic bone-like apatite formation on the surface of alkaline-treated titanium implant:State of the art. Biointerfaces 86, 390-396, 2011.

9. Faure, J., Balamurugan, A., Benhayoune, H., Torres, P., Balossier, G., Ferreira, J.M.

F., 2009. Morphological and chemical characterisation of biomimetic bone like apatite formation on Ti6Al4V titanium alloy. Mater. Sci. & Eng. C (29), 1252-1257, 2009. 10. Li, P.J., 2003. Biomimetic nano-apatite coating capable of promoting bone ingrowth. J Biomed Mater Res A 2003;6 6A(1):79–85, 2003.

10. Li et al 2002
11. Xiaobo, C., Yuncang L., Peter, D. H., Cui'e, W., 2009. Misrostructures and bond strengths of the calcium phosphate coatings formed on titanium from diffrent simulated body fluids. Materials Science end Engibneering C 29, 165-171, 2009.
12. Pasinli, A., Yuksel, M., Celik, E., Sener, S., Tas, C.A., 2010. A new approach in biomimetic synthesis of calcium phosphate coatings using lactic acid-Na lactate buffered body fluid solution. Acta Biomaterialia 6, 2282-2288, 2010.
13. Aydin I., Caglayan M. E., Pasinli A. :Hydroxyapatite coating of Ti6A14V alloys in alanin - alanine sodium salt environment with biomimetic method" Celal Bayar University Journal of Science, 2016.
14. Aydın, İ., Kırman, M., Pasinli, A., "Coating Ti6Al4V Alloy by Hydroxyapatite through Biomimetic Method using Aminoacetic Acid-Sodium Aminoacetate Buffer System and examination of features of the coating ", 1st International Mediterranean Science and Engineering Congress, 26-28 October, Adana, Turkey.
15. Aydın, İ., Engin, F., "Hydroxyapatite Coating on Ti6Al4V Alloy Surface Through Biomimetic Method Using Glycolic Acid - Sodium Gluconate Buffer System and Examination of Properties of the Coating", Journal of Polytechnic, 20(4), 2017.
16. Bonfield, W. Elasticity and viscoelasticity of cortical bone in natural and living. Biomaterials, eds. G.W. Hasting and P.Ducheyne(CRC Press, Boca Raton,FI), 1984, 43-60.
17. Audekereke, V. R., Martens, M. Mechanical properties of cancellous bone in natural and living, Biomaterials, eds. G. W. Hasting and P.Ducheyne(CRC Press, Boca Raton,FI), 1984, 89-98.
18. Kempson, G. E. relationship between the tensile properties of articular cartilage from the human knee and age. Annals of the Rheumatic Diseases. 1982, 41, 508-511.
19. Butler, D. L., Grood, E. S., Noyes, F. R., Zernicke, R. F., Bracket, K. Effects of structure and strain measurement techniques on the material properties of young human tendons and fascia. Journal of Biomechanics. 1984, 17, 579-596.
20. Kui C., Changbao R., Wenjian W., Piyi D., Ge S., Gaorong H., Sam Z. Bonding strength of fluoridated hydroxyapatite coatings: A comparative study on pull-out and scratch analysis. Thin Solid Films. 2009, 517, 5361-5364.
21. 21. Xiang, G., Yang, L., Fuzeng, R., Xiong, L. Integrity and zeta potential of fluoridated hydroxyapatite nanothick coatings for biomedical applications. Journal of The Mechanical Behavior of Biomedical Materials. 2011, 4, 1046-1056.
22. Dunstan B., Scott J., Robert S., Serena B. Using scratch testing to measure the adhesion strength of calcium phosphate coatings applied to poly(carbonate

urethane) substrates. Journal of The Mechanical Behavior of Biomedical Materials. 2012, 6, 128-138.

23. İ. Aydın, H. Çetinel, A. Pasinli, M. Yüksel: Fracturing and adhesion behavior of hydroxyapatite formed by a citric acid and sodium citrate buffer system, Materials Testing, 58 (2016) 2, pp 1 - 6 DOI:10.3139/120.110826

24. M. E. Caglayan,"Hydroxyapatite Coating of Ti6A14V Alloys in Alanin - Alanine Sodium Salt Environment with Biomimetic Method and Observing of Some Features", M.Sc. Thesis, Celal Bayar University, Turkey, 2016.

25. Zhang, S., Wang, Y. S., Zeng, X. T., Khor, K. A., Weng, W., Sun, D. E. Evaluation of adhesion strength and toughness of fluoridated hydroxyapatite coatings. Thin Solid Films. 2008, 516, 5162–5167.

26. Tsui, Y. C., Doyle, C., Clyne, T. W. Plasma sprayed hydroxyapatite coatings on titanium substrates Part 2: optimisation of coating properties. Biomaterials. 1998, 19, 2031-2043.

27. Marcelo, Henrique. Prado da. Silva., Alexandra, Fernandes. Lemos., José, Maria da. Fonte. Ferreira., José, Domingos. Santos. Mechanical characterisation of porous glass reinforced hydroxyapatite ceramics – bonelike. Materials Research. 2003, 6 (3), 321-325.

28. Mohammadi, Z., Ziaei-Moayyed, A.A., Mesgar, S. M. Adhesive and cohesive properties by indentation method of plasma-sprayed hydroxyapatite coatings. Applied Surface Science. 2003, 253, 4960–4965.

29. Bharati, S., Soundrapandian, C., Basu, D., Data, S. Studies on a novel bioactive glass and composite coating with hydroxyapatite on titanium based alloys: Effect of γ-sterilization on coating. Journal of the European Ceramic Society. 2009, 29, 2527–2535.28.

CHAPTER 3

DEVELOPMENT OF DESIGN MODEL WITH ARTIFICIAL INTELLIGENCE

Mustafa BOZDEMİR[1]

1. INTRODUCTION

The competition in the market makes it compulsory to reflect the needs of consumer or user to the product. Time and money losses caused by customer dissatisfaction or improper design cannot be accepted in market conditions. These facts directs the designers to developed more flexible systematic design models to prevent the negativity of conventional design methods. Systematic design techniques include complex design processes such as, documentation of the requirements, conceptual design , assessment of alternative products, and finalising function - form relation (Pahl and Beitz, 1996). In this study a systematic design model which has an expert system aided decision making capability was developed to design the machine tools which have complex mechanical system . The developed design model was applied to a computer program (TASITA) which has been used for machine tool systematic design. The program enables to design the systems, realising the relations between the customer requirements and design functions. The program finalizes the assessment of parameters of the design such as; machine tool structure form, power supply, control type, cutting tool and fixturing type of the workpice. Generally there are three stages in systematic design process. These are; documenting the requirements, conceptual design, and design of details. The first stage of systematic design is the "documenting the requirements". In this stage the required information and limitations of product are defined. In the conceptual design stage, the structure and function of the product are defined. In the last stage, the product design is made in detail taking into account the requirements and limitations identified for the product in previous stages (Ullman, 1992). Dimensioning of the product, material and manufacturing process selection has been done assessing the previously defined requirements and limitations (Hsu and Woon, 1998). The main problem of systematic design applications, is the selection of appropriate solution among the possible alternatives in conceptual design stage (Anderson and Crawford, 1989). Selection of the solution among alternatives can be made by "assessment charts", "mass ratio–matrix" or "reference method" (Roozenburg and Eekels, 1995). These conventional methods are not recommended, because they increase the time span of decision making process and reduce the reliability of the selected solution for the products which have a lot

1 Department of Mechanical and Metal Technologies, Kırıkkale Vocational High School, Kırıkkale University, Kırıkkale, Turkey

of alternative solutions (Roozenburg, 1993). To overcame these difficulties it is appropriate to use computer programs which have been developed for design. In his study Tice, Used process steps to prepare documentation of requirements and select appropriate solu0tion among alternatives. Graph/trees have also been used to model the physical representations of the design components. Besides modelling structural, behavioural and functional aspects of the product, graph and trees have also been used to model requirements and constraints (Tice, 1980). Identification of the component of the system and arrange them as a catalogue is an important phase of systematic design (Kusiak and Szezebicki, 1992; Hatamura, 1999).

2. DESIGN MODEL

The models which show the representation of solutions are used to overcome the difficulties confronted during design stage. In the design model, the process is started by identifying the existing problem. The design models can be classified as prescriptive, descriptive, computer based and the others. The TASITA Program which has been developed for design of machine tools is a prescriptive based model . Sub stages of developed model have been given in figure 1.

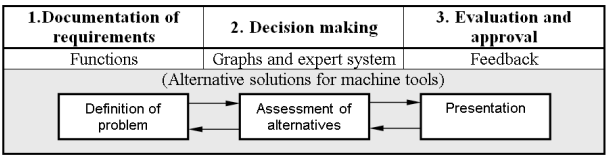

Figure 1. Stages of design model

Figure 1. Stages of design model

2.1. Documentation of Requirements

Documentation of requirements stage is the first stage of systematic design model. In this stage, documentation of the requirements is prepared using the identification of the machine tool, constrains and requirements of the user. The stage of documentation of requirements is used as main function in assessment of design alternatives. The information obtained from the documentation of requirements is used to select the proper alternative among solutions for conceptual design. Functionality, integrity, competency and usefulness of the system must be taken into consideration during documentation of requirements process (Kota, 1990; Kota S. and Ward, 1990; Rinderle and Finger, 1990; Suh, 1900). After definition of the problem which arises in the documentation of requirements, the problem can be solved using Pahl- Beitz's function structure, which is used in systematic design technique. Function structure of machine tool is identified using the main purpose of the problem, user requirements and design restrictions. When constituting the whole function structure of the machine tool, the properties of workpice

and cutting tool are identified. The whole of the information about the system e.g. energy type of the system, the material, signal and the information that exits from the system must be identified on the function .The function structure of a lathe is given Figure 2. Identification of the structure of the function is the first step in the representation of design. After constituting the function structure, it is divided into functions which include sub systems, the relation and connections between sub- systems are explained.

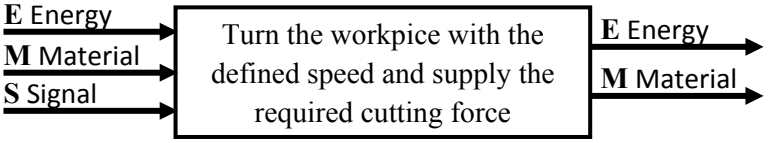

Figure 2. The whole function structure lathe

Identification of system structures and relations is the starting point of conceptual design. The all of the alternatives of mechanical structures for sub- system structure must be known. This situation enables to develop alternative solutions. The structure of the main function may not contain detailed explanations for the solution of the problem. For this reason the whole structure of the function is divided into, sub structure functions. During the assessment process of sub structures, the properties of the system e.g. power flow, material, signal and the relations between these parameters taken into consideration. When dividing the main function every sub function arranged such as to compromise one of the physical representation of the lathe. In the stage of the documentation of requirements, the artificial intelligence decision making system needs some answers of the questions to identify the capacity of the lathe. Some of the questions that can be used by decision making system may be defined as follow.

- What is the kind of manufacturing category that the machine tool will be used**?**
- Will same or different kind of workpice be machined by machine tool?
- What are the maximum dimensions of the workpices that will be machined with machine tool?
- Has the workshop a special energy supplier?
- What is the number of the ordered machine tool?
- Does the customer want any special specification with the machine tool?

To prepare the documentations of requirements and identify the aim of the design some tables may be developed. During the stage of documentation of requirements the all of the factors such as identification the structure of the system, manufacturing and marketing must be assessed. The aim of the documentation of requirements for systematic design of a lathe is given in table 1.

Table 1. Documentation of requirements for lathe

Lathe design	Main Functions	Sub functions
Identification	Identification of the problem	A1. Structure of functions A2. Structure of sub-function A3. Preparation of graphs A4. Preparation of catalogues
The structure of the system	Type of the structure	B1. Strength B2. Vibration damping
	Drive mechanism	B3. Required cutting power must be achieved B4. Vibration dampening
	Fixture of work piece	B5. Fixturing force B6. Moderate turning motion B7. Easy and quickly fixturing
	Fixturing mechanism of cutting tool	B8. Durable B9. Vibration dampening B10. Rapid cutting tool change B11. Required cutting force must be supplied B12. Motion in require axis
	Ergonomics	B13. Easiness for use B14. Safety precautions B15. Compatible to operator
	Compatibility	B16. Compatibility of the component of the system. B17. Compatibility of product and documentation of requirements
Manufacturing	Product policy	C1. Delivery time span C2. Efficiency of the product
	Product development	C3. Prototype production C4. Continual product control C5. Reservation of allocation for enhance product quality
	Product planning	C6. Investment planning C7. Planning of restrictions
	Prototype	C8. Long term usage test C9. Testing of properties of machine tools
	Manufacturing	C10. Production costs C11. Manufacturing of components C12. Stoking of manufactured components
	Assembling	C13. Assembling of sub systems C14. Assembling of the system
Marketing-dispatching	Money policy	D1. Total cost of product D2. Commercial cost of product
	Additional services	D3. Service after sales and guaranty possibilities D4. Delivery and installation

2.2. Decision Making Stage

In the developed design model a decision making system which is similar with Kusiak's decision making system was used it in systematic design of lathe. The most appropriate method for representation of information in systematic design technique is the graphical representation. The relations between the needs of user and the function of the machine tool can be identified by graphical representation. After this process it is very easy to transform the identifications made in tree form to into meaningful sentences using "If–Then" template. The sentences obtained from "If–Then" template are used to form the database of expert systems. Assessment charts, product assessment technique and artificial intelligence techniques can be used to select the most moderate design among solutions which are obtained from the conceptual design process. In this study, detailed design data for lathe design has been added to expert system data base which was developed for to be used in design model for lathe . In this export system, the properties and function of each of the component have been identified. Four different cutting tool motion mechanism and their structural properties are given in Table 2 which are used on lathe. The developed lathe design program has a wide variety of data base which contains the lathe base structure, power systems, power and motion transmission systems, workpice fixturing system, cooling system etc. The developed TASITA program uses two different knowledge bases for the design of classical lathe and computer numerical controlled (CNC) lathe. These knowledge bases contain the all design properties of system components. The structure of the decision making mechanism of the expert system is given in Figure 3. Selection criteria of classical lathe and CNC are in the first and second knowledge base of the program respectively as seen in Figure 3 (Bozdemir, 2003). Decision making mechanism shorten the time needed to assess the initially identified requirements and alternative solutions.

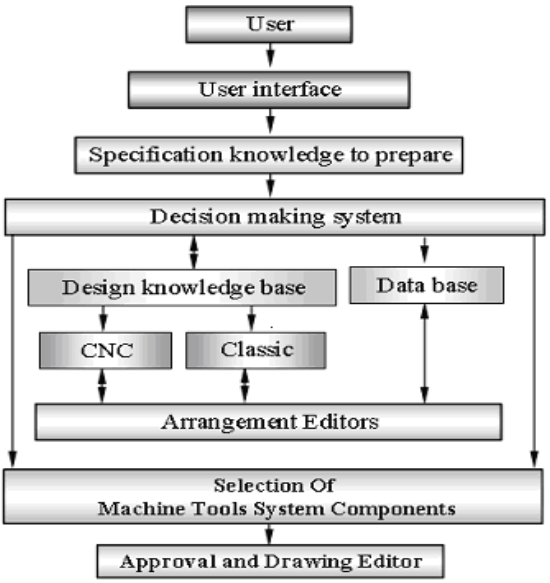

Figure 3. Expert system aided decision making mechanism

Using "If–Then" design template in the decision making mechanism of TA-SITA a flexible program data base has been obtained which enables to add, expend or change the design properties. A part of knowledge base developing process is shown in Figure 4 for the functions of sub structure of lath.

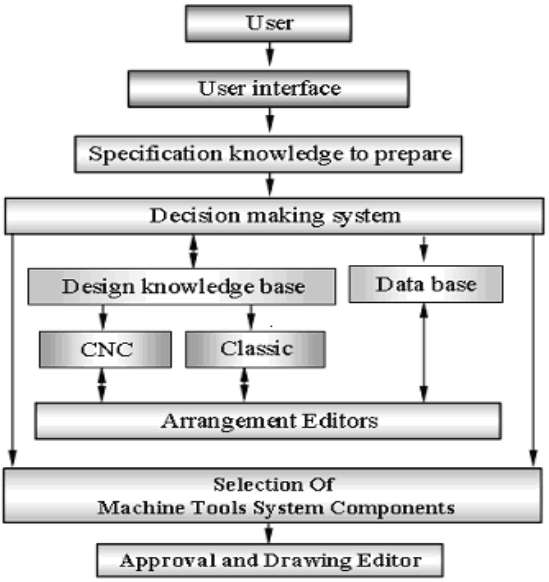

Figure 4. Part of the knowledge base developing process for lathe

2.3. Evaluation and Approval Stage

At his stage, it is possible to make changes and modifications which are required to supply feed backs to conceptual design and documentation of requirements stages. The designer is asked tool for his approval to finalize the decision making process. The designer has the possibility to make changes on the decision recommended by the expert system. At the end of this process a solution folder is obtained which contains the design details.

3. STRUCTURE of TASITA

The TASITA program has been developed for application of these possibilities to design process. It is possible to enter, to change, to correct or to erase the data of design knowledge base or data base of program. Decision making mechanism of the program interacts with these knowledge and data bases. This situation enables the program to assess the all of the data obtained from the documentation of requirements. The inter face of TASITA (Figure 5) is used to identify and asses the user requirements (14).

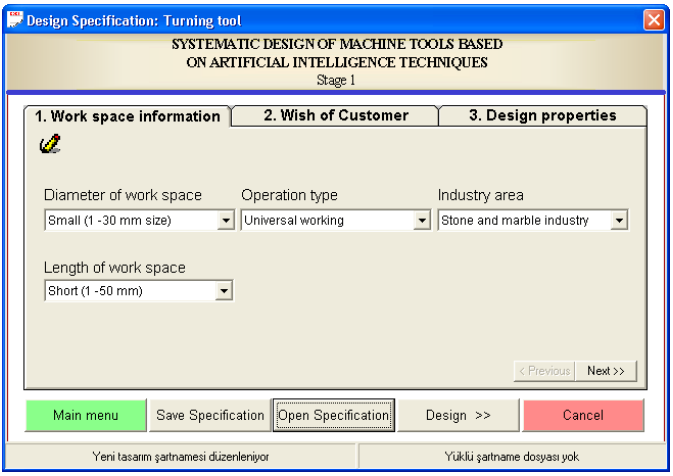

Figure 5.The menu of documentation of requirements

It is an important possibility to use computers in the assessing the requirements of user, finding the best solution at the end of the conceptual design stage, identifying the relation between function and form, preparing the design report and shortening the time required for design.

After the stage of documentation of requirements the program runs the decision making stage as seen in Figure 6.

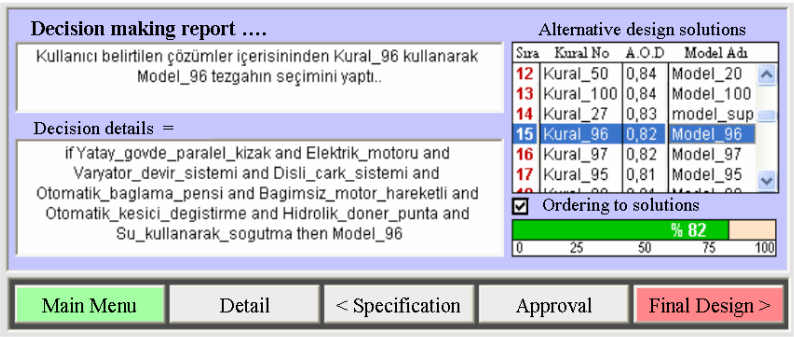

Figure 6. Decision result list of expert system.

In the decision making mechanism, the program enables to select alternative solution which contains the rule number, mass ratio value and the model name of the machine tool. The alternative solutions are listed for mass ratio results. In user supported decision making process it is possible to assess the similarity of the alternatives with visual graphics. It is possible to return to the stage of the documentation of requirements by pressing specification button. The information about solution which is selected by user or TASITA is seen in decision details window. After selection of solution pressing detail button, rule information is transformed into function–form relation. Matching of the function and form relation process of TASITA is seen in Figure 7. After completing the matching process the program enables to reach the detailed design information of sub function structures. This information is used to prepare the final report of the design. The functions which are identified by decision making mechanism are transformed to form structure and shown with a schematic plan. The specification of the selected function is given on this plan.

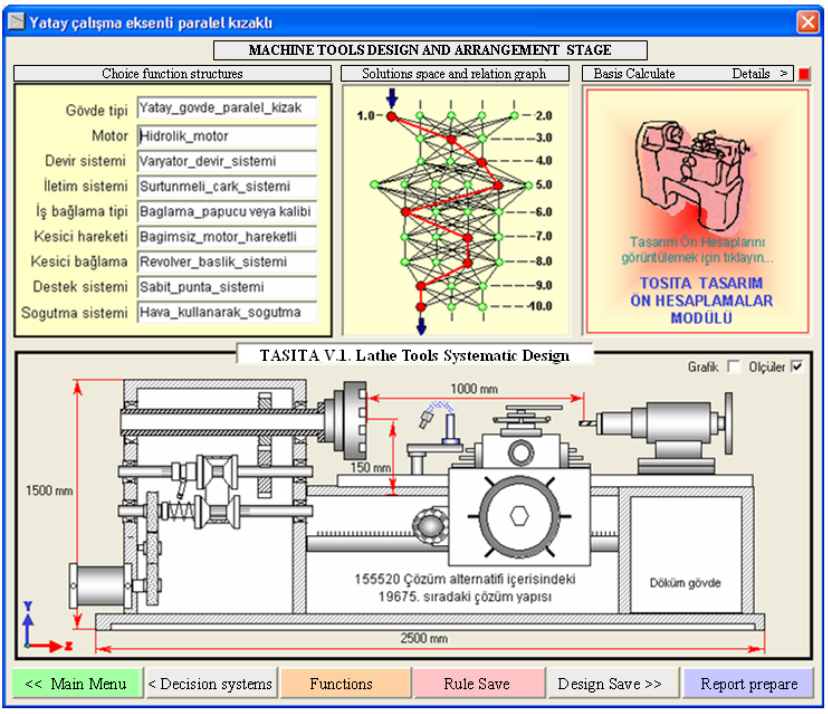

Figure 7. Matching processes of function and form.

4. CONCLUSION

It is an important problem and time consuming to redesign the complex mechanical systems for new conditions. Selecting the best alternative of the design solution, shorten the design time and increase the customer satisfaction in this study a design model for machine tools is introduced. A design application of lathe was performed for lathe. The expert system of the program uses the data base of machine tools which are designed and design knowledge of the components. The developed program (TASITA) has been arranged as a flexible structure to enable to enter the data and knowledge base of machine tools. The following results have been obtained from the study which contains the development of systematic design model and its application to lathe.

- The developed design model enables to interrelate between the documented requirements and conceptual design and decreases the time required for the design.
- Appropriate design lowers the total cost of the machine tool.
- Systematic design model can be used to prepare the documentation of requirements, asses the alternative designs, decision making, interrelate between function and forms and prepare the final report

stage by stage.

- The flexible structure of the program enables to designer to add new parameter to the data and knowledge base of the program.
- Developed design model can be used by the manufacturers of machine tools and also can be used in technical education schools in related courses.

REFERANCES

1. Pahl, G. ve Beitz, W., 1996. Engineering Design-A Systematic Approach, The Design Council, London, UK.
2. Ullman, D.G., 1992. The Mechanical Design Process, McGraw-Hill, Inc., USA.
3. Hsu W. and Woon M., 1998. Current research in the conceptual design of mechanical products, Computer aided design, Vol: 30, No: 5, Pp : 377-389.
4. Anderson D.C., Crawford R.H., 1989. Knowledge management for preliminary computer aided mechanical design, Organization of engineering knowledge for product modelling in Computer integrated manufacturing, Pp : 15-38.
5. Roozenburg N.F.M and Eekels j., 1995. Product Design: Fundamental and methods, John Willey & Sonns.
6. Roozenburg N.F.M., 1993. On the pattern of reasoning in innovative design, Design studies, Vol: 14-1, Pp: 6-18.
7. Tice W., 1980. The application of axiomatic design rules to an engine lathe case study, S.M. Thesis, Massachusetts Institute Of Technology, Massachusetts.
8. Kusiak A. And Szezebicki E., 1992. A formal approach to specifications in conceptual design, ASME Transactions: Jour. of Mech. Des., Vol: 114, Pp: 659-667.
9. Hatamura Y., 1999. The practice of machine design, Clarendon press, Oxford.
10. .Kota S., 1990. Qualitative motion synthesis: Toward automating mechanical systems configuration. In "Proceedings of the NFS Design and Manufacturing systems conference", Pp: 77-91, Society of manufacturing engineers.
11. Kota S. and Ward A., 1990. Functions, structures, and constraints conceptual design. In "Proceedings of the international conference on design theory and methodology", Pp: 239-250, ASME press, New York.
12. .Rinderle J.R. and Finger S., 1990. A Transformational approach to mechanical design synthesis, "In proceedings of the NFS Design and manufacturing systems conference", Pp: 67-75, Society of manufacturing engineers, Dearborn.
13. Suh N., 1990. The principles of design, Oxford University press, New York.
14. Bozdemir M., 2003. Systematic design of machine tools based on artificial intelligence techniques, Ph.D. Thesis, Gazi University Instute of science and technology, Ankara.

COMPOSITE MODELING ON MODULUS OF ELASTICITY OF LAYERED CLAY SOILS

İsmail ZORLUER[1], Süleyman GÜCEK, Tayfun UYGUNOĞLU

1. Introduction

In nature, soils usually are not found as homogeneously. In most of the cases, the foundations are built on a natural soil deposits exhibiting varying strength and strain characteristics. A very common kind of such of soil deposits is a soil layer of finite thickness overlying a thick layer of another soil; of different strength characteristics than overlying soil [1].The failure mechanism depends on soil properties and the thickness of each layer. In some cases where the top layer is relatively thick and consists of weak soil, the failure may be limited in the top layer only and the strength of the remaining lower layers has no influence. In many other cases, however, the failure mechanism may contain two or more layers [2].

Foundation engineering problems can be solved by two methods as experimentally, by conducting model or full-scale tests or analytically, by using methods such as finite elements. A more desirable solution for engineering practice is a lower bound estimate, as it results in a secure design and, if used in conjunction with an upper limit solution, serves to bracket the actual collapse load from above and below [3].Previously, Mısır and others, experienced equivalence in a single-layered system in their study on soil specimen between Terzaghi bearing capacity values and values from computer program. In a layered soil system, however, Terzaghi bearing capacity values were not equal with the values from the values from the computer program; moreover, difference in values reached up to the rate of 50%. The result of Terzaghi bearing capacity was also hyperbolic. Regarding this, theoretical approach for stratified soil is thought to be untrustworthy [4]. This also tells us that the relation between nonlinear stress and deformation is more realistic than linear approach.

Conte and Dente [5] carried out settlement analysis of layered soil systems by using the Stiffness method to understand the effect of the inclusion of a soft layer or stiff layer, placed at various depths within a uniform soil deposit on the settlement of the footing. Madhav and Sharma [6] studied the bearing capacity of soft-clay deposits overlain by a stiffer layer or crust. The bearing capacity of the lower soft soil was estimated considering the load spread outside the footing width as a variable surcharge stress.One-dimen-

1 Corresponding author: Ismail ZORLUER, Civil Engineering Department, Faculty of Engineering, AfyonKocatepe University, 03200 Afyonkarahisar

sional (1-D) finite element (FE) methodfor a highlynon-linear 1-D elasticvisco-plastic (1-D EVP) modelproposedbyZhuandYin[7]forconsolidationanalysis of layeredclaysoils. Authorsreportedthatthe FE modelingresultswere in goodagreementwiththemeasuredresults. Forsomeboundaryconditions, changes of factors in onelayerwillhavesomeeffects on theconsolidationbehavior of anotherlayerduetothedifferentconsolidationrates. Merifield et al. [8] appliednumerical bound analysis to evaluate the undrained bearing capacity of a rigid surface footing resting on a two-layer clay deposit. A comparison is performed between existing limit analysis, empirical and semi-empirical solutions. It was reported that the latter can overestimate or underestimate the bearing capacity by as much as 20% for certain problem geometries. Fox et al. [9]presented a numerical model, called CS3, for one-dimensional, large strain consolidation of layered soils. Verification controls show excellent agreement with available analytical and numerical solutions. Several numeric examples were used to illustrate the capabilities of CS3 and highlight errors that may occur when multilayer systems were modeled as a single layer with average properties. Finally, settlement estimates obtained using CS3 were in good agreement with field measurements for the Gloucester test fill. Pu and Fox developed a numerical model for one-dimensional large strain consolidation of a layered soil stratum. The model can also accommodate depth-dependent loading and variable pre-consolidation stress profiles. An overview of the model is presented and a parametric study is performed to illustrate the effects of large strain and depth-dependent loading on consolidation response of layered soils. Deb et al. [1]developeda simple foundation model for representing the behavior of layered soil system. Different soft and granular soil layers have been represented by shear layer of different shear modulus and springs of different stiffness, respectively, by authors. It has been observed that when a granular layer is placed over soft soil, the settlement is more predominant under loaded region for granular layer with low shear modulus as compared with the granular layer with high shear modulus where the rise in settlement is observed throughout. The settlement response is generally influenced by an appreciable amount as long as the stiffness of one soft stratum is 20 times more/less than the stiffness of other soft stratum.Shiau et al. [10] developed rigorous plasticity solutions for the ultimate bearing capacity of a strip footing resting on a sand layer over the clay layer by applying enhanced upper and lower bound techniques. They reported that most of the researches carried out regarding the layered soil system are from the viewpoint of the bearing capacity of the layered soil system.

In this study, layered specimens with different thickness which are made of two different clay soils were exposed to axial strength experiments. Effects of change in curing period on strength of specimen were also stated. In modeling phase, 6 composite models were implemented on specimens prepared. Values between experimental results and model results were observed to be the closest in Reuss model.

2. Experimental study

2.1 Materials

Two different clay soil used in this study was obtained one from ANS Campus of AfyonKocatepe University in Afyonkarahisar, and other from Meselik Campus of Eskisehir Osmangazi University in Turkey. The Clays are named as ANS (A) clay and Meselik (M) clay respectively.

The A clay soil had 90,92 % of particles passing the US No. 200 sieve (< 0.075 mm) and was classified as high-plasticity clay (CH) according to the Unified Soil Classification System (USCS). The specific gravity of the clay is 2.49, pH is 9.1, liquid limit is 60,36 %, and plastic limit is 28,20%. The M clay soil had 75 % of particles passing the US No. 200 sieve (< 0.075 mm) and was classified as high-plasticity clay (CH) according to the Unified Soil Classification System (USCS). The specific gravity of the clay is 2.69, pH is 9.1, liquid limit is 63,96 %, and plastic limit is 30,13%. The physical and compaction properties of the clay soils are shown in Table 1.

Table 1. Physical and compaction properties of clay materials.

Properties	A Clay	M Clay
0,075 mm > (%)	90,92	75
4,76 mm > (%)	100	99
Liquid limit (%) (w_L)	60,36	63,96
Plastic limit (%) (w_P)	28,20	30,13
PlastisityİndisiI (PI)	32,16	33,83
Spesific Gravity (Gs)	2,49	2,69
Soil Class	CH	CH
δ_{dmax}(g/cm^3)	1,47	1,51
w_{opt}(%)	20	18

δ_{dmax}: maximum dry unit weight, **w_{opt}**: optimum water cotent.

2.2 Soil identification tests

Soil identification tests were performed according to TS 1900-1 [11] standard. The distribution of particle sizes larger than 0.075 mm was defined by sieving, whereas the distribution of particle sizes smaller than 0.075 mm was determined by hydrometer (152 H type). For sieve analysis, the soil specimen was washed above a 0.075-mm sieve and dried in the drying oven. Then, it was sieved by a sieve set. For hydrometer analysis, 50 g of material (smaller than 0.075 mm) was mixed with a solution of chemical dispersant (Na2PO7) and stirred with a mixer. Distilled water was added to this mixture to obtain 1000 ml of solution. It was measured by hydrometer from this solution.

For consistency limits, the specimen was dried and sieved on a 0.425-mm sieve. The Casagrande device was used for liquid limit. Water was added to the specimen and mixed. The specimen was placed into the metal cup portion

of the device. A groove was constituted down its center with a standardized tool. The metal cup was repeatedly dropped 10 mm onto a hard rubber base. The water content at which it takes 25 drops of the cup to cause the groove to close over a distance of 13 mm is defined as the liquid limit. The plastic limit was determined by rolling out a thread of the fine portion of a soil on a flat, nonporous surface. The plastic limit is described as the water content where the thread breaks apart at a diameter of 3 mm.

For standard compaction test, water was mixed with the specimen. The wetted specimen was compacted in the standard compaction mold (diameter, 105 mm; height, 115.5 mm) in three layers of approximately equal mass, each layer being given 25 blows from a 2.5- kg Proctor rammer dropped from a height of 305 mm above the specimen. This process was repeated three to five times with increasing amounts of mixing (or molding) water. Maximum dry density and optimum water content were determined from relationships between dry density and water content of these processes. Compositions of the mixtures and compaction characteristics are given in Table 1.

For sample preparation, the specimens were compacted with standard proctor compaction energy and optimum water content as two-layered. Specimen height was formed from ¾ M clay and ¼ A clay, from ½ M clay and ½ A clay, from ¼ M clay and ¾ A clay, from 1A clay, from 1M clay (Fig. 1). After compaction, a sharpened brass pipe with an inner diameter of 38 mm and height of 76 mm was used to take specimens from the compaction mold. Three specimens were obtained from this mold for every different layered specimen. The specimens were sealed in plastic wrap three times and covered with a wet cloth to control humidity. The cloth was wetted every day, and then the specimens were cured for 7, 14, and 28 days. Triplicated specimens underwent an unconfined compressive test as quality control, and the averages of these three tests were reported as results. Total specimen numbers are

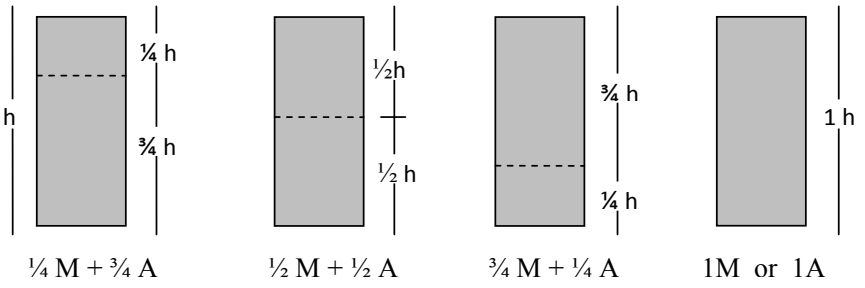

Figure 1. Heights of layered specimens

2.3. Unconfined compressive strength test

The unconfined compressive strength (qu) is a measure of the strength of mixtures for the purpose of soil stabilization. It shows the effects of additive materials on soil strength. An unconfined compressive strength test followed the procedures outlined in TS 1900-2 [12]. A strain rate of 1%/min was maintained during this test.Specimens and unconfined compression test device are shown in Figure 2.

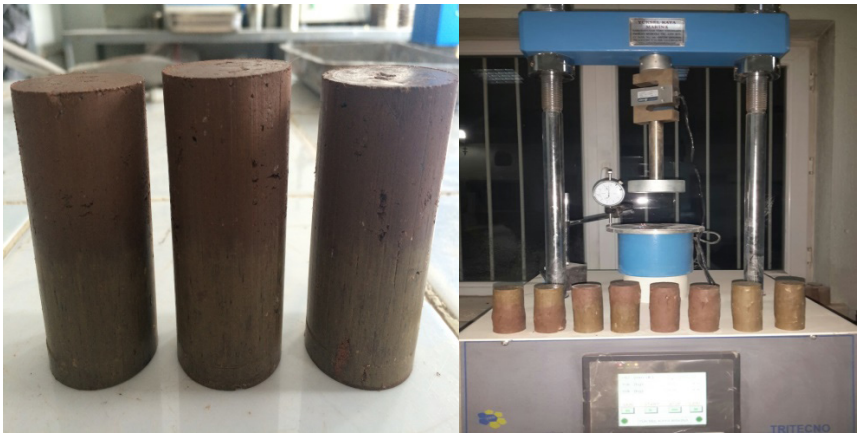

Figure 2. Specimens and unconfined compression test device

Elasticity Module is the rate of stress-strain which soil reacts under the loading conditions. It is described numerically as tangent or secant gradient of stress-strain curve. Elasticity module for each specimen was determined by computing best slope of the line produced with least square method on excel to dots from start to 40% of specimen strength. In computing of elasticity module, 40% of stress strength of elasticity area in stress-strain relation was accepted as stress value [13].

3. Composite modeling

In our experimental study is based on “Layered Composite Model”. Laminated Composite is obtaining new parts in desired shape or size by adding same or different sort of materials with solder and glue. In this sort of material, at least two phases are located within the form of the composite as strata. To create a layered composite specimenAfyon ANS clay (A) and EskişehirMeşelik clay (M), physical and mechanical property of which are different than each other were used. To assign E-module of specimens which were produced as composite material, Voigt, Reuss, Hirsch-Dougill, Popovics, Counto and Hashin models, which are implemented on simple composite systems, were used(Fig. 3) [14-16].

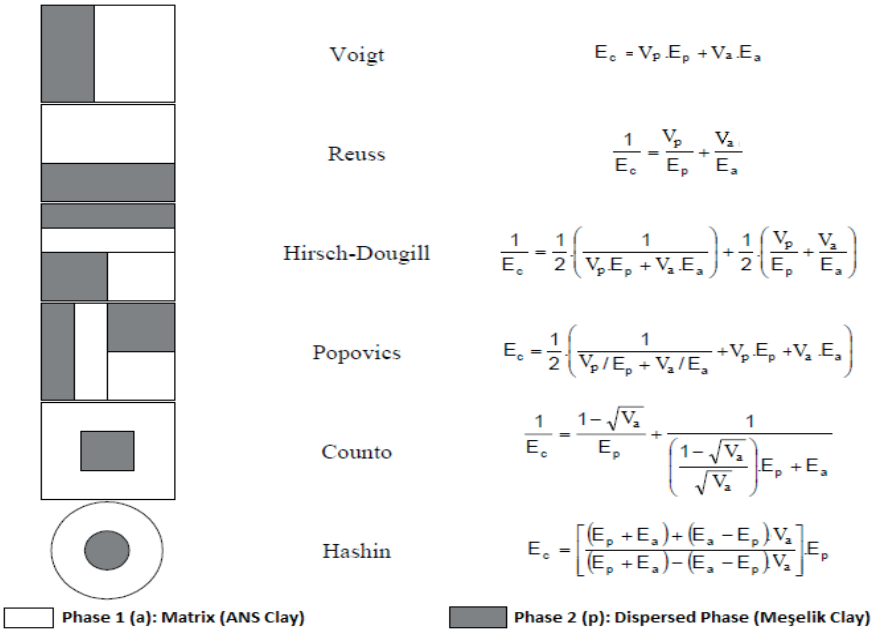

Figure 3. Composite models

In models, Ep and Ea is modulus of elasticity of distributed and matrix phase, respectively. Vp and Va is volume fraction of distributed and matrix phase, respectively. Ec is modulus of elasticity of composite, i.e. layered clay soil.

4. Results and discussions

Examining of the results of unconfinedcompressive test, increase in both curing period and strength was observed. The highest stress value was on the clay while the lowest was on the clay M. Stress values started from 25 kPa approximately, and reached to 50 kPa with the effect of curing period. The more the rate of clay A was increased in compositions, the more elasticity moduli were increased relatively. Values were observed to decrease when creating a clay layer to the clay 1A in line with the rates of M¼, M½, M ¾, M (Figure 4-6).Unconfined compressive strength of the clay 1A exceeded the value of 25 kPa at the end of 7-day period. The lowest stress value was observed on the specimen of the clay 1M with 10 kPa (Figure 4).

Stress value of unconfined compressive strength of the clay 1A was about 28 kPa. Even though the composite of M ¼ + A ¾ approached to the value of 1A, a decrease was observed with the increase of the clay M rate. The lowest stress value was on the clay 1M specimen as 14 kPa (Figure 5).Unconfined compressive strength of the clay 1A reached its peak 50 kPa at the end of 28-day curing period. Stress values were observed to decrease as the type and rate of clay A changed. The lowest stress value was on the clay 1M as 17 kPa

(Figure 6).

An increase in strength was observed relatively to the increase in the rate of composition and curing period(Figure 7). In all composition rates were observed increase in strength depending on curing period. In all compositions, the lowest strength value was observed on 1M with 10 kPa while the highest on 1A with 50kPa. As can be seen, the more the rate of the clay A in layered composite increased, the more the strength increased. Regarding the compositions of M ¾ + A ¼, M ½ + A ½and M ¼ + A ¾, the strength also increased as the rate of the clay A increased.

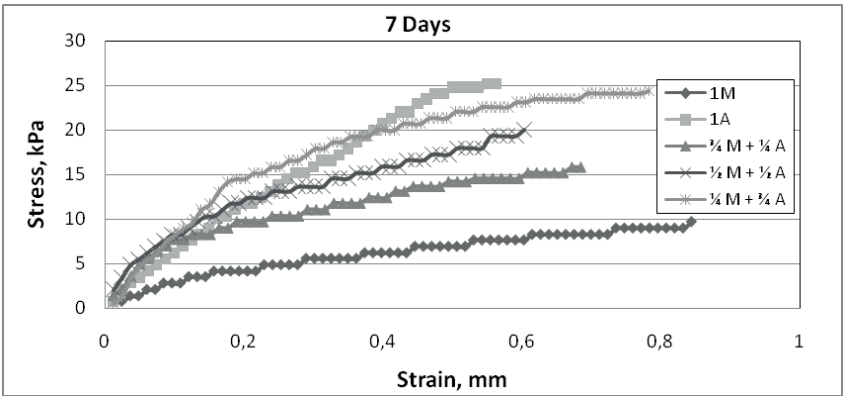

Figure 4.7-Day Values of Stress – Deformation

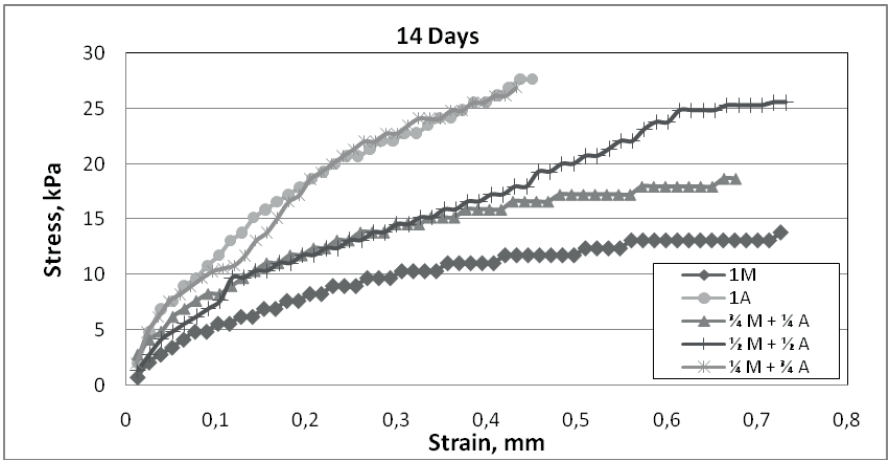

Figure 5.14-Day Values of Stress – Deformation

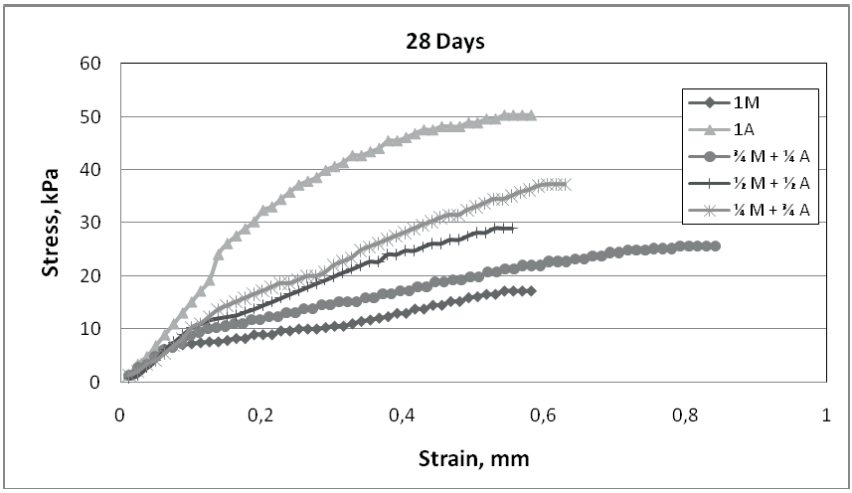

Figure 6.28-Day Values of Stress – Deformation

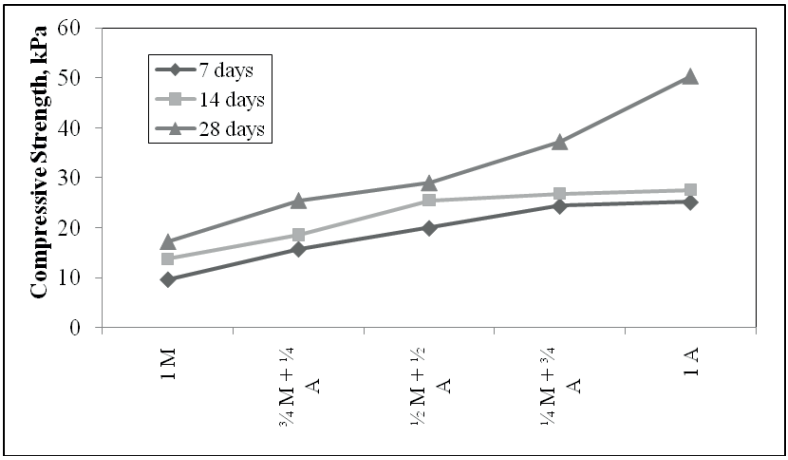

Figure 7. Effect of Curing Period on Compress Strength

The highest E-module value was on the specimen of the 28-day 1A clay with 17500 kPa while the lowest was on the specimen of 7-day 1M clay with 2200 kPa(Figure 8). The highest e-module value was on 28-day M ¼ + A ¾ clay with 9500 kPa while the lowest was on the specimen of 7-day M ¾ + A ¼ clay with 7500 kPa among layered composite specimens. Increase in clays in pure state was high while increase in layered composite specimens was close to one another.

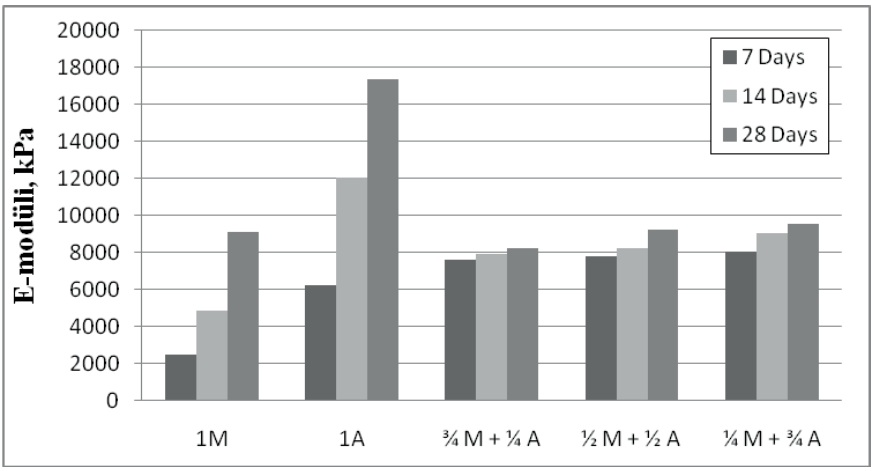

Figure 8. Effect of Curing Period on E-Module

E-moduli of all 7-day specimens of layered composite models were observed below the value of the reference specimens, which was about 7800 kPa(Figure 9). E-moduli of all layered composite specimens were observed below the value of the reference specimen, which is about 3000-5000 kPa.E-moduli of all 14-day samples of layered composite models were observed near the value of the reference specimen, which was about 8500 kPa. E-moduli of all specimens of layered composite models were about 6000-10000 kPa(Figure 10).E-moduli of all specimens of layered composite models were above the value of the reference specimen, which was about 9000 kPa(Figure 11). E-moduli of all specimens of layered composite models were above the value of the reference specimen, which was about 10000-15000 kPa.

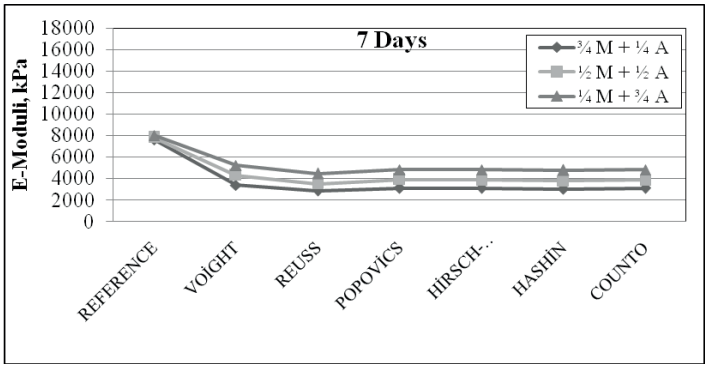

Figure 9. Comparison of composite models for 7 days aged clay specimens

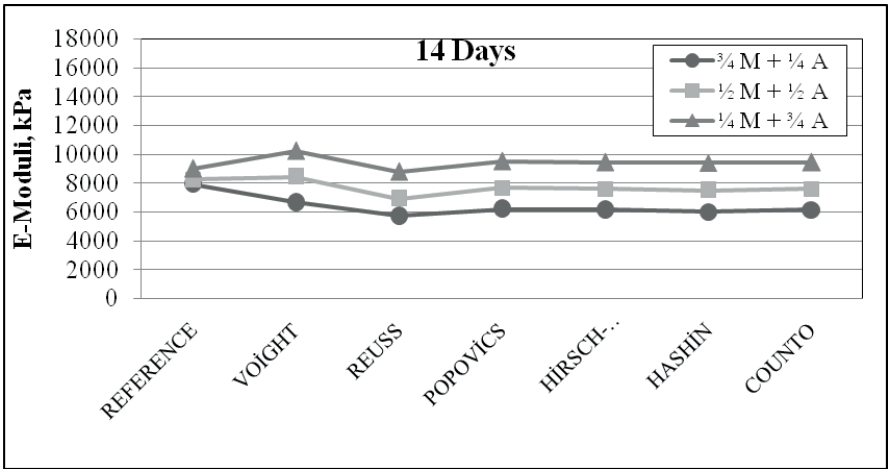

Figure 10. Comparison of composite models for 14 days aged clay specimens

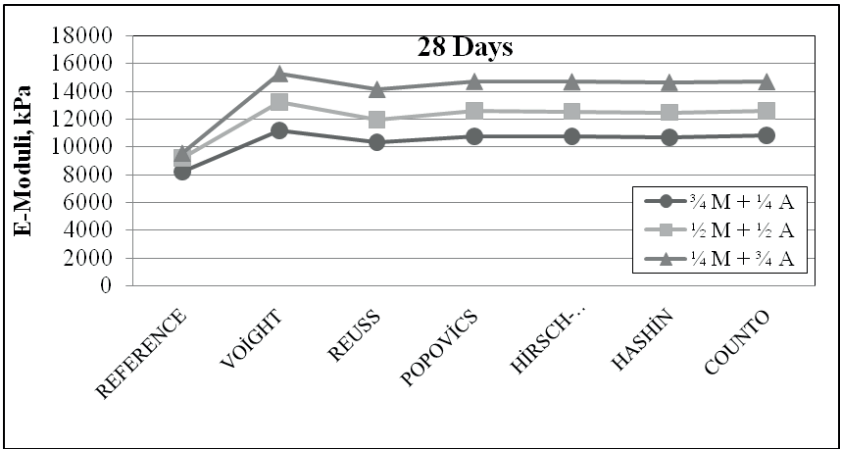

Figure 11. Comparison of composite models for 28 days aged clay specimens

The lowest error rate for model results of e-module among specimen of layered composites was on Voight model on the 14-day composition of M ½ + A ½ with the value of 2,484 % while the highest was on Reuss model on 7-day composition of M ¾ + A ¼ with the value of -62,171 %(Table 2).

5. Conclusions

This paper describes the experimental measurement of E-moduli (Young's modulus) of layered clay soil at differentagesunder compression test. Moreover, predictive composite models were developed to estimate the age-dependent E-moduli of layered clay soil using the volume fractions and prop-

erties of the constituents. The main conclusions are summarized as follows.

- E-moduli of 7-day samples of all composite models are below the value of the reference specimen, which is about 7800 kPa.
- E-moduli of 14-day samples of all composite models are near the value of the reference specimen, which is about 8500 kPa.
- E-moduli of 28-day samples of all composite models are above the value of the reference specimen, which is about 9000 kPa.
- Increase rate considering curing period of e-module value of the Meşelikspecimen is about 90% - 100% while the clay A is about 50% - 90%.
- Increase rate considering curing period of e-moduli of the specimens in form of layered composite is about 4-12%. The lowest strength is observed on 1M with the value of 10 kPa while the highest is on the clay 1A with the value of 50 kPa.
- The lowest error rate considering layered composite models is on Voight model on the 14-day composition of M ½ + A ½ with 2.484% while the highest is on Reuss model on 7-day composition of M ¾ + A ¼ with -62,171%.
- The more the rate of the clay A increases, the more the strength increases in layered composite specimens. On Figure 7 can be seen increase in strength as the clay A increases regarding the rates of the layeredspecimens of M ¾ + A ¼, M ½ + A ½ and M ¼ + A ¾.

Consequently, the bearing capacity decreases as thickness of the top layer increases for a soft-over-strong clay profile, whereas an inverse trend for a strong-over-soft clay profile. Different failure mechanisms and displacement fields are observed for strong-over-soft clay profile and soft-over-strong clay profile. A comparison of the composite modeling solutions with experimental solutions shows a good agreement. This implies that the modulus of elasticity of 14 days aged layered clay soil can be predicted appropriately by employing the Reuss composite model when the volume fraction of constituents is known.

References

1. Deb, K., Dey, A., Chandra, S. 2007. Modeling of layered soil system. First Indian Young Geotechnical Engineers Conference (FIYGEC), Jawaharlal Nehru Technological University, College of Engineering, Hyderabad.
2. Burd H.J. andFrydman S. 1997.Bearingcapacity of plane-strainfootings on layeredsoils, Can. Geotech. J. 34: 241–253.
3. Griffiths, D.V. 1982. Computation of bearingcapacityfactorsusingfiniteelements. Géotechnique, 32(3): 195–202.
4. Terzaghi, K. &Peck, R.B. 1967. Soilmechanics in engineeringpractice. 2nd. Ed., John Wiley, New York.

5. Conte, E. andDente, G. 1993. Settlementanalysis of layeredsoilsystemsbystiffnessmethod. Journal of GeotechnicalEngineering, ASCE, 119(4), 780-785

6. Madhav, M. R. andSharma, J. S. N. 1991. BearingCapacity of ClayOverlainbyStiffSoil. Journal of GeotechnicalEngineering, ASCE, 117(12) 1941-1948.

7. Fox, P.J., Pu, H., Berles, J.D. 2014. CS3: Large Strain Consolidation Model for Layered Soils, J. Geotech. Geoenviron. Eng., 140(8): 1-13

8. Shiau, J.S., Lyamin, A.V., Sloan, S.W. 2003.Bearing capacity of a sand layer on clay by finite element limit analysis. Canadian Geotechnical Journal, 40(5), 900-915.

9. Zhu, G., Yin, J.H. 1999. Finite element analysis of consolidation of layered clay soils using an elastic visco-plastic model, International Journal for Numerical and Analytical Methods in Geomechanics, 23, 355-374.

10. Merifield, R.S., Sloan, S.W., Yu, H.S. 1999. Rigorous plasticity solutions for the bearing capacity of two-layered clays, Geotechnique, 49(4), 471-490.

11. TS 1900-1. 2006. Methods of testing soils for civil engineering purposes in the laboratory – Part 1: Determination of physical properties. Turkish Standard, Ankara, Turkey.

12. TS 1900-2.2006. Methods of testing soils for çivil engineering purposes in the laboratory – Part 2: Determination of mechanical properties. Turkish Standard, Ankara, Turkey.

13. Oluokun F. A., Burdette E. G., andDeatherage J. H. 1991.Elasticmodulus, Poisson'sratio, andcompressivestrengthrelationshipsat earlyages, ACI MaterialsJournal, 88(1), 3–10, 1991.

14. Popovics, S., andErdey, M., 1970.Estimation of theModulus of Elasticity of Concrete-LikeCompositeMaterials, MaterialsandStructures, ResearchandTesting (RILEM, Paris), 3(16) 253-260.

15. Ersoy HY. 2002. Compositematerials. Istanbul: Literatur Yayıncılık[in Turkish].

16. Tanacan L, Ersoy HY. 2000. Mechanicalproperties of firedclay–perlite asa compositematerial. J Mater CivilEng, ASCE, 2(1):55–9.

17. PolytechnicUniversity, HungHom, Kowloon, Hong Kong

18. Contractgrantsponsor: The Hong Kong PolytechnicUniversity

19. Contractgrantsponsor: UGC (Grant No. pdyU 63/96E) of Hong Kong SAR Government of China

20. CCC 0363—9061/99/040355—20$17.50 Received 20 May 1997

21. Copyright(1999 John Wiley&Sons, Ltd. Revised 21 April 1998

22. INTERNATIONAL JOURNAL FOR NUMERICAL AND ANALYTICAL METHODS IN GEOMECHANICS

23. Int. J. Numer. Anal. Meth. Geomech., 23, 355—374 (1999)

CHAPTER 5

COMPARISON OF CONTROL METHODS FOR A QUADROTOR BY USING OPTIMIZATION ALGORITHM

Muharrem Selim CAN[1], Hamdi ERCAN[2],

Introduction

In the last decade, the popularity of unmanned aerial vehicles has increased and this has led to the development of control strategies as well. Researchers have focused on the development of more precise and effective control systems. In the literature, the design of the control system for the flight of a quadrotor in the indoor environment has been investigated. The quadrotor control system has been developed to avoid obstacles. LQR control method has been used to control the quadrotor. According to results, quadrotor avoids obstacles and is in equilibrium (Budiyono et. al., 2015). In another study, LQR method has been used for a quadrotor's attitude control (Reyes, 2013). In another study, changes in angular velocities, euler angles and position of the quadrotor have been investigated using LQR and PID methods. LQR and PID control methods responses have been compared for the quadrotor (Khatoon, 2014). Futhermore, fixed wing aircraft has also been controlled by using LQR control method (Can, 2018). In a different study, PSO optimized LQR and LQR are compared to control a fixed-wing aircraft. According to results, the optimized LQR method by using PSO is more successful than LQR method (Can, 2018). In a other study, the control of a quadrotor in the windy area has been examined by LQR method (Tran, 2015). PID and LQ control have been developed for attitude control of a multimotor and PID and LQ control methods has been compared (Rinaldi, 2014).

Dynamic Equations of Quadrotor

The total force acting on the quadrotor by Newton's law is shown in Equation (1). Total force acting on the quadrotor, acceleration of the quadrotor and angular velocities are represented **F,** $\dot{v}$ and ω, respectively.

$$F = m\dot{v} + \omega \times v \tag{1}$$

Total moment acting on the quadrotor are represented by Equation (2). M

1 (Research Assistant); İskenderun Technical University. Department of Aviation Electric and Electronics . E-mail:mselim.can@iste.edu.tr

2 (Assoc. Prof. Dr.); Erciyes University. Department of Avionics. E-mail: hamdiercan@erciyes.edu.tr

(2)

$$M = I\dot{\omega} + \omega \times I\omega$$

$\dot{v}_x$

, $\dot{v}_y$ and $\dot{v}_z$ indicate accelerations with respect to x, y and z in Following Equation (3) and (4). R_b^v and g are transformation matrix and gravitational acceleration, respectively.

(3)

$$\begin{bmatrix} \dot{v}_x \\ \dot{v}_y \\ \dot{v}_z \end{bmatrix} = \begin{bmatrix} 0 \\ 0 \\ g \end{bmatrix} + \frac{1}{m} R_b^v \begin{bmatrix} 0 \\ 0 \\ u_1 \end{bmatrix}$$

(4)

$$\begin{bmatrix} \dot{v}_x \\ \dot{v}_y \\ \dot{v}_z \end{bmatrix} = \begin{bmatrix} 0 \\ 0 \\ g \end{bmatrix} + \frac{1}{m} \begin{bmatrix} c\theta c\varphi & s\phi s\theta c\varphi - c\phi s\varphi & c\phi s\theta c\varphi + s\phi\varphi \\ c\theta c\varphi & s\phi s\theta s\varphi + c\phi c\varphi & c\phi s\theta s\varphi - s\phi c\varphi \\ -s\theta & s\phi c\theta & c\phi c\theta \end{bmatrix} \begin{bmatrix} 0 \\ 0 \\ u_1 \end{bmatrix}$$

The inertial coordinate system and the body coordinate system are shown in Figure 1. F1, F2, F3 and F4 show the four motor forces.

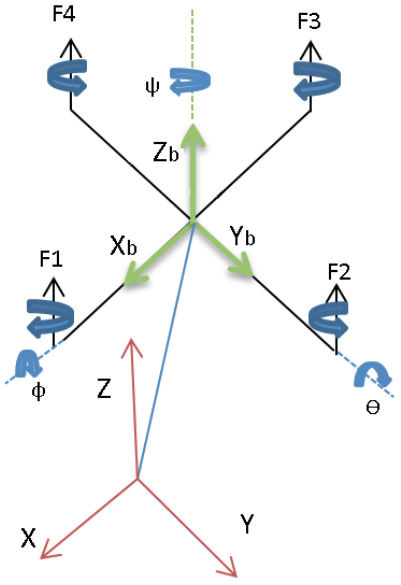

Figure 1

The properties of the simulated UAV are shown in Table 1 below.

Table 1 Quadrotor's Properties

Mass	0.5 kg
Arm Length	0.25 m
I_{xx}	0.006 kg m^2
I_{yy}	0.006 kg m^2
I_{zz}	0.02 kg m^2

Since the quadrotor is symmetrical, the moment of inertia is in the form of a diagonal matrix and is shown in Equation (5).

$$I=\begin{bmatrix} I_{xx} & 0 & 0 \\ 0 & I_{yy} & 0 \\ 0 & 0 & I_{zz} \end{bmatrix} \tag{5}$$

Following Equation (6) shows relation between rate change of angular velocities and moments.

$$\begin{bmatrix} \dot{p} \\ \dot{q} \\ \dot{r} \end{bmatrix} = \frac{1}{m}\begin{bmatrix} \frac{1}{I_{xx}}(I_{yy}-I_{zz})qr \\ \frac{1}{I_{yy}}(I_{zz}-I_{xx})pr \\ \frac{1}{I_{zz}}(I_{xx}-I_{yy})pq \end{bmatrix}_{+}\begin{bmatrix} \frac{1}{I_{xx}} & 0 & 0 \\ 0 & \frac{1}{I_{yy}} & 0 \\ g & g & \frac{1}{I_{zz}} \end{bmatrix}\begin{bmatrix} u_{2x} \\ u_{2y} \\ u_{2z} \end{bmatrix} \tag{6}$$

PID Control Method

PID method is widely the preferred control technique for industrial control system applications. It preferred due to has simple structure. The PID control method has three parameters that affect the performance of the control system, which are Kp, Kd, Ki. The performance of the control system is increased by determining optimum Kp, Kd, Ki parameters (Khatoon, 2014; Yit, 2016). Equation (7) shows mathematical PID equation. The structure of the PID control system is given in Figure (2).

$$u(t) = K_p e(t) + K_d \frac{de(t)}{dt} + K_i \int_0^t e(\tau)\, d\tau \tag{7}$$

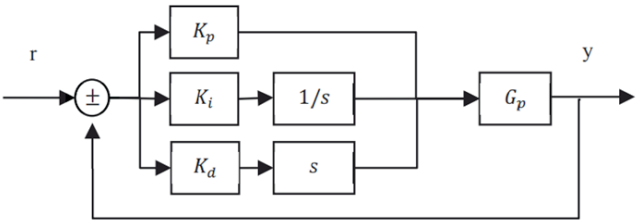

Figure 2 PID control structure

Linear Quadratic Regulator Control Method

The linear state space model is given in Equation (8) and (9). Matrix A and vector x indicate the transition matrix and states respectively (Yu, 2013). Matrix B and vector u indicate input matrix and input vector respectively (Tran, 2015).

$$\dot{x}(t) = Ax(t) + Bu(t) \tag{8}$$

$$y(t) = Cx(t) + Du(t) \tag{9}$$

In order to design a control system using the LQR method, cost function given in Equation (10) is desired to minimize. Q and R are weight matrices. x and u are state variable and input variable, respectively.

$$J = \int_0^\infty (x(t)^T Q x(t) + u(t)^T R u(t)) dt \tag{10}$$

The following Equation (11) Riccati equation is solved for X and then the K matrix is obtained by substituting it in Equation (12).

$$0 = A^T X + XA - XBR^{-1}B^T X + Q \tag{11}$$

The cost function is minimized and the gain K in Equation (12) is obtained.

$$K = -R^{-1}B^T X \tag{12}$$

Equation (13) shows the control rule that minimizes the cost function given in Equation (10).

$$u(t) = -Kx(t) \tag{13}$$

Bat Algorithm

The bat algorithm has been developed to inspire by the survival of bats using echo signals. The microbats emit high sound pulses at various pulse rates and then listen to sound echo. Some bats become aware of the outside world by using the echolocation method at fixed frequencies. While bats are hunting and avoiding from obstacles, they are detected their prey or barriers by sending echo signals at a certain frequency (Yang, 2010). Sound wave impulses emitted by bats may vary according to hunting strategies. Furthermore, bandwidth of the sound signals they emit varies according to the bat species. Bats' position and velocities are represented in Equation (14-16). Bats' new positions and velocities are also updated with these equations.

$$f_i = f_{min} + (f_{max} - f_{min})\beta \quad (14)$$

$$v_i^t = v_i^{t-1} + (x_i^t - x_*)f_i \quad (15)$$

$$x_i^t = x_i^{t-1} + v_i^t \quad (16)$$

Bat algorithm Pseudo code has been shown in Figure 3.

Objective function (x), $x = (x_1, ..., x_d)^T$
Initialize the bat population x_i ($i = 1, 2, ..., n$) and v_i
Define pulse frequency f_i at x_i
Initialize pulse rates r_i and the loudness A_i
while (t <Max number of iterations)
Generate new solutions by adjusting frequency,
and updating velocities and locations/solutions
if (rand > r_i)
Select a solution among the best solutions
Generate a local solution around the selected best solution
end if
Generate a new solution by flying randomly
if (rand < A_i & $f(x_i) < f(x_*)$)
Accept the new solutions
Increase r_i and reduce A_i
end if
Rank the bats and find the current best x_*
end while
Postprocess results and visualization

Figure 3 Bat Algorithm Pseudo Code (Yang, 2010)

Optimization of the Control Parameters

Optimization algorithms are often used in the solution of many engineer-

ing problems as well as in designing control systems. The Optimization algorithms have been developed and implemented for solving numerical complex problems. In this study, the optimization algorithms are used to control a quadrotor. The parameters of the PID and LQR methods can be optimized to improve control performance of the quadrotor. The parameters to be optimized in the LQR control method are the Q and R matrices that affect the performance of the system. These Q and R matrices are shown in Equation (17) and (18).

$$Q = \begin{bmatrix} Q_1 & 0 & 0 & 0 \\ 0 & Q_2 & 0 & 0 \\ 0 & 0 & Q_3 & 0 \\ 0 & 0 & 0 & Q_4 \end{bmatrix} \tag{17}$$

$$R = \begin{bmatrix} R_1 & 0 & 0 & 0 \\ 0 & R_2 & 0 & 0 \\ 0 & 0 & R_3 & 0 \\ 0 & 0 & 0 & R_4 \end{bmatrix} \tag{18}$$

Simulation Results

In this study, the development of a control system for position control and attitude control for a quadrotor has been investigated. The equations of motion are obtained for controlling the quadrotor. Optimization algorithms are used to find the global minimum or maximum in many numerical optimization problems. The optimization algorithm can be contributed to achieve better performance with control methods. PID and LQR methods are preferred to control the quadrotor. The PID control method is chosen because of its simple structure likewise the LQR method is chosen for its robust structure. PID control technique is easy to implement because it has simple structure. Both the PID and LQR methods contain parameters that need to be tuned. Manual determination of the parameters of the PID and LQR methods is a challenging process. Therefore, optimization algorithms are used to determine the parameters. As shown in Figure 4, the optimized LQR control method for position control in the x direction is more successful than the optimized PID control method in terms of shorter settling time, less rise time and less overshoot.

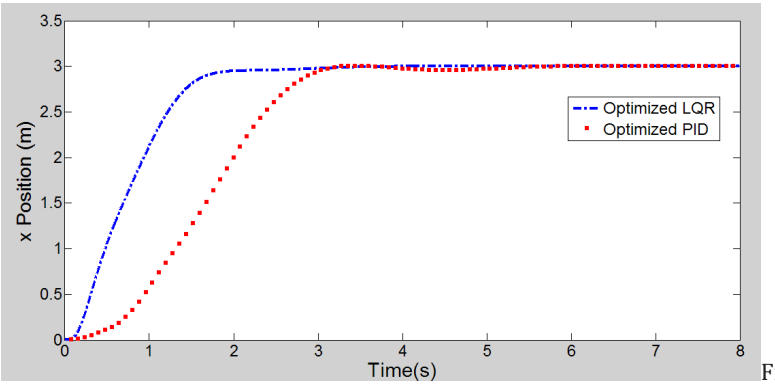

Figure 4 Comparision of LQR control method and the optimized PID control method for quadrotor.

It can be seen in Figure 5, the optimized LQR control method for position control in the y direction is more successful than the optimized PID control method in terms of shorter settling time, less rise time and less overshoot.

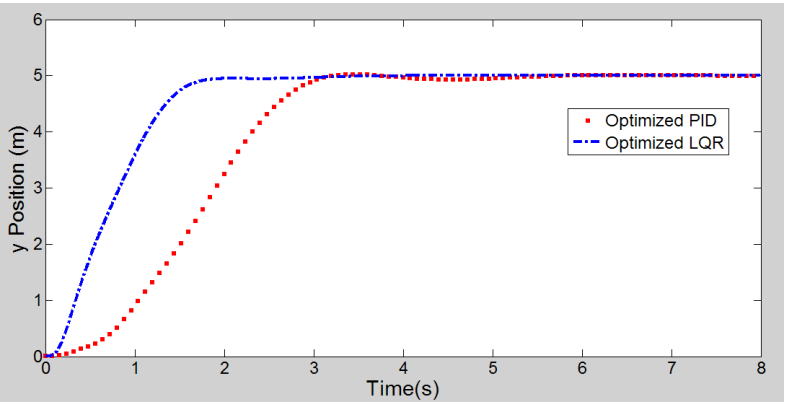

Figure 5 Comparison of LQR control method and the optimized PID control method for quadrotor.

It is clear in Figure 6, the optimized LQR control method for position control in the z direction is more successful than the optimized PID control method in terms of shorter settling time, less rise time and less overshoot.

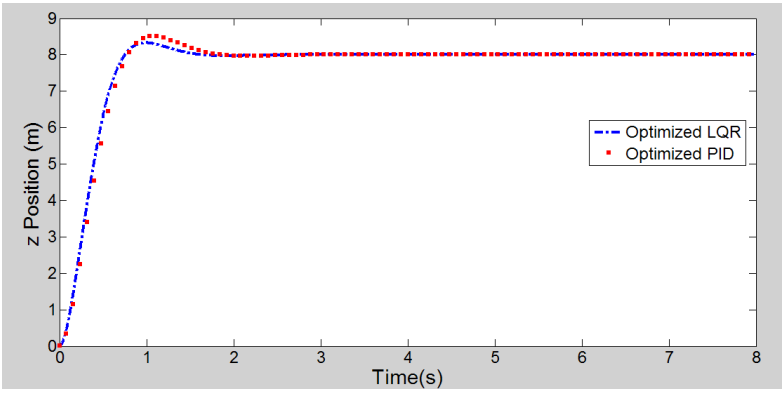

Figure 6 Comparison of LQR control method and the optimized PID control method for z direction quadrotor.

The position error in the x direction for both controllers is shown in Figure 7. For position control using the LQR method, the error converges faster to zero.

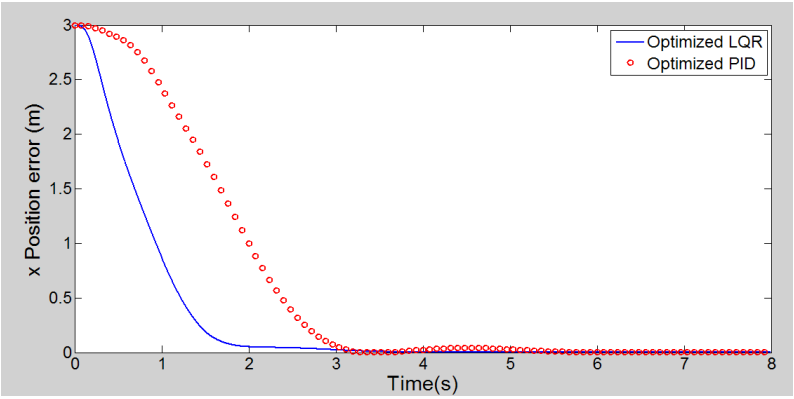

Figure 7 Comparison of LQR method and the optimized PID method for x axis error.

The position error in the y direction for both controllers is shown in Figure 8. For position control using the LQR method, the error converges faster to zero.

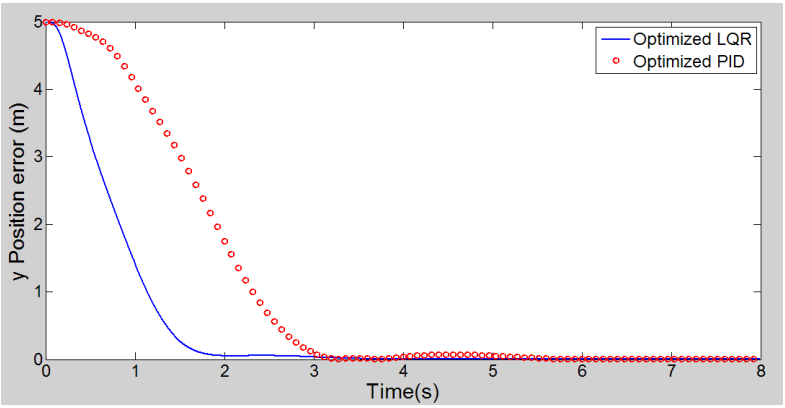

Figure 8 Comparison of LQR method and the optimized PID method for y axis error.

The altitude errors for PID and LQR control are shown Figure 9. According to the graph, error converges to zero faster for LQR control method than PID control.

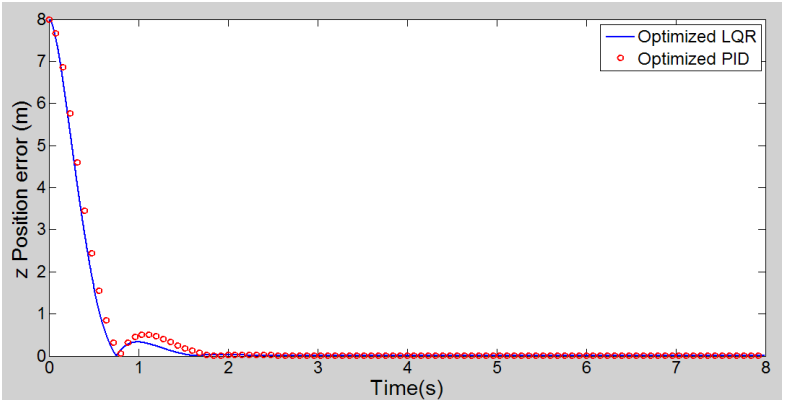

Figure 9 Comparison of LQR method and the optimized PID method for x axis error.

In this study, position and attitude control are performed using LQR method and PID method. Based on these results, the LQR method has less rise time and settling time than the PID method. Similarly, it can be seen the LQR method has less position error along the x, y and z axes than the PID method has.

LQR method and PID method which have been optimized by using Bat Algorithm are compared in Table 2, Table 3 and Table 4. According to Table 2, BAT optimized LQR method which is used to control quadrotor along x axis is provided better performances with respect to rise time, settling time, overshoot, peak and steady-state error.

Table 2 Simulation results along x axis

	Optimized LQR	Optimized PID
Rise Time (s)	1.1382	1.8066
Setting Time (s)	1.8837	2.9936
Overshoot (%)	0	0.1808
Peak (m)	3	3.0054
Steady-State Error	8.1232×10^{-7}	0.0012

According to Table 3, BAT optimized LQR method which is used to control quadrotor along y axis is provided better performances with respect to rise time, settling time, overshoot, peak and steady-state error.

Table 3 Simulation results along y axis

	Optimized LQR	Optimized PID
Rise Time (s)	1.1093	1.8064
Setting Time (s)	1.7326	2.9927
Overshoot (%)	0	0.3780
Peak (m)	5	5.0189
Steady-State Error	1.3361×10^{-7}	0.0021

According to Table 4, BAT optimized LQR method which is used to control quadrotor along z axis is provided better performances with respect to rise time, settling time, overshoot, peak and steady-state error. For both controllers steady-state error in the z-axis has been occurred much less than x and y axis.

Table 4 Simulation results along z axis

	Optimized LQR	Optimized PID
Rise Time (s)	0.4886	0.5146
Setting Time (s)	1.2937	1.5470
Overshoot (%)	3.9680	6.5068
Peak (m)	8.3174	8.5205
Steady-State Error	1.2348×10^{-10}	6.4139×10^{-7}

Conclusion

PID and LQR methods have been applied to control a quadrotor. The performance of PID and LQR methods have been compared for position and attitude control. In both methods, bat algorithm has been used to determine the control parameters. In the data obtained, the LQR method allowed the UAV to reach the desired position faster. The LQR method has a lower rise time, a settling time, overshoot and a steady state error. As shown in Table 2, Table 3 and Table 4 the optimized LQR method is more successful than the optimized PID method. Furthermore, according to Table 2, Table 3 and Table 4

optimized LQR has more advantage for the performance of system responses than optimized PID method.

References

1. Budiyono, A., Lee, G., Kim, G. B., Park, J., Kang, T., & Yoon, K. J. (2015). Control system design of a quad-rotor with collision detection. Aircraft Engineering and Aerospace Technology: An International Journal, 87(1), 59-66.
2. Can, S.,M., Ercan, H., Tekin, A.,S. (2018). Optimization of Steady State Flight Parameters for a Given Trim Condition. 4th International Conference On Engineering And Natural Sciences (ICENS 2018) (pp.672-679)
3. Ercan H., Can, S., M. (2018). Roll Control Of Aircraft Using Optimization Algorithms And Lqr Method. 2nd International Congress on Multidisciplinary Studies 4th-5th May, 2018.
4. Khatoon, S., Gupta, D., & Das, L. K. (2014, September). PID & LQR control for a quadrotor: Modeling and simulation. In Advances in Computing, Communications and Informatics (ICACCI, 2014 International Conference on (pp. 796-802). IEEE.
5. Reyes-Valeria, E., Enriquez-Caldera, R., Camacho-Lara, S., & Guichard, J. (2013, March). LQR control for a quadrotor using unit quaternions: Modeling and simulation. In Electronics, Communications and Computing (CONIELECOMP), 2013 International Conference on (pp. 172-178). IEEE.
6. Rinaldi, F., Gargioli, A., Quagliotti, F. (2014). PID and LQ regulation of a multirotor attitude: mathematical modeling, simulations and experimental results. Journal of Intelligent & Robotic Systems, Vol.73 (1-4), pp. 33-50.
7. Tran, N. K., Bulka, E., & Nahon, M. (2015, June). Quadrotor control in a wind field. In Unmanned Aircraft Systems (ICUAS), 2015 International Conference on (pp. 320-328). IEEE.
8. Yang, X. S. (2010). A new metaheuristic bat-inspired algorithm. In Nature inspired cooperative strategies for optimization (NICSO 2010) (pp. 65-74). Springer, Berlin, Heidelberg.
9. Yit, K. K., Rajendran, P., Wee, L. K. (2016). Proportional-derivative linear quadratic regulator controller design for improved longitudinal motion control of unmanned aerial vehicles. International Journal of Micro Air Vehicles, Vol.8 (1), pp. 41-50.
10. Yu, B., Zhang, Y., Minchala, I., & Qu, Y. (2013, October). Fault-tolerant control with linear quadratic and model predictive control techniques against actuator faults in a quadrotor UAV. In Control and Fault-Tolerant Systems (SysTol), 2013 Conference on (pp. 661-666). IEEE.

CHAPTER 6

INSTEAD OF ASPHALTITE FOR HEATING PURPOSES: SOLAR ENERGY

Öykü BİLGİN[1], Süreyya ECE[2]

1. Introduction

The global increase in population has led to increased levels of energy consumption. Fossil fuels are heavily used to generate the amount of energy needed. Natural bitumen asphaltite ore, a dark-colored and hard petroleum-based fuel that resembles coal and is composed of a combination of hard-to-melt organic compounds, is one of the most commonly used fossil fuels. Given that asphaltite ore, which is directly used for heating to meet the ever-increasing energy needs, cannot be replenished, its accelerated consumption may also inflict damage on the environment. In contrast, generating energy by means of renewable energy resources is not harmful to humans or the environment. In other words, renewable energy resources are environmentally friendly.

Renewable energy resources can be used forgenerating electricity, heat energy, and biomass-based fuel. The generated electricity can be used immediately. After it is regulated because it can be transferred to the main electrical grids. Through the co-generation method, biomass can be used to obtain both electricity and heat energy (DIKA, 2010). Solar energy has been estimated to meet our electricity needs to a great extent if used efficiently.

To satisfy their energy needs, Europeancountries are investing remarkable amounts of money and resources on solar energy technologies inaddition towind-based technologies despitethe relativelylow amount of sunshinereceived in those countries. In Turkey, whichreceives more sunshinethan that in other Europeancountries, this potential is underutilized.In particular, the southeastern provinces of Turkey experience sunny days with little or no cloud cover for most of the year.Among the cities in the southeastern provinces, Şırnak Province receives sunshine for the highest duration. Moreover, this province holds a considerable amount of asphaltite ore mines as well. It is safe to say that Şırnak Province is one of the most potent places in Turkey in terms of both solar energy and fossil fuel potential.However,solar electricity is not generated in the province. Solar energy is used only for heating water. Consequently, the population of the city use large amounts of unprocessed, raw asphaltite ore during winter for heating purposes.

1 ŞırnakUniversity, Faculty of Engineering, Department of MiningEngineering, 73000, Şırnak

2 ŞırnakUniversity, Faculty of EconomicsandAdministrativeSciences,Department of Business Administration, 73000, Şırnak

In this study, we aim to draw attention to the environmental destruction occurring as a result of the direct use of asphaltite ore for heating and to provide information on how the solar energy potential of the region can be used to meet its residential electricity needs. Furthermore, we demonstrate how the electricity needs of Şırnak Province can be satisfied using solar energy, in addition to the solar energy potential of the region.

2. Asphaltite Mine

Asphaltite is a hydrocarbon derived from petroleum of high caloric value. Such hydrocarbons,namely, asphaltite and asphalt pyrobitumen , fill up rock crevasses and are found in lodes. The location of asphaltite depends on factors such as hydrostatic pressure, gas pressure, gravitation, and temperature, all of which cause petroleum migration. Liquid or quasi-liquid asphalt in motion may reach up to the rock surface by following various cracks and crevasses. Asphaltite is a non-volatile material and it does not generally include any oxygenated compounds,so it does not melt when heated up and which is not dissolved in carbon-sulfur with dark color with the hardness level of 2-3 based on the Mohsscale (Orhun, 1969; Gündoğdu, 2009).

The characteristic features of asphaltite and asphalt-type materials are presented in Table 1. As can be seen from this table, asphaltites are characterized by their high melting points (120–315 °C). Natural asphalts tend to soften at temperatures of 15–160 °C. The most distinguishing feature of asphaltite obtained from asphaltpyrobitumen is its thermo- fusibility and solubility in carbon-sulfur (Gündoğdu, 2009).

Table 1: Characteristic features of asphaltite and various types of asphalt materials

Features	Asphaltites			Asphaltic pro bitumen		
	Gilsonite	Bitumen	Grahamite	Versalite	Albertite	Impsonite
Color	Black	Black	Black	Black	Black	Black
Specific weight	1.03-1.1	1.1-1.15	1.15-1.2	1.05-1.07	1.07-1.1	1.10-1.25
Stiffness	2	2	2-3	2-3	2	2-3
Penetration	0-3	0-5	0	0-5	0	0
Melting point	120-175	175-315	insoluble	insoluble	insoluble	insoluble
Babit carbon	10-20	20-35	35-55	5-25	25-50	50-85
Oxygen	0-2	0-2	0-2	0-2	0-3	0-3
Mineral matter	little-1	little-5	little-50	little-10	little-10	little-10
Resolution in Cs_2	98-100	95-100	45-100	5-10	2-10	little-6

Source: Gündoğdu, 2009

In addition to being used for heating and as a fuel asphaltite is used for various purposes such as the production of car tires, electrical insulating materials, battery jackets, expanded rubber, water-resistant cables, and synthetic petroleum (Bilgin and Kantarcı, 2015). The use of asphaltite is not desirable owing to the environmental concerns it poses given its very high sulfur content (Sezer, 2007).

At the present rate of consumption, fossil fuelswill not satisfy the community's energy needs in the long run. Moreover, fossil fuels have harmful side effects such as pollution and greenhouse gas emission that threaten human health. The use of fossil fuels causes climate change in the long run (Lewis and Crabtree, 2005).

3. Solar Energy

3.1. Solar energy potential in Turkey and Worldwide

3.1.1. Solar Energy in the World

Considering the global trendsit can be seen that the number of solar energy systems, installedrecently is on the rise; in particular, states in the European Union offer incentivesto benefit from this clean source of energy and the to attract investments. Germany,owing to the incentives it enacted, accounts for 47% of the photovoltaic (PV) solar systems installed in the world despite its disadvantageous location compared to other countries in terms of the sunshine duration and global radiation valuesSpain (16%), Japan (12%) and Germany, together account for 75% of the total installed solar energy systems worldwide. In terms of the total installed power, a global growth rate of 78% was achieved in 2008 compared to the previous yearwhereas a rate of 52% was recorded in 2009 . The average annual growth rate over 2006–2009 was 42% (DIKA, 2010).Most of the energy, used in the world, is derived from the primary energy resources. such as fossil fuels. According to 2011 data,12274.6 Mtep (Million Ton) Equivalent Petroleumof primary energy resources were used worldwide. Petroleum (33.1%), coal (30.3%), and natural gas (23.7%)used. Other energy resources include renewableforms, such as wind, solar,forms, such as wind, solar, biofuel, and geothermal energy resources. In the same year, the amount of electricity generated from primary energy was 22018.1 TWh. The primary energy resources with thelargest shares in electricity production were coal (41%), natural gas (21%), and hydro- energy (16%) (Koç and Şenel, 2013).

3.1.2 Solar Energy in Turkey

In Turkey, the primary energy production was 32228.9 Btep (Billion Ton Equivalent petroleum) in 2011. The resource-based distribution of primary energy generation is as follows lignite (50%), hydro-based (14%), wood (8%), oil (8%), geothermal (5%), and pit coal (4%). In 2011, the production of primary energy from resources such as lignite, geothermal, wind, and solar energy systems increased compared to that in 2010, while the production of the primary energy from wood and animal and plant wastesdecreased. The

total energy consumption of Turkey in 2011 stood at 114480.2 Btep , and Turkey ranked 23rd in terms of energy consumption worldwide. Most of the country's energy needs are met by oil and natural gas, which are necessarily imported into Turkey. The shares of various energy resources in the energy consumption pie are as follows: natural gas (33%), oil (27%), pit coal (15%), lignite (14%), and hydropower (4%). The coverage ratio of domestic energy resourcesin terms of satisfying the energy consumption needs has declined rapidly within years. It stood at 48.10% in 1990 and has since declined to 28.20% in 2011 (Koç and Şenel, 2013).

As of the end of July 2017 natural gas, coal, hydro-power, wind energy, geothermal energy, and other sources accounted for 34%, 31%, 24%, 6%, 2%, and 3%, respectively, of the energy production in the country (Enerji, 2017a).

Turkey has abundant solar energy potential. According to the Solar Energy Potential Atlas (SEPA)compiled by EIE byconsidering regions with 4,600 m^2 of usable area and more than 1.650 kWh m^2 of annual solar radiationthe technical potential for annual solar-based electricity generation in Turkey was calculated to be 380 billion kWh.

In Turkey, solar energy is used for heating water using rooftop solar water heaters (DIKA, 2010).

The total installed solar collector area in Turkey as of 2012; 18,640,000 m^2 (approximately). The annual plenary solar collector production is estimated to be 1,164,000 m^2, whereas vacuum-tube-based collector production isestimated to be 57.,600 m2. It is known that 50% of planar solar collectors and all vacuum -tube -based collectors are used within the country. In 2015, approximately 811,000 TEP (Ton equivalent petroleum) heat energy was generated using solar collectors. In 2015, it was calculated that 528,000 TEP of the total energy generated was used for residential purposes, while 283,000 TEP was utilized for industrial purposes. In Turkey, as of the end of 2016, 34 solar energy plants with an installed capacity of 402 MW obtained preliminary licenses, while two solar energy plants with a combined installed capacity of 12.9 MW obtained operating licenses. Considering unlicensed electricity generation plants the total number of solar energy plants stood at around 1,043 as of the end of 2016, whereas the installed capacity of those plants stood at 819.6 MW. With the addition of the two licensed plants, the total installed capacity reached 832.5 MW (Enerji, 2017b).Turkey, thanks to its geographical location, has a high solar energy potential, and according to SEPA the total annual sunshine duration in the country is 2,737 h (daily average: 7.5 h), while the amount of solar energy received per year is 1,527 kWh/m^2 (daily total: 4.2 kWh/m^2) (Enerji, 2017b). The solar energy potential map of Turkey is shown in Figure 1.

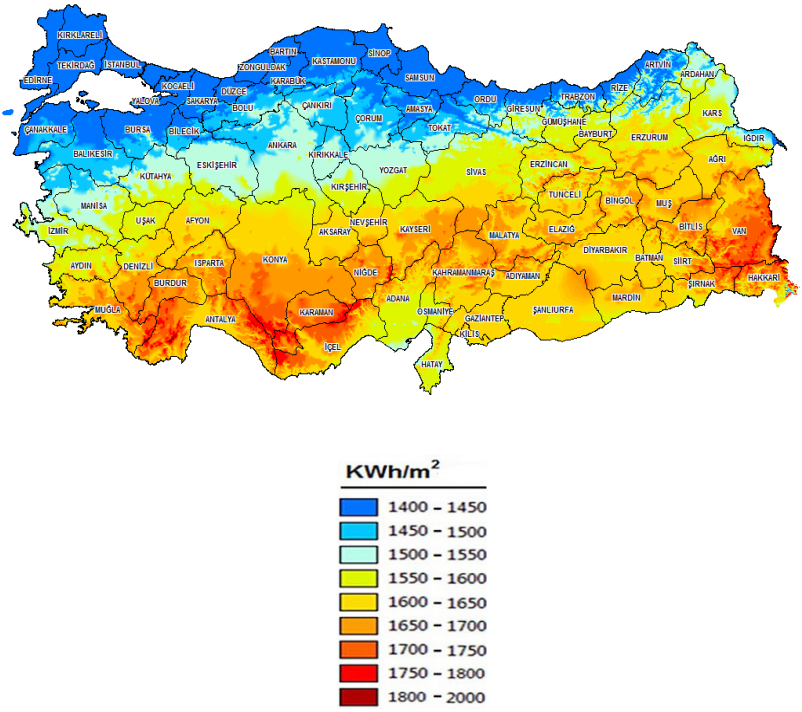

Figure 1: Annual solar energy potential value map of Turkey (kWh/m^2)
Source: EnerjiAtlası, 2017

According to Table 2, the months during which the most and least energy is produced are June and December, respectively. Among the regions, Southeastern Anatolia and Mediterranean (shoreline) Regionsare the ones with the highest solar insolation. Except for the Black Sea region, where solar energy production is virtually nonexistent, 1,110 kWh of solar power can be generated per square-meter per year, and the total number of sunshine hours is 2,640/year. It can be said thequantity of solar energy that Turkey receives per year is around 1.015 kWh (Varınca and Gönüllü, 2006). Table 2 presents the distribution of annual total solar energy potential in Turkey by region.

Table 2: Distribution of annual total solar energy potential in Turkey by region

Region	Total average solar energy	Max. solar energy (June)	Min.solar energy (December)	Average sunshine duration	Max. average sunshine duration (June)	Min. average sunshine duration (December)
	kWh/m^{2}-year	kWh/m^2	kWh/m^2	hour/year	hour	hour
Southeast of Anatolia	1.460	1.980	729	2.993	407	126
Mediterranean	1.390	1.869	476	2.956	360	101
East of Anatolia	1.365	1.863	431	2.664	371	96
Central Anatolia	1.314	1.855	412	2.628	381	98
Aegean	1.304	1.723	420	2.738	373	165
Marmara	1.168	1.529	345	2.409	351	87
Black Sea	1.120	1.315	409	1.971	273	82

Source: Varınca & Gönüllü, 2006

As can be seen from Table 2, the Southeast Anatolian Region has the highest solar energy potential in Turkey and Şırnak Province is located in this region. The amount of solar energy that the Southeast Anatolian Region receives per year (per sqm) corresponds to 16% of the total solar energy received by Turkey in one year. Incidentally, the annual average sunshine hours in the Southeast Anatolian Region corresponds to 16% of the average sunshine hours in Turkey in total.

In Turkey, solar energy is most commonly used in water heating systems. The total area of installed solar collectors in Turkey stood at 7.5 million m^2 in 2001. These indicated systems, which are predominantly located in the Mediterranean and Aegean regions, generate around 290,000 TEP of heat each year. Over 100 companies are engaged in manufacturing such systems in Turkey, and it is estimated that 2,000 people are employed in this industry. The annual production of solar collectors is around 750,000 m^2 and a part of this production is exported (Varınca and Gönüllü, 2006).

3.2. Solar Energy Technologies

Solar power is a type of radiation-based power generated as a result of nuclear fusion (conversion of hydrogen gas into helium) that occurs at the core of the Sun. The intensity of solar energy is around 1370 W/m^2 outside the Earth's atmosphere. However, the amount that actually reaches the surface of the Earth varies between 0 and 1100 W/m^2 owing to the effect of the atmosphere. However, even this small portion of energy that reaches the Earth is considerably more than the energy consumption of humans. Research on the use of solar energy gained momentum after the 70's and with technological advancement of solar energy systems, their costs decreased, which helped establish them as viable and clean means of energy production. The Sun is the source of all other energy sources in a direct or indirect manner, except for nuclear energy (EIE, 2017).

Even so, as complete energy systems, solar energy conversion systems continue to be expensive. Solar energy must be cost-effective to become widespread and be considered as a primary energy source. To this end, it is necessary to convert and store the energy obtained from the Sun. Developments in nanotechnology, biotechnology, materials science, and physics can provide new approaches to cost efficiency to increase the dissemination of solar energy. Through improvements in science and technology, the costs of existing PV energy production methods can be reduced. Moreover, such improvements are expected to facilitate the capture and storage of solar energy at the lowest level (Lewis, 2007).

Solar energy technologies vary in terms of materials and the technology used, and accordingly they are divided into two main groups, namely, PV and thermal solar technologies.

3.2.1. PV Solar Technologies

PV solar systems generate electricity from sunlight using solar cells or PV cellsmade of semiconductor materials. When sun rays are incident on a solar panel, electron exchange occurs in the semiconductors within the solar cell, and this exchange generates electric currents. These solar panels convert sun rays within a certain wavelength into electricity. The rays from the other wavelengths are absorbed by the other components of a solar panel and are converted into heat or are simply reflected (Cengiz and Mamiş, 2016).

The use of solar cells is usually economically feasible in areas that are far from major settlements and where the electric grid is not extensive; therefore, solar energy systems can be used to provide signal services and to meet the electric needs of rural areas. In Turkey, the installed capacity of solar cells that are currently used in telecom stations, fire observation posts of the Under Secretariat of Forestry, lighthouses, and highway illumination is approximately 300 kW. While there are no problems in terms of resources for the utilization of solar energy in Turkey, there are a few regional differences in terms of to the methods used for electricity production. PV systems can generate electricity under any weather conditions, clear or overcast. By contrast, concentrator systems (thermal and mechanical conversion) require direct radiation or clear weather. Therefore, thermal and mechanical generators should be employed in the Southeast Anatolian and Mediterranean regions, whereas PV systems are suitable for use in all other regions, except for the Southern Black Sea region (Varınca and Gönüllü, 2006).

In PV systems, thermal radiation originating from the Sun is converted to electricity using solar panels, and the generated energy is used after converting it into a usable form by an inverter. In thermal systems, sun rays are directed toward a certain point using special mirrors, and a liquid such as water or oil is heated at this point. The pressurized vapor generated in this process is used to generate energy in a thermal cycle. Solar cells (PV cells) are made of semiconductor materials that directly convert any incident solar

irradiation into electricity. The area of solar cells, which are usually shaped into squares, circles, or rectangles, is usually 100 cm^2, while their thickness is 0.1–0.4 mm (EIE, 2017).

Solar cells can be used for any application where electricity is required. Depending on the application, PV modules are paired with batteries, inverters, battery charge controllers, and various supplementary electronic circuits to form a PV system. In the past, these systems were used only in regions that were far away from major settlements with no access to the main electrical grid because transporting fuel to generators in such locations was difficult and costly. Today, solar energy systems are being used commonly in areas with a connection to the grid, especially on the roofs of residences (with grid connections). In addition, they are being used to build large-scale power plants. Apart from the aforementioned applications, it is possible to use solar energy systems in combination with diesel generators or other power generation systems (EIE, 2017).

The typical standalone (used independent from the grid) applications of the PV systems are at communication stations; radio and phone systems in rural areas; cathodic protection of oil pipelines; corrosion protection of metal structures (such as bridges and towers); telemeter measurements conducted at electricity and water distribution stations and meteorology stations; indoor or outdoor lighting; electrical appliances such as TV, radio, and refrigerator in mountain cabins or houses in remote locations; agricultural irrigation or water pumping for residential use; forest observation posts; lighthouses; emergency-security-alarm systems; earthquake and weather observation posts; and cooling for drugs and vaccines (EIE, 2017).

Concentrator PV systems are among the most widely used systems for converting solar energy into electricity. In such systems, the solar rays incident on silicon-based planar PV panels are converted into electricity. However, the surfaces of cells used in such systems are large and the amount of material used is high, which means efficiency is low and cost is high. Non-silicon thin film or concentrator photovoltaic (CPV) technologies may decrease the use of silicon and other semiconducting materials. In this way, the electricity generated by solar power plants will be able to compete with grid-based electricity produced using conventional fossil fuels. Although the manufacturing cost of thin film devices is relatively low, they are used rarely and their source materials (such as Ga and In) are expensive, which restrict their widespread use despite their high efficiency and reliability. The advantages of CPV modules compared to planar PV modules are as follows:

- The cost of the active semiconductor material that produces the same amount of energy from the solar power received over a given area is 1/1000 compared to that of the materials used in other PV systems.
- The cost of electricity generated from the Sun is less than half of the cost of the electricity we use at present.

- The efficiency of CPV modules is twice that of planar PV systems (EIE, 2017).

3.2.2. Thermal Solar Technologies

Thermal solar technologies can be categorized into two groups, namely, low-temperature collector systems and concentrators.

a. Low-temperature solar collector systems:

- Planar Solar Collectors: These devices transfer solar energy to a fluid in the form of heat. Such solar collectors are most widely used solar energy applications owing to their simplicity and low cost. They are used for heating water in residences, swimming pools, and industrial facilities (Uçgül andErgün, 2012).
- Evacuated Solar Collectors: These systems comprise two intertwined glass tubes. The air between the tubes is evacuated using vacuum technology to limit any heat loss. Owing to vacuum insulation between the two glass layers, such systems pose zero risk of freezing during winter, which means the use of anti-freeze formulations is unnecessary. Water heating systems with evacuated solar collectors are more expensive compared to systems with panel collectors (Ersöz and Yıldız, 2013).
- Solar Pool Heaters: The large amounts of energy required to heat the water in swimming pools, which are provided by various sources at present, cost users significant amounts of money. In this regard, heating up swimming pools using solar energy is an attractivealternative (Akbulut et al., 2006). The black-colored floor of a swimming pool with a depth of approximately 5–6 m is used to catch solar radiation to heat water to 90 °C (EIE, 2017).
- Solar Chimneys: Solar chimneys are based on a physics principle dictating that heated air rises. The air within solar collectors is hot and it exits the chimney. This cycle of motion of the air spins the turbines at the entry of the chimneys, which generates electricity (Türkmen et al., 2009). More energy is produced as the height of the chimney increases. The efficiency of the chimney depends not on the temperature rise but on the ambient air temperature. Therefore, the efficiency of such systems is directly proportional to the height of the chimney and the ambient air temperature (Aydınol andAslan, 2009).
- Water Purification Systems: These systems mainly comprise a shallow pool. The surface of the pool is covered with inclined transparent glass meshes. The water, vaporized in the pool, condenses on the indicated covers. Such systems have long been used in some settlements wherein clean water sources may not be available (EIE, 2017). Solar-powered water pumps do not require daily maintenance because they can be installed in any location with substantial amounts of solar

insolation. Although the initial installation costs and setup costs of such pumps are high, their operational and maintenance costs are very low. Therefore, they break even swiftly, especially in places with high solar radiation potential (Atay et al., 2009).

- Solar Architecture: As a result of a few changes to the structure and design of buildings, heating, cooling, and lighting can be achieved. By using passive natural heat transfer mechanisms, solar energy can be collected, stored, and distributed. In addition, active components such as solar collectors and PV modules can be used.
- Product Drying and Greenhouses: These are agricultural applications of solar energy. While such systems can be primitive and passive in terms of their design and structure, they may contain active components that facilitate air circulation.
- Solar Cookers: Solar heat is collected in bowl- or box-shaped solar cookers, the interiors of which are coated with reflective materials, to cook meals (EIE, 2017).

b. Concentrating systems

- Parabolic Chamfer Collectors: Parabolic solar collectors are the most widely used solar technology compared to the other thermoelectric systems. These collectors comprise a concentrating array with a parabolic cross-section. The reflective surfaces inside the collectors concentrate solar energy onto a dark-colored absorbent tube that stretches longitudinally across the center of the collector. The collectors are usually placed on a single-axis tracking system that tracks the east to west traversal of the Sun. While heat transfer oil is used in the absorbent tube as the heat transfer fluid, researchers are testing the use of water, which is less expensive and does not inflict damage on the environment. The collected heat is then transferred to a plant for generating electricity. The cost and space required per MW of power generated are 5 million Euro and 3,500 m^2, respectively (EIE, 2017).
- Parabolic Dish Systems: In these systems, a dish concentrates solar radiation onto a collector. The system tracks the Sun. The collected heat is directly used by a heat engine on the collector. Parabolic dish systems can be used for small-scale applications for individual users or larger-scale applications for power plants (Cengiz and Mamiş, 2016). In the conversion of solar energy into electricity via the Dish–Sterling combination method, an efficiency ratio of 30% can be achieved. This technology is very expensive owing to its 1 million Euro cost per 10 kW (EIE, 2017).
- Central Collector Systems: Mirrors called heliostats, which are more than 100 m^2 in size and have individual focusing capabilities, reflect and intensify solar energy on a heat exchanger with a high absorption

coefficient, also called a receiver. In such systems, liquid salt or air is used as the heat transfer fluid, and temperatures of up to 800 °C are achieved. While the cost per MW is 3.5–4.5 million Euro, a designated space of 35,000 m^2/MW is required (EIE, 2017).

- Fresnel Lens Technology: Fresnel solar power systems work by reflecting and intensifying solar energy to increase the temperature of the fluid within the absorbent. Depending on the demand, the red-hot steam produced by the system may be used as a thermal source by itself or be used to generate electricity via a turbine. In addition, given that that the height of such systems is low, they have few structural requirements (Uçgül andErgün, 2012).

In this system, which is less expensive compared to the parabolic chamfer system, efficiency may be increased by lowering the receiver height. However, because doing so would decrease the solar energy collection area, a greater number of panels would be required, which would increase the overall system cost (EIE, 2017).

- Concentrating Solar Energy Systems: Concentrating Solar Energy Systems (CSP) are among the few renewable energy technologies that show potential in terms of satisfying future energy demands. An integrated study conducted in Africa and Europe shows that CSP technologies may help to attain ambitious climate protection goals (Viebahn et al., 2011).
- Linear Concentrators: Parabolic chamfer collectors comprise parabolic arrays with parabolic cross-sections that provide linear concentration. In these systems that are used in applications where mid-range temperatures are required, it is sufficient to track the Sun with one-dimensional traversing because solar energy would be concentrated on a single line.
- Point Concentrators: This type of systems, which tracks the Sun along two planes and perform point concentration, are divided into two groups, namely, parabolic dishes and central receivers. The parabolic dish collectors track the Sun along two planes and constantly reflect the Sun onto the focal spot. In the central receiver system, an array comprising planar mirrors called heliostats that can perform individual focusing reflects solar energy onto a heat exchanger or receiver installed on a tower(EIE, 2017).

Solar thermal power plants are power production systems that use solar energy as the primary source of energy. While these systems operate based on the same principle, they differ in terms of solar energy collection methods, i.e. the collectors they use. In power plants, wherein parabolic chamfer collectors are used as the collection component, fluid is circulated within the absorbent tube fitted at the focal center of the collectors. Thereafter, hot steam is generated from the liquid heated using heat exchangers. In systems that use parabolic dish collectors, either the same method is used or electricity is

directly produced via a motor (Stirling) fitted at the center. In systems with central receivers, solar rays are reflected on a heat exchanger called the receiver by means of planar mirrors (heliostats). In the receiver, electricity is generated using the fluid and conventional methods (EIE, 2017).

4. Asphaltite Mining in Şırnak Region and Solar Power

4.1. Environmental Impact of Asphaltite Mining

The most important asphaltite mineral deposits in Turkey are in Şırnak and Silopi. Asphaltite ash contains a few rare minerals such as nickel, molybdenum, vanadium, and uranium, and it is used in fossil fuel plants as solid fuel owing to its high thermal yield (Bilgin and Kantarcı, 2015). The net calorific value of asphaltite varies between 2,800 and 5,800 kcal/kg. However, it contains sulfur (3%–8%) and ash (32%–35%). According to the TKI data of 2012, the asphaltite mines in Şırnak Province are estimated to be 104.60 million tons (TKI, 2013). These asphaltite mines, which were idle for many years owing to a terrorist problem in the region, have been reopened for operation recently and have been contributing to the regional economy and energy balance of the country (DPT, 2007). The total asphaltite production of Turkey in 2010 was 1,293,000 tons (MMO, 2012).

The asphaltite mining methods used within Şırnak City limits are open-pit mining and underground mining. The explosives used for mine production are compliant with the Explosive Substances Directive. The asphaltite extracted from the mines is generally reduced to various sizes, namely, orange, nut, and walnut, bagged in a packing section, and put out on the market. Some portion of the asphaltite produced is sold after it is mixed with molasses and lime. The asphaltite streak and stockpile at the Şırnak Mine Site are shown in Figure 2.

Figure 2: Photographs of asphaltite streak and stockpile at Şırnak Mine Site

In addition to heating, a part of the asphaltite produced in this region is used in fossil fuel plants operated in Silopi. One of the indicated plants extracts asphaltite coal from the mine, thus contributing to the generation/sale of electricity. Around 2,000 people are employed by this industry, including 1,000 people at the mining site (half of these people are from Şırnak and other cities in the region), and because asphaltite is not directly used in the indicated power plants, there is no damage to the environment as is caused in case of personal use of the ore.

4.2 PotentialandUtilization of SolarEnergy

In Şırnak Province, electricity production using PV or thermoelectric technologies is not undertaken, mainly because these systems require high levels of investment and that investing in this field through the current renewable energy act is not economically feasible. In Şırnak province, solar energy is utilized for heating water on residential rooftops via roof-installed solar panels (Eren et al., 2011). Figure 3 shows the annual solar energy distribution map of Şırnak Province.

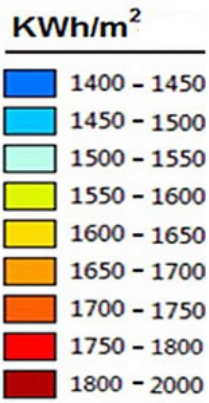

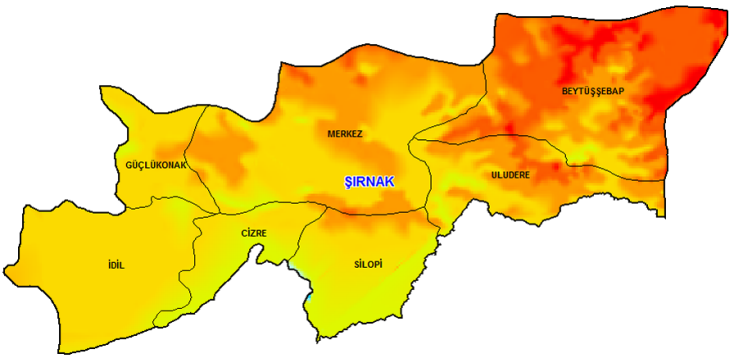

Figure 3: Annual Solar Energy Distribution Map of Şırnak Province.
Source: Energy Atlas, 2017b.

According to a report compiled by the Electrical Power Resources Survey and Development Administration, there are large areas available and convenient for solar installation in Şırnak Region, in addition to the fact that solar insolation in the region is quite high. In Şırnak, it is possible to implement solar-energy-powered cooling systems. The Southeastern Anatolian Project Administration now reviews pilot projects, in which the fields, where the feasibility studies that contain reduced costs can be converted into practice since in it estimated that such systems would be in high demand throughout the region. In this region, where agricultural activities are widespread, the use of renewable energy resources in agricultural fields can be realized via solar energy systems integrated into the greenhouse and drip irrigation systems. The monthly sunshine periods and the radiation values in Şırnak Province indicate that this region is suitable for the installation of high yield solar systems within Turkey. Table 3 lists the monthly sunshine periods in Şırnak Province and Turkey.

Table 3: Monthly Sunshine Periods in Şırnak Province and in Turkey

Sunrise Times		
Months	**Şırnak**	**Turkey**
January	4.32	4.11
February	5.52	5.22
March	6.65	6.27
April	7.61	7.46
May	9.87	9.10
June	12.12	10.81
July	12.42	11.31
August	11.67	10.70
September	9.90	9.23
October	7.38	6.87
November	5.86	5.15
December	4.50	3.75

Source: DİKA, 2010

It is clear from this table that the monthly sunshine duration in Şırnak Province is above the average value for Turkey. While the average annual sunshine duration in Turkey is 7.50 h, in Şırnak Province, it is 8.15 h. The lowest sunshine duration in Şırnak Province is 4.50 h in December and 4.32 h in January, while the highest sunshine duration is 12.12 h in June, 12.14 h in July, and 11.67 h in August. Table 4 shows the monthly radiation values for Turkey and Şırnak.

Table 4: Monthly Radiation Values of Turkey and Şırnak

Global Radiation Values		
Months	**Şırnak**	**Turkey**
January	1.95	1.79
February	2.63	2.50
March	4.14	3.87
April	5.12	4.93
May	6.29	6.14
June	6.78	6.57
July	6.73	6.50
August	5.93	5.81
September	5.10	4.81
October	3.74	3.46
November	2.44	2.14
December	1.81	1.59

Source: DİKA, 2010

From Table 4, it can be inferred that the radiation values in Şırnak Province are higher than the average for Turkey. While the average radiation value in Turkey is 4.18 (annual value), the average radiation value in Şırnak Province within a year is 4.39. The lowest values in Şırnak Province were measured in December and January, whereas the highest values were measured in May, June, July, and August. Considering the values in Tables 3 and 4, the estimated electrical energy that can be generated in a month by using a 1 kW fixed-angle crystal silicon PV panel in Şırnak is given in Table 5 (DIKA, 2010).

Table 5: Estimated Electrical Energy that can be Generated within a Month by Using a 1 Kw Fixed-Angle Crystal Silicon PV Panel in Şırnak

Monthly Total Electricity Production Values (kWh)	
Months	**Şırnak**
January	70.3
February	81.4
March	118
April	121
May	135
June	137

July	138
August	134
September	131
October	115
November	84
December	71.4
Toplam	1336.10

Source: DİKA, 2010

The values in Table 5 show that the electricity production using a 1 kW solar panel is possible during almost all months. In addition, calculations show that peak electric production months are May, June, July, August, and September. Because the temperature during the indicated months is very high in Şırnak Province (over 40 °C), the population in this region generally use air-conditioning units for cooling. This leads to increased power consumption during the indicated months. Similarly, people in the region use electric heaters to meet their heating needs in winter months, in addition to coal-fueled radiators and stoves. Dense smog with high sulfur content (%S) generated by intense asphaltite burning is mixed with air. In addition to increased electricity consumption, this leads to heavy air pollution during the winter months. It is projected that meeting this spike in the energy consumption during the winter and summer months with solar energy is the right choice in terms of the production-consumption balance and prevention of air pollution. However, despite the very high potential for solar energy in the region, this potential is underutilized and solar energy is used just for heating water. By using PV solar energy systems, residential electricity needs can be met in addition to water heating needs. Figure 4 shows a schematic of electricity generation in a sample residence using a PV system.

Figure 4: Example of Electricity Generation in a Residence Using a PV System.

Source:GüneşEnerjisi, 2017.

It can be said that the PV part of the solar energy system is the heart of the entire system. The solar module comprises several separate PV cells connected in series or parallel. The number of cells in a solar module and the arrangement of these cells affect the energy produced. It is possible to adjust the cells in the module to produce a certain voltage and current to meet specific electrical needs (Rehman et al., 2007).

If the electricity requirement of a residence is to be met partially, the generated energy is fed into the main grid and in cases where sufficient energy is not produced, electricity is received from the grid. In such a system, there is no need to store energy. Only conversion of DC electricity to ensure compatibility with the grid is required (EIE, 2017). To satisfy all energy needs of a building, the electricity produced during the day is consumed and the excess amount is stored in batteries. During the night, electricity demand is supplied using the energy stored in the batteries. Standalone systems that are designed to supply the entire electricity demand have higher installation costs because such systems require additional consumable materials and more powerful systems (GüneşEnerjisi, 2017). However, as a greater number of the indicated systems are installed, the general energy needs of Şırnak Province can be met with environment-friendly and renewable solar energy instead of fossil fuels, and the high installation costs of such systems will be offset in the future, and any investment will generate a profit in the long term.

5. Conclusion

The rapid increase in population worldwide has created societies, namely, consumer societies, that consume more than they produce. To meet the demands of such consumer societies, companies produce intensely while aiming to increase their earnings. However, in doing so, these companies do not consider the effects of such rampant production on human health or on the ecological balance. Factors such as the scarcity of raw materials and damage to the environment due to manufacturing waste have gradually started to come into focus. Thus, conscious consumers have forced companies to review their manufacturing processes. Companies are increasingly trying to benefit from renewable energy sources such as solar energy systems. Although the initial cost of a solar energy system that can produce electricity is high, it must be noted that producing electricity using imported fossil fuels is expensive as well, and it makes people in a region dependent on regions exporting such fuels. Thanks to the technological advancements, the cost of producing electricity from solar irradiation is decreasing by the day.

PV modules are used for solar energy production. To ensure that PV panels are cost-effective from the viewpoint of electricity production (meaning economical), additional systems can be integrated into PV panels systems to increase the yield of PV panels, such that the break-even point is reached earlier than it would without such an integration. This can further lower the overall cost of the PV panels. The most important systems that may increase the yield of PV panels are sun-tracking solar tracking systems and air-conditioning systems. Although air-conditioning systems may only provide a small

boost in terms of the yield of the PV panels, they can be preferred depending on the location and case. However, PV panels should be directed to track the Sun throughout the day by means of sun trackers to optimize the use of solar energy (Cengiz and Mamiş, 2016).

The most important parameters to be considered in the design of solar-powered thermal power plants are the selection of location, evaluation of solar energy and climate, and optimization of the parameters. When choosing an ideal spot for the plant, factors such as low annual rainfall, open and fogless atmosphere, low air pollution, distance from woodlands and groves, and low wind speed are important. The region in which the plant would be installed should have at least 2,000 hours/year of sunshine and should have a solar insolation value of at least 1.500 kWh/m^2/year. In addition, the number of days with 4 h of sunshine should not be less than 150 per year (EIE, 2017).

It is estimated that the cost of producing electricity will decrease significantly when a solar energy system is built by considering the aforementioned parameters. Today, companies, within the scope of the environmental social responsibility, have started planning their manufacturing activities in a way that would not harm the environment. However, there is still a long way ahead for companies in this regard. In addition, companies that undertake environmental activities need to announce such efforts to people through promotional activities. These companies impact the behavior of consumers, and they can ensure that consumers who are aware of environmental problems show consumption-oriented behaviors that are protective of the environment (Ece and Ergeneli, 2015). It will not be sufficient for companies that are active in the energy business to invest in solar energy systems in Şırnak Region to generate electricity from solar power. This new system should be adopted by the people in the region, and installation of the indicated system and its use to meet the electric needs of residences should come from the people as well. For this, first, the companies should inform people about the harmful effects of asphaltite ore on both human health and on the environment when it is directly burned. It should also be shown that although the installation of a system that can produce electricity from solar energy is costly, it is healthier and efficient. As indicated above, it should be noted that companies play significant roles in influencing the consumption behavior and decisions of individuals.

References

1. Akbulut, U., Kıncay, O., and Köşker, F.,(2006).GüneşEnerjisinin KapalıOlimpik YüzmeHavuzlarındaKullanımı. TesisatMühendisliğiDergisi. 96, 11–20.

2. Atay, Ü.,Işıker, Y., and Yeşilata, B.,(2009).Fotovoltaik Güç Destekli Mikro Sulama Sistemi Projesi-1: GenelEsaslar, V. Renewable Energy Resources Symposium. YEKSEM' 2009. June 19–21, 2009. Diyarbakır, Turkey.

3. Aydınol, M. and Aslan, T.,(2009).GüneşBacası Yardımıyla Labaratuar ŞartlarındaElektrikÜretimi (Model Çalışma), V. Renewable Energy Resources Symposium.YEKSEM' 2009. June 19–21, 2009. Diyarbakır, Turkey.

4. Bilgin, O. and Kantarcı, S.,(2015).Şırnak Asfaltitlerinin Önemi. 24. International Mining Congress and Exhibition.Imcet2015. April 14–17, 2015. Antalya, Turkey.

5. Cengiz, M.S. and Mamiş, M.S.,(2016).Termal Güneş Enerjisi KullanımıveCsp Sistemlerin Verimlilik Analizi.BEÜ Fen BilimleriDergisi.5, 1–13.

6. DIKA.(2010) Diclebölgesi (TRC3) enerjiraporu.http://www.dika.org.tr/photos/files/enerji_raporu.pdf (Accessed December 1, 2017.

7. DPT. (2007) Dokuzuncukalkınmaplanı: Madencilik. file:///C:/Users/Konti/Downloads/oik690%20(2).pdf. (Accessed November 2, 2017).

8. Ece, S. and Ergeneli, A.,(2015). The Effect of Individuals' Perceptions Toward Firms' Environmental Social Responsibility Activities on Pro-Environmental Behavior.3rd International Academic Conference in Paris.IACP.August 10–11, 2015. Paris, France.

9. EIE.(2017) Güneşenerjisiveteknolojileri. http://www.eie.g.,ov.tr/yenilenebilir/g_enj_tekno.aspx (Accessed December 1, 2017).

10. Enerji.(2017a) Elektrik.http://www.enerji.gov.tr/tr-TR/Sayfalar/Elektrik (Accessed December 1, 2017).

11. Enerji.(2017b) Elektrik.http://www.enerji.gov.tr/tr-TR/Sayfalar/Gunes (Accessed December 1, 2017).

12. Eren, C., Uçar, S., and Yıldırım, M. (2011) Şırnakiliçevre durum raporu. http://www.csb.gov.tr/db/ced/editordosya/sirnak_icdr2011.pdf. (Accessed December 10, 2017).

13. Ersöz, M.A. and Yıldız, A., 2013.Isı BoruluVakumTüpGüneşKollektörlerinde Optimum BoruÇapınınBelirlenmesi.TesisatMühendisliği. 5, 5–17.

14. Gündoğdu, C.,(2009). Determine the Properties of Asphaltite Asphalt and Compare with Refinery Asphalt. Unpublished M.SC.thesis. KaradenizTeknikÜniversitesi,Trabzon, Turkey.

15. GüneşEnerjisi. (2017) Shunt technologies. http://www.shunttech.com/binalarda-gunes-enerjisi-nasil-kullanilir/. (Accessed December 10, 2017).

16. Koç, E. and Şenel, MC.,(2013).DünyadaveTürkiye'deEnerjiDurumu. MühendisveMakina. 54, 32–44.

17. Lewis, N.S. and Crabtree, G. (2005) Basic research needs for solar energy utilization. [online] Report of the basic energy sciences workshop on solar energy utilization, Office of Sciences, April 18–21, 2005, Maryland.

18. Lewis, N.S., 2007.Toward Cost-Effective Solar Energy Use.Science. 315, 798–801.

19. MMO. (2012) Türkiye'ninenerjigörünümü. http://www1.mmo.org.tr/resimler/dosya_ekler/dd924b618b4d692_ek.pdf. (Accessed November 1, 2017).

20. Orhun, F., (1969). Güneydoğu Türkiye'deki Asfaltik Maddelerin Özellikleri, Metamorfoz Dereceleri Ve Klasifikasyon Problemleri. Maden Tetkik ve Arama Enstitüsü Dergisi.72,146–158.

21. Rehman, S., Bader, M. A., and Al-Moallem, S. A.,(2007). Cost of Solar Energy Generated Using PV Panels.Renewable and Sustainable Energy Reviews. 11, 1843–1857.

22. Sezer, M.K., (2007).Şırnak-SilopiAsfaltitiilePolietileninEşpirolizivePirolizÜrünleri ninDeğerlendirilmesiPublished PhD. thesis.Ankara Üniversitesi, Ankara, Turkey.

23. TKI.(2013) Yıllıkfaaliyet raporu. http://www.tki.gov.tr/depo/2017/2012 yillikfaaliyetraporu.pdf. (Accessed November 2, 2017).

24. Türkmen, E., Kurban, M., and Filik, Ü. B.,(2009).Güneş Bacalarıve Türkiye'de Kullananılabilirliği. V. Renewable Energy Resources Symposium. YEKSEM'2009. June 19–21, 2009. Diyarbakır, Turkey.

25. Uçgül, İ. and Ergün, E., (2012).DoğrusalFresnel GüneşGüçSistemi. SüleymanDemirelÜniversitesiYekarum E-Dergi. 1, 11–17.

26. Varınca, K. B. and Gönüllü, M. T., (2006).Türkiye'deGüneşEnerjisiPotansiyelive Bu PotansiyelinKullanımDerecesi, YöntemiveYaygınlığıÜzerinebirAraştırma. I. National Solar and Hydrogen Energy Congress. UGHEK'2006.June 21–23, 2006. Eskişehir, Turkey.

27. Viebahn, L., Yolanda, P., and Trieb, F., (2011). The Potential Role of Concentrated Solar Power (CSP) in Africa and Europe—ADynamic Assessment of Technology Development, Cost Development and Life Cycle Inventories until 2050.Energy Policy.8, 4420–4430.

CHAPTER 7

QUADRATIC SURFACE FITTING WITH ORTHOGONAL DISTANCES

Sebahattin BEKTAŞ

Introduction

A second-order algebraic surface given by the general equation

$$a x^2 + b y^2 + c z^2 + 2 f y z + 2 g z x + 2 h x y + 2 p x + 2 q y + 2 r z + d = 0.$$

Quadratic surfaces are also called quadrics, and there are 17 standard-form types. A quadratic surface intersects every plane in a (proper or degenerate) conic section. In addition, the cone consisting of all tangents from a fixed point to a quadratic surface cuts every plane in a conic section, and the points of contact of this cone with the surface form a conic section (Hilbert and Cohn-Vossen 1999, p. 12).

Examples of quadratic surfaces include the cone, cylinder, ellipsoid, elliptic cone, elliptic cylinder, elliptic hyperboloid, elliptic paraboloid, hyperbolic cylinder, hyperbolic paraboloid, paraboloid, sphere, and spheroid.

In this chapter, In this section, we will perform quadratic surface fitting through the ellipsoid, which is a very large area of application. we present techniques for fitting which are based on minimizing the sum of the squares of the geometric distances between the data and the quadratic surface. The literature often uses “orthogonal fitting” in place of “geometric fitting” or “best-fit”. For many different purposes, the best-fit ellipsoid fitting to a set of points is required. The problem of fitting ellipsoid is encountered frequently in theimage processing, face recognition, computer games, geodesy etc. Today, increasing GPS and satellite measurements precision will allow usto determine amore realistic Earth ellipsoid. Several studies have shown that the Earth, other planets, natural satellites, asteroids and comets can be modeled as triaxial ellipsoids Burša and Šima (1980), Iz et al (2011). Determining the reference ellipsoid for the Earth is an important ellipsoid fitting application, because all geodetic calculations are performed on the reference ellipsoid. Algebraic fitting methods solve the linear least squares (LS) problem, and are relatively straightforward and fast. Fitting orthogonal ellipsoid is a difficult issue. Usually, it is impossible to reach a solution with classic LS algorithms. Because they are often faced with the problem of convergence. Therefore, it is necessary to use special algorithms e.g. nonlinear least square algorithms. We propose to use geometric fitting as opposed to algebraic fitting. This is computationally more intensive, but it provides scope for placing visually apparent constraints on ellipsoid parameter estimation and is free from curvature bias Ray and Srivastava (2008).

Fitting an ellipsoid to an arbitrary set of points is a problem of fundamental importance in many wide fields of applied science ranging from astronomy, geodesy, digital image processing and robotics to metrology etc. Ellipsoids, though a bit simple in representing 3D shapes in general, are the only bounded and centric quadrics that can provide information of center and orientation of an object. Fitting ellipsoid has been discussed widely and some excellent work has been done in literature. However, most of these fitting techniques are algebraic fitting, but not orthogonal fitting. Various "least- squares" fitting approaches have been formulated over the years Zhang (1997), but they all fall into two categories; (1) algebraic methods, which are extensively used due to their linear nature, simplicity and computationally efficiency, and (2) geometric methods that solve a nonlinear problemRay and Srivastava (2008).

We could not find enough studies with numerical examples in the literature. Turner et al(1999) gave a numerical application, but the application's data are not given.No other comparable orthogonal fitting ellipsoid application could be found in literature. Against this background, the purpose of the study is to give an orthogonal fitting ellipsoid with numerical examples. In this article, we demonstrate that the geometric fitting approach, provides a more robust alternative than algebraic fitting approach-although it is computationally more intensive.

This chapter has eight parts. First, the basic ellipsoid will introduce some mathematical equationsto explainthe concepts. Then, it reviews the extended literature relevant to ellipsoid fitting. And we discussed in this research which estimators is used. Next, comes the part which deals with algebraic fitting, orthogonal fitting and numerical example. You will find ellipsoid fitting application based on both *l_1-norm* and *l_2-norm* methods. The paper concludes with a discussion of theoretical and managerial implications and directions for further research.

1.1 Ellipsoid

An ellipsoid is a closed quadric surface that is analogue of an ellipse. Ellipsoid has three different axes ($a_X > a_Y > b$) in Figure 1. Mathematical literature often uses "ellipsoid" in place of "Triaxial ellipsoid or General ellipsoid". Scientific literature (particularly geodesy) often uses "ellipsoid" in place of "biaxial ellipsoid, rotational ellipsoid or ellipsoid revolution". Older literature uses 'spheroid' in place of rotational ellipsoid. The standard equation of an ellipsoid centered at the origin of a Cartesian coordinate system and aligned with the axes is shown with this formula:

$$\frac{x^2}{a_x^2}+\frac{y^2}{a_y^2}+\frac{z^2}{b^2}=1 \qquad (1)$$

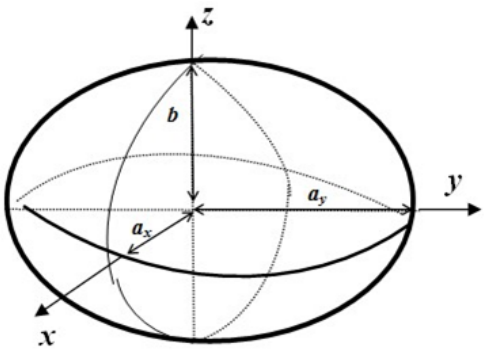

Figure 1: Ellipsoid

Although ellipsoid equation is quite simple and smooth, computations are quite difficult on the ellipsoid. The main reason for this difficulty is the lack of symmetry. Generally, an ellipsoid is defined with 9 parameters. These parameters are; 3 coordinates of center (X_0,Y_0,Z_0), 3 semi-axes (a_x, a_y, b) and 3 rotational angles (ε,,ω) which represent rotations around x-,y- and z- axes respectively in Figure 2. These angles control the orientation of the ellipsoid.

R_1,R_2,$R_3$are plane rotation matrices

$$\underline{R}_1(\varepsilon)=\begin{bmatrix}1 & 0 & 0\\ 0 & \cos\varepsilon & \sin\varepsilon\\ 0 & -\sin\varepsilon & \cos\varepsilon\end{bmatrix},\ \underline{R}_2(\psi)=\begin{bmatrix}\cos\psi & 0 & -\sin\psi\\ 0 & 1 & 0\\ \sin\psi & 0 & \cos\psi\end{bmatrix},\ \underline{R}_3(\omega)=\begin{bmatrix}\cos\omega & \sin\omega & 0\\ -\sin\omega & \cos\omega & 0\\ 0 & 0 & 1\end{bmatrix} \quad (2)$$

R-rotation matrix is obtained from R_1,R_2,$R_3$by multiplying the reverse order

$$\underline{R}=\underline{R}_3(\omega)\underline{R}_2(\psi)\underline{R}_1(\varepsilon)$$

$$\underline{R}=\begin{bmatrix}\cos\psi\cos\omega & \cos\varepsilon\sin\omega+\sin\varepsilon\sin\psi\cos\omega & \sin\varepsilon\sin\omega-\cos\varepsilon\sin\psi\cos\omega\\ -\cos\psi\sin\omega & \cos\varepsilon\cos\omega-\sin\varepsilon\sin\psi\sin\omega & \sin\varepsilon\cos\omega+\cos\varepsilon\sin\psi\sin\omega\\ \sin\psi & -\sin\varepsilon\cos\psi & \cos\varepsilon\cos\psi\end{bmatrix} \quad (3)$$

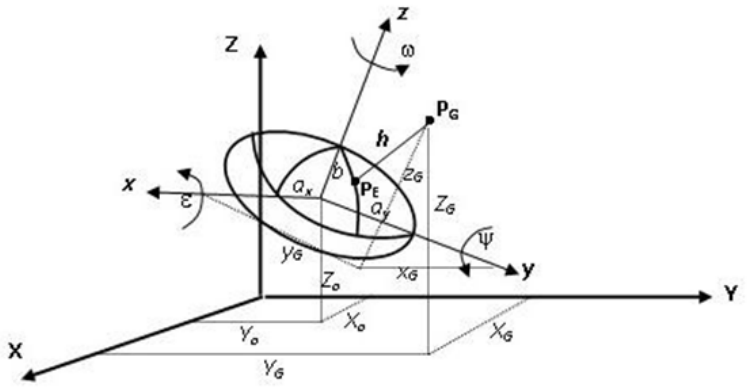

Figure 2: Shifted - oriented ellipsoid

FittingEllipsoid

For the solution of the fitting problem, the linear or linearized relationship, written between the given data points and unknown parameters (one equation per data points), consists of equations, including unknown parameters.

Here, *A* is design matrix, *x* is unknown parameters, *l*is measurements vector or data points, For this minimization problem to have a unique solution the necessary conditions is to be *n*>=

9 and the data points lie in general position (e.g., not all data points should lie is an elliptic plane). Throughout this paper, we assume that these conditions are satisfied.

u=9 : number of unknown parameter

n: number of given data point (or measurements)

f=*n*-*u* :degree of freedom

-If *f*= 0 there is only one (exact) solution, algebraic solution

-If *f*<0 there is no solution. The solutioncan be found with based on the extra constraint

-If *f*> 0 is most commonly encountered situation. The given data points (or measurements), which are much greater than the required number cause discrepancy, and in this case, the solution is not unique. There is an over determined system. Because *n* > *u*, in other words the number of equations is greater than the number of unknowns.

The system of linear equations (3) must be solved. Therefore, this system must be consistent with the rang of design matrix, and design matrix extended with constant terms, must be equal, so that *rang(A) =rang(A:l)*; whereas, the system of (3) is inconsistent, because *x* unknown parameters that provide (3), can not be calculated. In this case, *rang(A) ≤ u*. The extended matrix with *l* measurements *rang(A:l)* is generally more than *rang(A)* . There is no solution of inconsistent equations, and only the approximate solution of the system can be derived. The equation system with approximate solution is calculated by adding residuals (or corrections) at the right side of (4).

$$A_{n,u} \,.\, \delta x_u = l_n + \varepsilon_n \qquad (5)$$

Depending on the choice of residuals vector, infinite solutions can be obtained. The unique solution can be derived only according to an estimator (objective function). For example, the

LS always give an unique solution Bektas and Sisman (2010). Here, the question of which estimation method to use comes to mind?

3.Which Estimator Should Be Used?

It is hoped that the residuals will be small. The more suitable estimation method is one that creates smaller residuals. It is seen that usually the objective functions are formed based on the minimization of corrections or a function of corrections. There are numerous estimators, some of these are l_1-norm, l_2-norm,l_p-norm, Fair, Huber, Cauchy, German-McClure, Welsch and Tukey. Two estimator methods come to the forefront.The most used estimators are shown below:

(i) [εε] = min..(l2-norm) Least Squares Method (LSM)

Squares Method (LSM)

(ii) [Iε I] = min.(l1-norm) LeastAbsolute Values Method (LAVM).

3.1. The Comparison of l_1 andl_2-Norm Methods

The solution of the l_2-norm method is always unique, and this solution is easily calculated. The l_2-norm method is widely used in parameters estimation. The l_2-norm method has indisputable superiority in parameter estimation.

The disadvantages of the l_2-norm method are that is affected by outlying (gross errors) and it distributes to the sensitivity measurements. In this case, ellipsoid fitting is a very nice application.

With least-squares techniques, even one or two outliers in a large set can wreak havoc! Outlying data give an effect so strong in the minimization that the parameters thus estimated by those outlying data are distorted. Nu-

merous studies have been conducted, which clearly show that least-squares estimators are vulnerable to the violation of these assumptions. Sometimes, even when the data contains only one bad measurement, l_2-norm method estimates may be completely perturbed Zhang (1997).

The solution of the l_1-norm method is not always unique, and there may be several solutions. Also, the solution of the l_1-norm method is not generally obtained directly, but iteratively calculations are made. Therefore, the solution is not easily calculated like in the l_2-norm method. Notwithstanding, when the computational tools, computer capacity and speed are considered, the difficulty of calculations are eliminated. The advantages of the l_1-norm method are non-sensitivity against measurements, including gross errors, and the solution is not or is little affected by these measurements.

The author of this study proposed and used the l_2-norm method in the solution of parameter estimation (optimization problems, adjustment calculus), after the measurement group cleaned up gross and systematic errors using the l_1-norm method. For further information see Bektas and Sisman (2010).

4.AlgebraicEllipsoidFittingMethods

The general equation of an ellipsoid is given as

$$A'x^2 + B'y^2 + C'z^2 + 2D'xy + 2E'xz + 2F'yz + 2G'x + 2H'y + 2I'z + K' = 0 \quad (6)$$

(5) contains ten parameters. In fact, nine of those ten parameters are independent. For example, if all the coefficients in this equation multiply by (-1/K'), we get a new equation which contains nine unknown parameters, and its constant term will be equal to "-1".

$$Ax^2 + By^2 + Cz^2 + 2Dxy + 2Exz + 2Fyz + 2Gx + 2Hy + 2Iz - 1 = 0 \quad (7)$$

In this algorithm, we need to check whether a fitted shape is an ellipsoid. In theory, the conditions that ensure a quadratic surface to be an ellipsoid have been well investigated and explicitly stated in analytic geometry textbooks. An ellipsoid can be degenerated into other kinds of elliptic quadrics, such as an elliptic paraboloid. Therefore, a proper constraint must be added. Li and Griffiths gave the following definitions Li and Griffiths (2004).

$$i = A + B + C \quad (8)$$

$$j = AB + BC + AC - F^2 - E^2 - D^2 \quad (9)$$

However $4j - i^2 > 0$ is just a sufficient condition to guarantee that an equation of second degree in three variables represent an ellipsoid, but it is not necessary. In this paper, we assume that these conditions are satisfied.

The algebraic method is a linear problem. It is solving the problem directly and easily. The fitting ellipsoid to a given the data set ($(x,y,z)_i$, $i=1,2,...,n$), is obtained by the solution in the LS sense of in the following:

$$\Omega.v = l \qquad (10)$$

Where

nxu= Design matrix

$v_u = [A\ B\ C\ D\ E\ F\ G\ H\ I]^T$ unknown conic parameters

$l_n = [1\ \ 1\ \ 1\ldots1]^T$ unit vector : right side vector ith row of the nx9 matrix

$$[x_i^2\ \ y_i^2\ \ z_i^2\ \ 2x_iy_i\ \ 2x_iz_i\ \ 2y_iz_i\ \ 2x_i\ \ 2y_i\ \ 2z_i] \qquad (11)$$

It is solved easily in the LS sense as below or

$$v=(\Omega^T\Omega)^{-1}\Omega^T l \qquad (12)$$

it is solved easily by MATLAB as below

$$v=[x.^2\ \ y.^2\ \ z.^2\ \ 2x.*y.2x.*z.2y.*z.\ \ 2*x\ \ 2*y\ \ 2*z]\backslash ones(n) \qquad (13)$$

If there are differences in weights or correlations between given data points, P weight matrix is added in the solution, and then

K_{ll}:nx$n$variance-covariance matrix of data points

Residual (or correction) vector is computed as below

$$\varepsilon=[x.^2\ \ y.^2\ \ z.^2\ \ 2x.y.\ \ 2x.z.2y.z.\ \ 2x.2y.\ \ 2z.]\ .\ v\ -ones(n) \qquad (15)$$

LSoptimization give us

$[I\varepsilon I]$ = min.

Algebraic methods all have indisputable advantages of solving linear LS problems. Themethods for this are well known and fast. However, it is

intuitively unclear what it is we are minimizing geometrically in (6) is often referred to as the "algebraic distance" to be minimized Ray and Srivastava (2008). A geometric interpretation given by Bookstein (1979) clearly demonstrates that algebraic methods neglect points far from the center.

5.FittingOfEllipsoidUsingOrthogonal Distances

To overcome the problems with the algebraic distances, it is natural to replace them by the orthogonal distances which are invariant to transformations in Euclidean space and which do not exhibit the high curvature bias. An ellipsoid of best fit in the LS sense to the given data points can be found by minimizing the sum of the squares of the geometric distances from the data to the ellipsoid. The geometric distance is defined to be the distance between a data point and its closest point on the ellipsoid.

Determining best fit ellipsoid is a nonlinear least squares problem which in principle can be solved by using theLevenberg-Marquardt (LM)algorithm. Generally, non-linear least squares is a complicated issue. It is very difficult to develop methods which can find the global minimizer with certainty in this situation. When a local minimizer has been discovered, we do not know whether it is a global minimizer or one of the local minimizer Zisserman (2013). There are a variety of nonlinear optimization techniques. Such as Newton, Gauss-Newton, Gradient Descent, Levenberg-Marquardt approximation etc.However, these fitting techniques involve a highly nonlinear optimization procedure, which often stops at a local minimum and cannot guarantee an optimal solution Li and Griffiths (2004).

Away from the minimum, in regions of negative curvature, the Gauss-Newton approximation is not very good. In such regions, a simple steepest-descent step is probably the best plan. The Levenberg-Marquardt method is a mechanism for varying between steepest-descent and Gauss-Newton steps depending on how good the H_{GN} approximation is locally.

The Levenberg-Marquardt method uses the modified Hessian

$$H(x,\lambda) = H_{GN} + \lambda.I$$

(I : identity matrix))

- • When λ is small, H approximates the Gauss-Newton Hessian.
- • When λ is large, H is close to the identity, causing steepest-descent steps to be taken.

This algorithm does not require explicit line searches. More iterations than Gauss-Newton, but, no line search required, and more frequently converge suppose that we have a unknowns parameter set

$v = [A\ B\ C\ D\ E\ F\ G\ H\ I]^T$ are unknown conic parameters. The general conic equation for an ellipsoid is given as (6)

We will reach the solution by establishing relationships between variations in the conical coefficients and the orthogonal distances.

The initial parameters were derived from the algebraic fitting ellipsoid.

Projection coordinates (onto ellipsoid) of given $P_i$data points

$dv = 2.K.[D \quad B \quad F \quad H]^T$: ∂ / ∂ y partial derivative with respect to y- coor.(17)

$dw = 2.K.[E \quad F \quad C \quad I]^T$: ∂ / ∂ z partial derivative with respect to z- coor.(18)

*i*th row of the *n*x10 matrix *J* (jakobien matrix)

$$(1/e)\,[x_i^2 \quad y_i^2 \quad z_i^2 \quad 2x_i y_i \quad 2x_i z_i \quad 2y_i z_i \quad 2x_i \quad 2y_i \quad 2z_i \quad -1] \qquad (20)$$

*i*th row of the right side vector h_{nx1}

$$h_i = sign(z_i^e - z_i)\,sign(z_i^e)\sqrt{(x_i^e - x_i)^2 + (y_i^e - y_i)^2 + (z_i^e - z_i)^2} \qquad (21)$$

We obtained the below linearized equation

$$J_{nx10}.\,dv_{nx1} = h_{nx1} \qquad (22)$$

$$dv = [\,dA \quad dB \quad dC\,dD\,dE\,dF\,dG\,dH\,dI\,]^T \qquad (23)$$

The fitted orthogonal ellipsoid is obtained by the solution in the LS sense with the L-M

algorithm.

5.1 The Levenberg-Marquardt Algorithm

1-Solve algebraic methods and find initial values for *v set* $\lambda = 1$ *(say)*

2- Compute *J*-jacobien matrix and $h_i$orthogonal distances from all given data points

$$minh = h^T h$$

3-Solve $(J^T J + \lambda\, I)\, dv = J^T h$ $v = v + dv$, new conic parameter

Find again$h_i$orthogonal distances from all given data points

$newh = h^T h$

4- ifnewh<minh % yes there is improvement, reduce λ

minh=newh; λ=λ/2

goto 3

else % no improvement, increase λ

*λ=2*λ*

goto3

end

5.2. Finding Orthogonal Distances from the Ellipsoid

In this paper, we present techniques for ellipsoid fitting which are based on minimizing the sum of the squares of the geometric distances between the data and the ellipsoid. The most time-consuming part is the computation of the orthogonal distances between each point and the ellipsoid. Our aim to find the orthogonal distances from a shifted-oriented ellipsoid see Figure 2. For detailed information on this subject refer to Bektas (2014).

6.NumericalExample

For numerical applications 12 triplets (x,y,z) Cartesian coordinates were produced. Here data points coordinates,

x: [7 7 9 9 11 11 8 8 10 10 12 12]

y: [22 19 23 19 24 20 21 17 22 18 23 19]

z: [31 28 31 27 29 26 32 29 32 28 31 28]

The conical coefficients in the Least Squares Method is,

v=[-0.0006 -0.0008 -0.0010 0.0005 -0.0005 0.0003 0.0092 0.0050 0.0278]

Algebraic fitting results are as below

Ellipsoid center: 10.384 20.965 29.007

Ellipsoid radii: 7.4676 3.1643 2.0147

RSS=0.216

Orthogonal fitting results are as below.

Ellipsoid center: 11.7833 21.6933 28.4934

Ellipsoid radii : 11.1839 3.3463 1.7893

RSS=0.189

*RSS: The residual sum of squares of the orthogonal distances

7.Discussion

Orthogonal least-squares has a much sounder basis, but is usually difficult to implement. Why are algebraic distances usually not satisfactory? The big advantage of use of algebraic distances is the gain in computational efficiency, because closed-form solutions can usually be obtained. In general, however, the results are not satisfactory.The function to minimize is usually not invariant under Euclidean transformations. For example, the function with normalization K' = -1 in (5) is not invariant with respect to translations. This is a feature we dislike, because we usually do not know in practice where the best coordinate system to represent the data is. A point may contribute differently to the parameter estimation depending on its position on the conic. If a priori all points are corrupted by the same amountof noise, it is desirable for them to contribute the same way Zhang (1997). More importantly, algebraic methods have an inherent curvature bias – data corrupted by the same amount of noise will misfit unequally at different curvatures Ray and Srivastava (2008). Our experience tells us that if the coordinates of given points consists of a large number this will cause bad condition. Therefore, before fitting, you must shift the given coordinates to the center of gravity, after fitting operation the coordinates of ellipsoid's center must be shifted back to the previous position.

8.Conclusion

In this section, we discussed the ellipsoid's orthogonal fitting from quadratic surfaces. The problem offitting ellipsoid is encounteredfrequently intheimage processing, face recognition, computer games, geodesy- determiningmore realistic Earth ellipsoid etc. The paper has presented a new method of orthogonal fitting ellipsoid. The new method relies on solving an over determined system of nonlinear equations with the use of the L-M method. In conclusion, the presented method may be considered as fast, accurate and reliable and may be successfully used in other areas. The presented orthogonal fitting algorithm can be applied easily to biaxial ellipsoid, sphere and also other surfaces such as paraboloid, hyperboloid,etc.

References

1. Bektas, S., Sisman, Y. The comparison of L1 and L2-norm minimization methods,
2. International Journal of the Physical Sciences, 5(11), 1721 – 1727, 2010
3. Bektas, S. "Orthogonal Distance From An Ellipsoid, Boletim de CienciasGeodesicas, Vol. 20, No. 4 ISSN 1982-2170 , http://dx.doi.org/10.1590/S1982-21702014000400053 (in Press), 2014
4. Bektaş,S. ,**Shortest Distance From A Point To Triaxial Ellipsoid**, International Journal of Engineering and Applied sciences pp 22 - 26 Vol 04. No. 11 , 2014

5. Bookstein, F. L. Fitting conic sections to scattered data", Computer Graphics and Image Processing 9,56-71, 1979.

6. Burša M, Šima Z. Tri-axiality of the Earth, the Moon and Mars, Stud. Geoph. etGeod. 24(3):211–217, 980.

7. Eberly, D. Least Squares Fitting of Data", Geometric Tools, LLC, http://www.geometrictools.com, 2008.

8. Feltens, J. Vector method to compute the Cartesian (X, Y ,Z) to geodetic (, λ, h) transformation on a triaxial ellipsoid", Journal of Geod. 83:129–137, 2009.

9. Hilbert and Cohn-Vossen 1999.Geometry and the Imagination (AMS Chelsea Pub…(Hardcover) by David Hilbert, S. Cohn-Vossen,1999

10. İz, H. B., Ding X. L., Dai C. L.,Shum C. K. Polyaxial figures of the Moon, J. Geod. Sci., 1, 348-354, 2011.

11. Li, Q., Griffiths J.G. Least Squares Ellipsoid Specific Fitting, Proceedings of the Geometric

12. Modelling and Processing (GMP'04), 2004.

13. Ligas, M. Cartesian to geodetic coordinates conversion on a triaxial ellipsoid, Journal of Geod., 86, 249-256, 2012.

14. Ray, A., Srivastava D.C. Non-linear least squares ellipse fitting using the genetic algorithm with applications to strain analysis, Journal of Structural Geology 30 1593-1602. 2008.

15. Turner, D.A., Anderson I. J., Mason J.C., Cox, M.G.An algorithm for fitting an ellipsoid to data, Cite-dataseerXBeta, http://citeseerx.ist.psu.edu/viewdoc/summary?doi=10.1.1.36.2773, 1999.

16. Zhang, Z. Parameter estimation techniques: a tutorial with application to conic fitting, Image and Vision Computing 15,59-76, 1997.

17. XiangchaoZhang ,Xinnian Jiang, Paul Scott, Fitting data with quadric surfaces based on orthogonal distance regression,January 2010

18. Zisserman, A. C25 Optimization, 8 Lectures, Hilary Term 2013,2 Tutorial Sheets,Lectures 3- 6 (BK), 2013.

CHAPTER 8

THE NEW APPROACH FOR SWITCHING PERFORMANCE OF POWER MOSFET

Seyfettin GÜREL[1] , Sezai Alper TEKİN[2]

Introduction

In recent years, MOSFET have been popular in many areas when they are used in many applications for electronic applications from switching to amplification (Mc Arthur,2001). However, power MOSFET has also disadvantages because many parameters can affect MOSFET operation. These parameters are examined by scientists for specific applications in electronic circuits in the literature. In this study, body effect, frequency, slew rate, threshold voltage parameters are taken into consideration.

In order to turn on and turn off MOSFET, it is necessary to have minimum duration. This duration varies between the maximum and minimum values of duty ratio (k). Output voltage changes this duty ratio and load current's fluctuation is inversely proportional to switching frequency. For reducing fluctuation, the frequency should increase (Rashid, 2014).

Other parameter which changes output voltage is the slew rate. Slew rate expresses the maximum voltage change per unit time in a node of a circuit, due to limited current sink or source.Operational transconductance amplifiers (OTA) with high slew rate and large gain-bandwidth product (GBW) are necessary in this application (Zhao, 2018). This shows that there is an inversely proportional relation between switching speed and resistor (Slew Rate, 2018). The important parameter is threshold voltage (V_{TH}). This is the voltage which dominates current flow and it is formed by physical change (Siebel, 2012).

Another property which has the effect on MOSFET is body effect. The effect of body effect on a MOSFET's threshold voltage is expressed by Equation 1 (Kuntman, 2014).

$$V_{TH} = V_{T0} + \gamma \cdot [\sqrt{2\varphi_f - V_{SB}} - \sqrt{2\varphi_f}] \quad (1)$$

In Equation 1, γ is the factor of body effect, V_{T0} is the voltage when V_{SB} =0, Φ_F represents the change in the surface potential(Sedra, 2004).

1 Erciyes University, Department of EnergySystemsEngineering, Kayseri, TURKEY
2 Erciyes University, Department of Industrial Design Engineering, Kayseri, TURKEY

The scope of this working is to examine V_{BS} and V_{TH} voltages via Equation 1. As clearly seen in the equation, increasing with $V_{BS,}$ the value of V_{TH} decreases, and body effect will go up depending on this parameter. At the same time, drain current I_D will go down and R_D will be rising because of this fact (Ercan, 2015).

$t_{ir} = t_2 - t_1 = R \cdot C \cdot \ln\left(\frac{V_{GS}-V_{TH}}{V_{GS}-V_{GP}}\right)$ (2)

$t_{if} = R \cdot C \cdot \ln\left[\left(1+\frac{g_{fs}\cdot L_{src}}{R_D \cdot C_{iss}}\right)\cdot\frac{V_{GP}}{V_{TH}}\right]$ (3)

$C_{GS} = \frac{2}{3}\cdot W \cdot L \cdot C_{OX} \cdot \left(1-\frac{(V_{GD}-V_{TH})^2}{(V_{GD}+V_{GD}-2\cdot V_{TH}{}^2)}\right)$ (4)

$C_{GD} = \frac{2}{3}\cdot W \cdot L \cdot C_{OX} \cdot \left(1-\frac{(V_{GS}-V_{TH})^2}{(V_{GD}+V_{GD}-2\cdot V_{TH}{}^2)}\right)$ (5)

where C_{iss} *is* input capacitance, V_{GS} is gate-to-source voltage, V_{GP} is gate to plateu voltage, g_{fs} is transconductance, L_{src} is Inductance, V_{GD} isgate-to-drain voltage, V_{TH} is threshold voltage, Cox is oxide capacitance, W is width of the MOSFET channel and Lis the length of the MOSFET channel.

Methodology

Two circuit topologies are analyzed for determining power consumptions for these circuits which are illustrated Figure-1 and Figure-2 respectively.

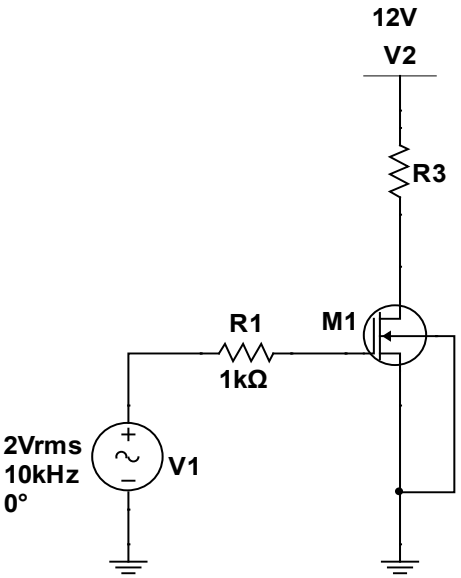

Figure-1. A Switching Circuit for Classical MOSFET

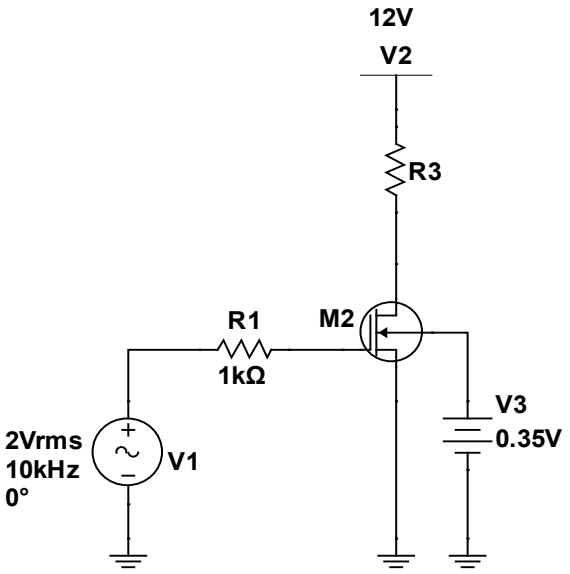

Figure-2.A SwitchingCircuitforClassical MOSFET withV_{th}=0.35V andR_2=1kΩ

For these separate circuit analogies, the time duration is increased, and the amount of power consumption is analyzed via SPICE.

After making simulations in simulation, Figure-3 can be seen for both power consumption and time duration of the two MOSFETs.

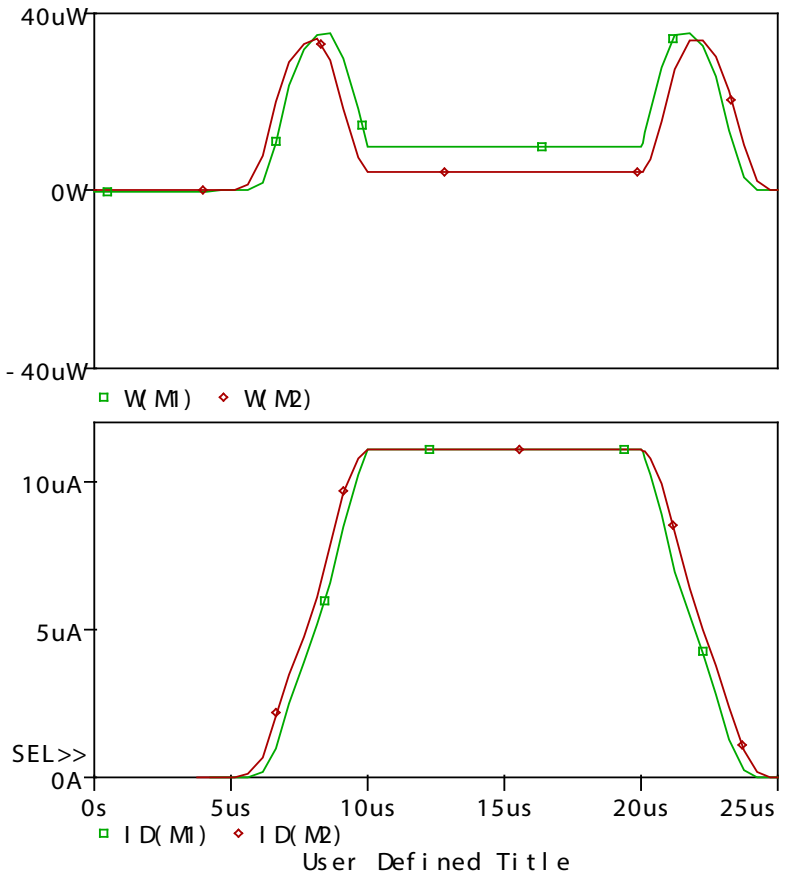

Figure-3. A plotfor time risingandfalling of MOSFETandpower

consumption of MOSFET

In addition to this, the rising and falling time of MOSFET is also drawn in simulation.

Figure-3 illustrates the drain currents of circuits in two case which are V_{th}=0 V and V_{th}=0.35 V. I_D (M1) is the drain current of classical switching circuit with V_{th}=0 V and I_D (M2) is the drain current of switching circuit with V_{th}=0.35 V and R_2=1kΩwith rising and falling times of MOSFETs. There is no change in R_2 between 100-1kΩ at this frequency. According to Equation 3, when V_{TH} increases, the rising time accelerates. Same phenomenon can be seen in Figure-4. This figure shows the power consumption of each circuit with V_{th}=0 V and V_th=0.35 V.

The power is reduced in rising time. In the falling time, threshold volt-

age is very high. Therefore, this problem may be solved by adaptive system to make threshold voltage zero(Feali,2018).In this structure, the falling time also shorten.

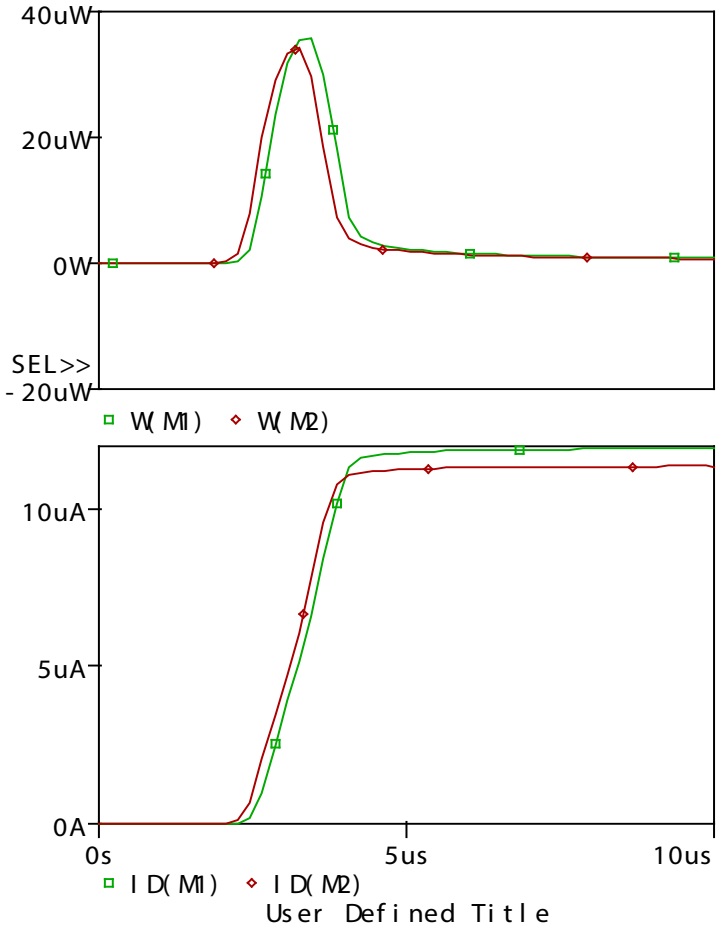

Figure-4. Therising time andpowerconsumption of MOSFET.

The alternative way to achieve low power consumption level can be used by Bi-directional MOSFETs in switching circuit which are already available commercially(Vishay,2009).

CONCLUSION

This study reveals that the time duration is related with the amount of power consumption. The power is reduced in rising time. In the falling time, threshold voltage is very high. Therefore, this problem may be solved by adaptive system to make threshold voltage zero.

Especially, it is controlled drain current of MOSFET with threshold voltage. This voltage is seen as 0.35 V and the resistor is 1kΩ. Simulations also validates theoretical approaches. This new approach can be used in DC-DC Converter design. Further workings may be carried out about the controlling the change in the falling time. In next studies, it will be used adaptive resistor and experimental workings will be done for this aim.

REFERENCES

1. Mc Arthur, R. (2001). Making use of Gate Charge Information in MOSFET and IGBT Data Sheets, Advanced Power Technology, Application Note APT0103 Rev-October 31.
2. Rashid M, H. (2014). Power Electronics, Devices, Circuits and Applications, 4th edition, pp.141.
3. Zhao, X., Wang, Y., Jai, D., Dong, L. (2018). Ultra-high current efficiency single-stage class-AB OTA with completely symmetric slew rate, International Journal of Electronics and Communications, 87, pp. 65-69.
4. Slew Rate (2018), http://www.onmyphd.com/?p=slew.rate.
5. Siebel, O. F., Schneider, M., C., Montoro-Galup, C. (2012). MOSFET threshold voltage: Definition, extraction, and some applications, Microelectronics Journal 43, pp. 329–336.
6. Kuntman, H. (2014). Analog Integrated Circuits Lecture Notes.
7. Ercan, H., Tekin, S. A., Alcı, M. (2015). "Low-voltage low-power multifunction current-controlled conveyor", International Journal of Electronics, Vol. 102, No. 3, pp. 444-461.
8. Sedra, A. S., Smith, Kenneth, C. (2004). Microelectronic Circuits, 5th edition, Oxford University Press,pp.258.
9. Bi-directional P-Channel MOSFET/Power Switch, Vishay Siliconix(2009), https://www.vishay.com/docs/70785/70785.pdf
10. Feali, M. S., Ahmadi, A., Hayati, M. (2018). Implementation of adaptive neuron based on memristor and memcapacitor emulators, Neurocomputing 000, pp. 1-11.

FACTORS AFFECTING ON PROFESSION CHOICE AND PROFESSION EXPECTATIONS OF ENVIRONMENTAL ENGINEERING STUDENTS

F.Füsun UYSAL[1] Müjgan YILMAZ[2] Esra TINMAZ KÖSE[1]

INTRODUCTION

Profession is defined as job and opinion field in which somebody contionously works or a job from which somebody earns his/her life. Profession is a continous job which requires a certain training and wants knowledge, skill, expertise and interest.

Profession is very important event in one person's life, a person in the period of chosing a profession selects a certain work environment,a certain life style and tries to prove hisself/herself in this chosen way by success. If a person selects profession in the direction of his/her skill,interest and wishes,he or she becomes successful,efficient and happy.If a person selects his/her profession randomly without bearing in mind,he/she becomes unhappy [1].

Selecting a profession consciously plays an important role in view of both person and country's future because a person selects a process which is going to form person's all life by making decision and also selects living environment and peopleconnected [2].

The education levels of citizens and human resource potentials also play an important role in social and economical improvements of countries.That's why, the selection of university and department is one of the most important decision steps of person and has quite important effect in person's future. Because of the fact that this step determines person's future profession,it must be seriously and carefully managed [3]

The profession selection step can be affected by many factors such as socio-demographic properties,work advantages,skilll and interest [4].

Instead of the only one criterion in profession selection, it is known that many criteria such as income advantages of profession,carrier possibility,job quaranteed key elements etc. are under consideration.Behaving rationalistically in profession selection can become true only by taking individuals'crite-

1 Department of Environmental Engineering, University of Namık Kemal, Çorlu/Tekirdağ, Türkiye

2 Department of Çerkezköy Vocational School, University of Namık Kemal, Çerkezköy/Tekirdağ, Türkiye

ria into consideration [2].

Individuals knowing of their interests and skills will seek an appropriate carrier to themselves actively [5].Besides it is known as a fact that family's economical and cultural levels affect young's profession both positevely and negatively.Resarch results show that youngs with high economical and social levels have a chance for selecting profession in the direction of skills and interests and can be supported by families.Youngs with lack of economical and cultural possibilities in families,are directed to jobs which bring great profits in a short time or bring honor [1].

Parents must realize themselves playing an important role in organizing carrier's journey of their children and independent carrier selections indicating first real step of a young person into adult.Parents must hold communication lines with their children open and must be as possible as supportive in bringing much information in carrier interest fields of their children [6].

Educational activities play an important role in training qualified man power in paralel to scientific developments.Higher education carrieers much more importance according to other institutions in view of providing information for profession.Environmental education has been given importance on the base of higher education all over the world from the point view of scientific and engineering solution of environmental problems which have started to become serious andto develop since 1970's [7].

Enviromental Engineering has started to be a seperate discipline,accepted all over the world,with the reasons of inreasing variety of environmental problems,the necessity of finding solution rapidly to new environmental problems and the complexity of environmental systems [8].

Environmental problems have started to be important with the reason of increasing industrialization and intensifying population in cities.Environmental eduaction has gained importance together with these problems and increasing investments in environmental sectors and the serious potential of employment have brought the requirement of qualified personnel.

METHOD

Data related with the method of descriptive research were given under the headlines of space and sampling, collection and analysis.

SPACE AND SAMPLING

The space of research covers 500 students at Environmental Engineering Departmet of Çorlu Engineering Faculty of Namık Kemal University.Because of the difficulty for reaching all of persons including the space of the research,determined values in the table proposed by Krejcie and Morgan related with the necessity of how much sample size taken against the size of space in researches in which evaluations are done according to proportions. Based on 233 samples proposed for 1000 space,233 persons were selected as sample from 500 space[9].

COLLECTION OF DATA

The survey was used as data colletion method in the research. In the preparation of the survey questions,the literature related with the research was looked over.Questions related with the subject,which will be improved,were collected in a question pool.By taking expert views,a scale was pepared by determining validity and reliability of questions in the question pool.

DATA ANALYSIS

Data,which are collected appropriate to the aim of the research,have been recorded in the electronic media by controlling. By analyzing data with SPSS 18.01(Statistical Package for the Social Sciences for Windows) statistical package program,frequency tables of variables were given with percentage values and chi-square statistical analysis was applied.

RESULTS

The distribution related with genders and ages of participants,education level of parents, incomes of families,attendant class in the faculty, type of graduated high school,taking suppport from university preparation courses,-placing in which entrance examination into environmental engineering department,preference order of participating students in the research are given in Table 1.

The variations of the information of participants about environmental engineeering profession before the entrance of department are shown in Table 2. According to the Table 2,the majority of students (63.9%) informed that they had information before making university and department preference. 39.6% of students, who have information, indicated that they had information from internet by searching and 38.35% of students,who have information,indiacted they learnt from person/people who does/do this job.

According to Table 3,48.5% of students participating in the research indicated that they chose willingly and 47.2%of them chose this department partially willingly.The percentage of students who chose unwillingly was 4.3%.When choosing reasons of students were viewed,24.5% of of students thought as a profession which will be much more imporatant in the future, 14.2 % of them chose this profession because of their families and %14.2 of them chose because of their score only enough for this department.

According to Table 4,looking at professional ideals of participating students after graduating the faculty, the majority (35.6%) of them wants to work as an engineer at public sector,29.6% wants to work as an engineer at private sector and 22.7% of them wants to have their own work. The lowest value (9.0%) belong to students prefering working in university.

As shown in Table 5,profesional ideals of students,after graduating from the faculty,shows a significant difference according to gender ($p<0.05$). It was seen that the majority of female participants (47.3%) wants to work as engineer at public sector. 32.3% of male participants wants to work as engineer at

private sector and 30.6% of them wants to have their own work. Working as academician at university is seen the least profession ideal among the others for both genders.

The variation of the participant students having knowledge about environmental engineering department before making university preference according to the willingly choosing the department is given in Table 6.As it can be seen in Table 6,there is a significant difference of students choosing environmental engineering department according to having knowledge about Environmental Engineering department.It was seen that the majority(67.8%) having knowledge chose the department willingly but the majority of students(75.0%) having any knowledge chose the department partially willingly.It was also seen that 0.7% of students having knowledge chose the department unwillingly.This percentage is a little bit higher among students having any knowledgee. The table shows us that 10.7%of students without any knowledge chose the department unwillingly.

Table 1. Number and Percentage Variation Related with Indivicual Properties of Participants

Variable	Group	f	%
Gender	Female	112	48.1
	Male	121	51.9
	Total	233	100.0
Age	17-19	53	22.7
	20-22	85	36.5
	23-25	82	35.2
	26and older	13	5.6
	Total	233	100.0
Education Level of Your Mother	Primary school	77	33.0
	Secondry school	50	21.5
	High school	76	32.6
	Associate degree	9	3.9
	Bachelor's degree	17	7.3
	Master and upper	4	1.7
	Total	233	100.0
Education Level of Your Father	Primary school	40	17.2
	Secondry school	34	14.6
	High school	93	39.9
	Associate degree	31	13.3
	Bachelor's degree	33	14.2
	Master and upper	2	0.9
	Total	233	100.0
Income of Your Family	1000 TL altı	12	5.2
	1000-2000	89	38.2
	2000-3000	74	31.8
	3000-4000	34	14.6
	4000 TL and upper	24	10.3
	Total	233	100.0
In which class are you student?	1. class	59	25.3
	2. class	48	20.6
	3. class	22	9.4
	4. class	43	18.5
	Higher	61	26.2
	Total	233	100.0
Type of school which you graduated	Anadolu High School	110	47.2
	Science School	2	0.9
	Vocational School	16	6.9
	Anadolu Vocational High School	6	2.6
	Classical High School	67	28.8
	Others	32	13.7
	Total	233	100.0
Did you take support from university Preparation courses?	Yes	144	61.8
	No	89	38.2
	Total	233	100.0
In which LYS entrance are you placed in Environmental Engineering Department?	1. entrance	133	57.1
	2. entrance	77	33.0
	3. entrance	21	9.0
	Upper	2	0.9
	Total	233	100.0
In which order was Environmental Engineering Department amongYour preferences	1.-6.preference	107	45.9
	7.-12. preference	72	30.9
	13.-18. preference	30	12.8
	19.-24. preference	18	7.7
	25.-30. preference	6	2.6
	Total	233	100.0

Table 2. Number and Percentage Values of Participants about having knowledge about Environmental Engineering Department

Varible	Group	f	%
Did you have knowledge about Environmental Engineering Department before making university Preference	Yes	149	63.9
	No	84	36.1
	Total	233	100.0

How did you learn Environmental Engineering Department before making university preference	From person/persons who does/do this job aound my environment	57	38.3
	Quide sevices in university preparotory schools	14	9.4
	University visits,organized in high schools	1	0.7
	From my teachers at high schools	12	8.1
	From internet by my research	59	39.6
	Carrier days organized at high school	2	1.3
	Diğer	4	2.7
	Total	149	100.0

Table 3. Number and Percentage Values related with parrticipants of choosing Environmental Engineering Profession

Varible	Group	f	%
Did you choose Environmental Engineering willingly?	Willingly chosen	113	48.5
	Unwillingly chosen	10	4.3
	Partially willingly chosen	110	47.2
	Total	233	100.0
What is your reason of choosing Environmental Engineering Department	Effect of my family	33	14.2
	Effect of my friends	10	4.3
	The reason od desiring this profession	29	12.4
	Advice of my teachers	19	8.2
	Advice of quide teachers in university preparation schools	6	2.6
	A profession with high income	6	2.6
	The reason of high job availability	27	11.6
	Appropriate for my talents	7	3.0
	A job respected in the society	4	1.7
	Because of a profession expected to become more important in the future	57	24.5
	My score enough for this department	33	14.2
	Others	2	0.9
	Total	233	100.0

Table 4. Number and Percentage Values Related with Professional Idealism After Graduating Environemnatl Engineering Department

Variable	Group	f	%
What is your Professional idealism after graduating the faculty	Working as engineer at government	83	35.6
	Working as engineer at private sector	69	29.6
	Going on at university as academician	21	9.0
	Having my own job	53	22.7
	Others	7	3.0
	Total	233	100.0

Table 5. Cross Table Results of Variations Related with Professional Idealism After Graduating the Faculty According to Gender

Professional Idealism after Graduating the Faculty Total			Working as engineer at government	Working as engineer at private sector	Working as academician at university	Having my own job	Other	
Gender	Female	f	53	30	11	16	2	112
		%	47.3%	26.8%	9.8%	14.3%	1.8%	100.0%
	Male	f	30	39	10	37	5	121
		%	24.8%	32.2%	8.3%	30.6%	4.1%	100.0%
Total		f	83	69	21	53	7	233
		%	35.6%	29.6%	9.0%	22.7%	3.0%	100.0%
X^2= 16,879 P= 0,002								

Table 6. Cross Table Results of the Variation of Students Having Knowledge About Environmental Profession Before making University Preference According to Willingly Chosen the University

Chosen Environmental Engieneering department Willingly Total			Unwillingly chosen	Partially willingly chosen	Willingly chosen	
Did youhave knowledge about EnvironmentalEngineering Department Before Making University Preference	Yes	f	1	47	101	149
		%	0.7%	31.5%	67.8%	100.0%
	No	f	9	63	12	84
		%	10.7%	75.0%	14.3%	100.0%
Total		f	10	110	113	233
		%	4.3%	47.2%	48.5%	100.0%
X^2= 65,813 P= 0,001						

CONCLUSION AND SUGGESTIONS

According to our research, the effect of family and friends,high job possibility,a profession which will be increase the importance in the future and the score only enough for this department show the most important criteria.The factors effective for choosing dentistry as a profession have been investigated for freshman students at Dentistry department of North Carolina Chapel Hill University in the USA. In this research, having a family member or a friend working in this profession was shown the most important factor in choosing the carrier [10]. In the research of Kıyak [11],which has been done on the basic criteria of chosing profession of classical high school students,indicated that the effective factors of job finding possibility,talent,interest,values,recognizing of personal properties (recognizing oneself),prizes(money, respect,-fame,etc.) were listed in order.According to a work done by Özyürek and Atıcı [12],it was brought up that school quide, family,friends,teachers and news on media were effective for students choosing a department in university.Our research findings show similarity (paralelism) with other research findings.

Professsional ideals of participants in our research show significant difference according to gender.While female students(47.3%) preferring working at public sector,this percentage is lower in male students(24.8%); it is shown that male students mostly prefer working at private sector(32.2%) and having their own job(30.6%).As demonstrated by Durer and others [13] In the examination of factors effective in career preferences in accounting field of business administration students,there is a significant difference to the importance given to carrier preference among male and female students.Majority of female students prefer working at public sector.These results confirm with our research.

Our research findings brought up that knowledge about Environmental Engineering before making profession preference was a high percentage such as 63.9%. Students informed that 39.6% had knowledge from internet by their search and 38.3% had knowledge from persons carrying out this profession around them.But university visits organized at high schools(%0.7) and carrier days(1.3%) were not so effective in profession selection.According to the work done by Saleem and the others [14],television,newspapers and social media tools were used so often by younger generation in order to search different professions and information related with job market.According to these findings,the effect of internet usage shows adjustable results with literature data.

Youngsters should collect necessary information about the history of profession,develoment,work qualities which are required in these profesions,the importance of talent and gender factor,job finding possibility in the future,validity of this job all over the country. They should also know profession well-which is planned to choose.Meetings,introducing professions, should be organized during their high school education and students should get information by inviting representatives from different professions.Families and teachers should help students to get knowledge.It should be provided to make choos-

ing consciously and students should be directed if they have talents and interest to professions,considered to choose.It should be kept in mind that they have the possibility to be unhappy when they are directed to a profession in which they do not have any interest and talent.The profession chosen by persons affect all their lives. The majority of students choosing Environmental Engineering learn information about the profession from internet or from persons carrying out this profession.Students are not enough informed about Environmental Engineering during their high school education.Our study shows that students having information choose the profession willingly.Increasing number of professions in today's world also gets appropriate profession to choose hard.

REFERENCES

1. Razon, N., 2015. Gencin Meslek Seçimini Etkileyen Faktörler, http://www.ekipnormarazon.com/makale-detay/gencin-meslek-secimini-etkileyen-faktorler
2. Pekkaya, M., Çolak, N., 2013.Determining the Priorities of Ratings Via AHP for the Factors that Effects in Choosing Professions forthe University Students, International Journal of Social Science, Volume 6, Issue 2, p. 797-818.
3. Sevendir and Yazıcı,2014. Examing the factors affecting the selection of mathematics proffession: A case study, Procedia-Social and Behavioral Sciences, 152, 642-647.
4. Çelik, N, Üzmez, U., 2014.Üniversite Öğrencilerinin Meslek Seçimini Etkileyen Faktörlerin Değerlendirilmesi Çağrı Merkezi Hizmetleri Örneği, Elektronik Mesleki Gelişim Ve Araştırma Dergisi, Cilt 2 Sayı 1, 94-105.
5. Kniveton,B.H. 2004. The Influence and Motivations on Which Sudents Base Their Choice of Career,Research in Education,72,47-57.
6. Qualifax The National Learner' Database The Parent's Role in Career Selection-How important is the role of the parent in the career guidance process? (17/06/2016) http://www.qualifax.ie/index.php?option=com_content&view=article&id=179&Itemid=207
7. Zeren, O., 1997. Türkiye'de Çevre Mühendisliği Eğitimi ve Karşılaşılan Sorunlar, International Journal of Environment, Vol 23 http://www.ekoloji.com.tr/resimler/23-1.pdf
8. Kilduff J., 2008. Developing a Body of Knowledge for Environmental Engineering, 38th ASEE/IEEE Frontiers in Education Conference, October 22 – 25, 2008, Saratoga Springs, NY, ABD.
9. Ural, A., Kılıç, İ., 2011.Bilimsel Araştırma Süreci, Detay Yayıncılık, Ankara
10. Wassel,J.R,Mauriello,S.M,Weintraub,J.A.,1992. Factors Influencing the Selection of Dental Hygiene as a Profession, J.Dental Hyg,66(2),81-88.
11. Kıyak, S, 2006. Genel Lise Öğrencilerinin Meslek Seçimi Yaparken Temel aldığı Kriterler, Yayınlanmamış Yüksek Lisans Tezi, Yeditepe Üniversitesi Sosyal Bilimler Enstitüsü, İstanbul.
12. Özyürek, R. ve Atıcı, M. 2002.Üniversite Öğrencilerinin Meslek Seçimi Kararlarında Kendilerine Yardım Eden Kaynakların Belirlenmesi, Türk Psikolojik Danışma ve

Rehberlik Dergisi, 2(17), 33-42.

13. Durer, S., Çalışkan, A.Ö., Akbaş, H. E., ve Gündoğdu, C. E., 2009.İşletme Bölümü Öğrencilerinin Muhasebe Alanında Kariyer Tercihlerini Etkileyen Faktörlerin İncelenmesi, Muhasebe ve Finansman Dergisi, 2009, Sayı:43

14. Saleem,N,Hanan,M.A,Saleem,I,Shamsad,R.M, 2014, Career Selection :Role of Parent's Profession, Mass Media and Personal Choice,Bulletein of Education and Research,Vol 36,No:2,25-37.

CHAPTER 10

INNOVATIVE APPROACHES IN ENGINEERING FUNCTIONALFOOD CONCEPT AND ENHANCEMENT OF THE FUNCTIONALITY

Tugba AKTAR[1]

INTRODUCTION

Functional foods are defined as certain food or food ingredients that have been associated with positive effects on consumer health, wellbeing beyond its nutritive value(Huggett and Verschuren, 1996). This functionality can be rooted from the components that are available naturally or can be added during the processing of the food which means functionality can be enhanced. Not only by enhancing the beneficial components, but also by reducing the negatively affecting components can be considered as functionality enhancement of the food.

The very first idea of functional foods was first introduced in Japan at the mid-1980s where also has the only specific approval process for the formulated functional foods. Japanese Government –Ministry of Education- funded 86 specific research programs on the "systematic analysis and development of food function". In the following ten years Japanese Government continued to fund the researches about logic regulation development about the functional foods. As mentioned earlier in the year of 1991 as a result of those researches, Japan introduce the new labeling program named FOSHU (Foods for Specified Health Use) to provide standard and approval process for the functional foods that includes 4 different categories (Roberfroid, 2000). With a similar motivation in the US around mid-1990s Food and Drug Administration investigated several food types in order to find the correlations with the risk of disease and cure to those certain diseases. Those investigations were used as evidence that selected foods had correlations with the risk of the disease and therefore can be described as functional. Meanwhile in Europe, the primary generation of functional foods involved addition of the supplements including calcium and vitamins. Even though still not legally categorized except Japan, functional foods recently became more and more popular and attracted the attention of the food scientists as well as consumers. On the other hand functional foods attracted the attention of the consumers followed by the food producers and researchers. The authorities also decided that European continent especially the European Union should emphasize the importance of the functional foods and investigate the missing links of the foods.

1 Department of Food Engineering, AlanyaAlaaddinKeykubat University, Antalya, TURKEY

Despite the industrial attack of the functional food supported by the governmental authorities, consumers started to hear about the functional foods by the upcoming of the "health conscious baby boomers" especially in the US (Meyer, 1998). The consumer awareness about it is very critical in order to market success as well as health development and for the functional foods we can say that the development is growing appreciably. The advanced technologies in the food industry are now capable of fulfilling the consumers demand on the healthier option for the food for the potential improvement on the technology of physical structure and composition of the food.

Mentioned increased in the consumer demand will and already did increase the market share and add value to potential market growth. The market study done in the year of 1998 by Waltham illustrated that functional food market has grown by $29 billion at late 1990s. The market potential involves the local, traditional and cultural characteristics of the consumer and therefore, should be designed specific to the target consumer group. If the market aims to be more universal it is necessary to provide scientific evidence to the function that has been claimed.

The initial role of the diet since the evolution of human is to provide nutrients (especially the essential ones) to carry out the metabolic requirements. Diet and nutrition should be supplying various functions in the body and sometimes as in functional food case may play a detrimental or beneficial roles for human health(Roberfroid, 2000).On the other hand despite feeding the bodily metabolisms requirements, we still eat for the feeling of satisfaction and joy. Therefore, it is true that food is essential for survival as well as it is still one of the most pleasurable human activities.

Recent researchers including nutritionists, food engineers, food scientists, and R&D experts are currently focusing on the functionality of the foods which may deliver beneficial components to health consumer group as well as delivering wellbeing to the vulnerable group of consumers (i.e. diabetes). These innovations will be particularly important in order to reduce health care costs, and to increase the life expectancy and quality of life especially for the elderly.

What is a Functional Food?

As broadly defined earlier in this chapter, Functional foods are defined as certain food or food ingredients that have been associated with positive effects on consumer health, wellbeing beyond its nutritive value (Huggett and Verschuren, 1996). Even before the invention of the terminology of "functional food", foods were consumed due to their many functions including essential contributions to vital metabolism. However, realization of the chemical composition and their functions which unveiled the idea of increasing those specific beneficial components generated the concept of functionality. Either single or multiple benefit delivering component containing foods are basically determined as functional foods which aims to improve the statement of wellbeing and health or reduction of the disease risk (Contor, 2001). It is

also necessary to state that the food should have psychological or physiological contribution beyond the traditional known effect(Clydesdale, 1997). The mostly accepted definition was stated at the meeting organized by the International Life Science Institute Europe as "a food can be regarded as functional if it is satisfactorily demonstrated to affect beneficially one or more target functions in the body, beyond adequate nutritional effects in a way which is relevant to either the state of wellbeing and health or the reduction of the risk of a disease"(Diplock *et al.*, 1999)

Functionalization of Foods

Function added food must have following several approaches. The very first aim is the elimination of the known deteriorative components (i.e. gluten for the celiac patients). For this approach it is necessary to be considering a vulnerable group for most of the time. This group of consumers involves two main categories of patients: elderly, babies and chronically ill consumers. Those perishable groups of consumers either require either a smooth/ soft texture due to limited dental development or removal of allergic or detrimental content from the food. Second approach involves the increasing of the already available functional component (i.e. vitamin C added orange juice). This approach is one of the mostly applied approaches in the industry. The third approach is the addition of not presented component to add functionality to the food (i.e. addition of fluoride to the water). Fourth approach on the other hand is the replacement of the excessive or deleterious component by beneficial component (i.e. using chicory inulin to replace sugar). The last approach is the increasing of the bioavailability of the functional component to improve the functionality (Roberfroid, 2000).

Literature Findings on the Food Substances

As highlighted earlier functional foods requires an evidence from epidemiological findings(Hasler, 1998). In the literature several food substances has been proven to be related with the health associated problems including cancer (Hasler, 1998). Here are the list of some well investigated food examples: green tea (Harbowy *et al.*, 1997),soy (Anderson, Johnstone and Cook-Newell, 1995; Messina, Barnes and Setchell, 1997; Nestel *et al.*, 1997; Hodgson *et al.*, 1998; Potter, 1998), cruciferous vegetables (Verhoeven *et al.*, 1996),tomatoes (Gerster, 1997), garlic (You *et al.*, 1988; Dorant *et al.*, 1993; Srivastava, Bordia and Verna, 1995; Nagourney, 1998), fish (Kromhout, Bosschieter and Coulander, 1985; Harris, 1996), citrus fruits (Hasegawa and Miyake, 1996; Gould, 1997), wine (Frankel *et al.*, 1993; Kanner *et al.*, 1994), and dairy products (Talamini *et al.*, 1984; van't Veer *et al.*, 1989; Sanders, 1994; Mitall and Garg, 1995).

Scientific Aspect of Functional Foods

The researchers design and test the functionality of the foods due to their positive effects on the human health. While doing this, it is necessary to involve the identification of the relationships and reaction potentials between

the components of the foods that may affect the beneficial content. By doing these interaction research researchers can build up strong basis to the functional food development as well as functional components chemistry. Meanwhile, by understanding of the mechanics and potential of the component, it will be possible to image the model of the chemicals and provide new ideas in terms of functionality. One good example to that is by understanding of the chemical structure and physical potential of a particular component; we can obtain the synergistic effects with the other chemical compounds and provide more than double effect by combining the two synergistic components together.

On the other hand functional food should provide consumers a healthier lif0e without changing their routine of eating or medicine intake (Jonas and Beckmann, 1998).Regarding this perspective Pascal, (1996) mentioned that food should remain as food, and must not be confused with medicines in terms of health benefit.

Future Plan for the Functional Foods

Keeping the previously mentioned content about the functional foods, researchers and functional food related bodies should be focusing on special targets. Determined targets involves the developments in the; gastrointestinal functions, redox and antioxidant systems, macronutrient metabolism, fetal and early life development, xenobiotic metabolism and mood and behavior improvement mechanisms (Roberfroid, 2000).

Conclusion

Functional foods are one of the highly increasing markets in the food industry. This demand is truly reasonable by the consumers and the functional foods deserve to be investigated, due to their possible contribution potential to the wellbeing and sometimes “healing” effect. Despite keeping the food nature of the product, the researchers still aim to follow the functions of the functioned food and enhance the functionality according to the plans that have been previously described as well as stepping towards the future plan.

References

1. Anderson, J. W., Johnstone, B. M. and Cook-Newell, M. E. (1995) ‘Meta-analysis of the effects of soy protein intake on serum lipids’, New England Journal of Medicine. Mass Medical Soc, 333(5), pp. 276–282.

2. Clydesdale, F. M. (1997) ‘A proposal for the establishment of scientific criteria for health claims for functional foods’, Nutrition reviews. Oxford University Press Oxford, UK, 55(12), pp. 413–422.

3. Contor, L. (2001) ‘Functional Food Science in Europe.’, Nutrition, metabolism, and cardiovascular diseases: NMCD, 11(4 Suppl), pp. 20–23.

4. Diplock, A. T., Aggett, P. J., Ashwell, M., Bornet, F., Fern, E. B. and Roberfroid, M. B. (1999) ‘Scientific concepts of functional foods in Europe: consensus document’,

British Journal of Nutrition, 81(1), pp. 1–27.

5. Dorant, E., van den Brandt, P. A., Goldbohm, R. A., Hermus, R. J. J. and Sturmans, F. (1993) 'Garlic and its significance for the prevention of cancer in humans: a critical view', British journal of cancer. Nature Publishing Group, 67(3), p. 424.

6. Frankel, E. N., German, J. B., Kinsella, J. E., Parks, E. and Kanner, J. (1993) 'Inhibition of oxidation of human low-density lipoprotein by phenolic substances in red wine', The Lancet. Elsevier, 341(8843), pp. 454–457.

7. Gerster, H. (1997) 'The potential role of lycopene for human health.', Journal of the American College of Nutrition. Taylor & Francis, 16(2), pp. 109–126.

8. Gould, M. N. (1997) 'Cancer chemoprevention and therapy by monoterpenes.', Environmental Health Perspectives. National Institute of Environmental Health Science, 105(Suppl 4), p. 977.

9. Harbowy, M. E., Balentine, D. A., Davies, A. P. and Cai, Y. (1997) 'Tea chemistry', Critical reviews in plant sciences. Taylor & Francis, 16(5), pp. 415–480.

10. Harris, W. S. (1996) 'n-3 fatty acids and lipoproteins: Comparison of results from human and animal studies', Lipids. Wiley Online Library, 31(3), pp. 243–252.

11. Hasegawa, S. and Miyake, M. (1996) 'Biochemistry and biological functions of citrus limonoids', Food Reviews International. Taylor & Francis, 12(4), pp. 413–435.

12. Hasler, C. M. (1998) 'Functional foods: their role in disease prevention and health promotion', FOOD TECHNOLOGY-CHAMPAIGN THEN CHICAGO-. Institute of Food Technologists, 52, pp. 63–147.

13. Hodgson, J. M., Puddey, I. B., Beilin, L. J., Mori, T. A. and Croft, K. D. (1998) 'Supplementation with isoflavonoid phytoestrogens does not alter serum lipid concentrations: a randomized controlled trial in humans', The Journal of nutrition. Oxford University Press, 128(4), pp. 728–732.

14. Huggett, A. C. and Verschuren, P. M. (1996) 'The safety assurance of functional foods', Nutrition reviews. Wiley Online Library, 54(11), pp. S132–S140.

15. Jonas, M. S. and Beckmann, S. C. (1998) 'Functional foods: Consumer perceptions in Denmark and England'. Aarhus School of Business, MAPP Centre.

16. Kanner, J., Frankel, E., Granit, R., German, B. and Kinsella, J. E. (1994) 'Natural antioxidants in grapes and wines', Journal of Agricultural and Food Chemistry. ACS Publications, 42(1), pp. 64–69.

17. Kromhout, D., Bosschieter, E. B. and Coulander, C. de L. (1985) 'The inverse relation between fish consumption and 20-year mortality from coronary heart disease', New England journal of medicine. Mass Medical Soc, 312(19), pp. 1205–1209.

18. Messina, M., Barnes, S. and Setchell, K. D. (1997) 'Phyto-oestrogens and breast cancer', The Lancet. Elsevier, 350(9083), pp. 971–972.

19. Meyer, A. (1998) 'The 1998 top 100® R&D survey', Food Processing, 58(8), pp. 32–40.

20. Mitall, B. K. and Garg, S. K. (1995) 'Anticarcinogenic, hypocholesterolemic, and antagonistic activities of Lactobacillus acidophilus', Critical reviews in microbiology. Taylor & Francis, 21(3), pp. 175–214.

21. Nagourney, R. A. (1998) 'Garlic: Medicinal food or nutritious medicine?', Journal of Medicinal Food, 1(1), pp. 13–28.

22. Nestel, P. J., Yamashita, T., Sasahara, T., Pomeroy, S., Dart, A., Komesaroff, P., Owen, A. and Abbey, M. (1997) 'Soy isoflavones improve systemic arterial compliance but not plasma lipids in menopausal and perimenopausal women', Arteriosclerosis, thrombosis, and vascular biology. Am Heart Assoc, 17(12), pp. 3392–3398.

23. Pascal, G. (1996) 'Functional foods in the European Union', Nutrition reviews. Wiley Online Library, 54(11), pp. S29–S32.

24. Potter, S. M. (1998) 'Soy protein and cardiovascular disease: the impact of bioactive components in soy', Nutrition reviews. Oxford University Press Oxford, UK, 56(8), pp. 231–235.

25. Roberfroid, M. B. (2000) 'Concepts and strategy of functional food science: the European perspective–', The American journal of clinical nutrition. Oxford University Press, 71(6), p. 1660S–1664S.

26. Sanders, M. E. (1994) 'Lactic acid bacteria as promoters of human health', in Functional foods. Springer, pp. 294–322.

27. Srivastava, K. C., Bordia, A. and Verna, S. K. (1995) 'Garlic (Allium sativum) for disease prevention', South African Journal of Science. BUREAU FOR SCIENTIFIC PUBLICATIONS, 91, p. 68.

28. Talamini, R., La Vecchia, C., Decarli, A., Franceschi, S., Grattoni, E., Grigoletto, E., Liberati, A. and Tognoni, G. (1984) 'Social factors, diet and breast cancer in a northern Italian population', British journal of cancer. Nature Publishing Group, 49(6), p. 723.

29. van't Veer, P., Dekker, J. M., Lamers, J. W. J., Kok, F. J., Schouten, E. G., Brants, H. A. M., Sturmans, F. and Hermus, R. J. J. (1989) 'Consumption of fermented milk products and breast cancer: a case-control study in The Netherlands', Cancer research. AACR, 49(14), pp. 4020–4023.

30. Verhoeven, D. T., Goldbohm, R. A., van Poppel, G., Verhagen, H. and van den Brandt, P. A. (1996) 'Epidemiological studies on brassica vegetables and cancer risk.', Cancer Epidemiology and Prevention Biomarkers. AACR, 5(9), pp. 733–748.

31. Waltham, M. S. (1998) 'Roadmaps to Market: Commercializing Functional Foods and Nutraceuticals, Decision Resources'. Inc.

32. You, W.-C., Blot, W. J., Chang, Y.-S., Ershow, A. G., Yang, Z.-T., An, Q., Henderson, B., Xu, G.-W., Fraumeni, J. F. and Wang, T.-G. (1988) 'Diet and high risk of stomach cancer in Shandong, China', Cancer research. AACR, 48(12), pp. 3518–3523.

CHAPTER 11

ACOUSTICAL PROPERTIES OF SANDWICH STRUCTURES DEVELOPED FROM CHICKEN FEATHER RACHIS MATERIAL

Nazim PAŞAYEV[1*], Müslüm EROL[2]**

1. INTRODUCTION

Noise as an air pollution is one of the most negative effects of industry as well as air pollution and water pollution. The fight against noise, which causes many health problems both physiologically and psychologically, has become one of the most important aspects of providing a healthy living and working environment.

Numerous sound insulation materials based on different principles have been developed to solve the noise problem. Among these materials the multi-layer constructions with sandwich structure form a group. There are studies in the literature about the ordinary sandwich construction sound insulation materials. In these studies, the effects of different characteristics of multilayer structures on the sound insulation properties have been investigated.

In his experiments on three-layered structures, Davern achieved the following result; the acoustic impedance of the material and the sound absorption coefficient depend on the porosity and density of the layers at considerable levels (Davern, 1977). Multilayer structures have been identified by their constructive analysis, in which the sound insulation properties of these structures are determined by their construction at significant levels. Dunn and Davern have made such an assumption by making an analytical analysis of three-layered echo-canceling porous materials that the outer layer should encourage the sound waves to enter the composition and the inner layers should provide sound energy reduction (Dunn & Davern, 1986).

An important component of multilayer sound insulation materials is the nonwoven surfaces. Numerous studies have been done starting from Zwikker and Kosten related to the sound absorption properties of nonwoven surfaces. (Zwikker & Kosten, 1949). These studies have shown that the porous materials exhibit high sound absorption coefficients at high frequencies, and low sound absorption coefficients at low and medium frequencies.

1 Prof.Dr., ErciyesUniversity, Faculty of Engineering, Lecturer of Textile Engineering Department, Kayseri/Turkey

2 Lecturer, Bingöl University,Technical Sciences Vocational School, Lecturer of Textile Technology Department, Bingöl/Turkey

In other words, porous nonwoven surfaces generally do not have the ability to absorb sound over a wide frequency range (Li et al., 2012). Accordingly, a number of studies have been carried out in order to improve the sound absorption properties of porous materials at medium and low frequencies. Some of these studies are related to the modeling of sound absorption of porous materials (Delany & Bazley, 1970; Allard & Champoux, 1992; Allard et al., 1993; Narang, 1995; Voronina, 1996; Shoshani & Yakubov, 1999; Shoshani & Yakubov, 2000; Shoshani & Yakubov, 2000). Due to these studies it was possible to develop effective materials for sound absorption. The studies on the material thickness, density and porosity, the amount of fibers in the material, characteristics of the fibers, orientation, shape of the material surface, fiber content of the material have provided the significant improvement of the sound absorption properties of nonwoven surfaces (Lee & Joo, 2004; Lou et al., 2005; Taşcan & Vaughn, 2008; Taşcan et al., 2009; Tai et al., 2010; Nazire et al., 2011; Küçük & Korkmaz, 2012).

A number of studies have been carried out to improve the sound absorption properties of fiber-containing porous materials through the use of different fibers and the application of production methods (Thilagavathi et.al., 2010; Fatima & Mohanty 2011; Ersoy & Kucuk, 2009; Fouladi et al., 2011; Zulkifli et al., 2009; Al Rahman et al., 2013; Koizumi et.al., 2012; del Rey et.al., 2007; Wassilieff, 1996; Shahani et al., 2013; Shahani et al., 2014).

Supporting nonwoven surfaces with different materials has resulted in improving the sound absorption properties at medium and low frequencies which has led to the development of multilayer sound insulation materials with better parameters (Joo & Lee 2003, Lin et al., 2010; Lin et al., 2011; Lin et al., 2011; Liu et al., 2012; Patinha et al., 2014). Sandwich structured sound insulation materials, which is a type of these materials, have been used successfully in many areas.

This paper is concerned with the development of sandwich structures that are obtained from processed chicken feather materials most of which are waste and by-product in the production of chicken meat.

2. MATERIAL AND METHOD

2.1. Approach

Studies on bird feathers have revealed many interesting features of this material (Martínez-Hernández & Velasco-Santos, 2012). Among these properties, the internal structure of the material is in the foreground. Inhomogeneous structured bird feather consists of a rachis which forms the spine and a fibrous structure that comes from the rachis. Figure 1 shows SEM views taken by us from the side of the inner structure of the chicken feather rachis (CFR) (*a*) and the chicken feather fibers (CFF) (*b*). This internal structure consists of micro cells with sizes of 5-10μm in the fibers and 5-20μm in the rachis.

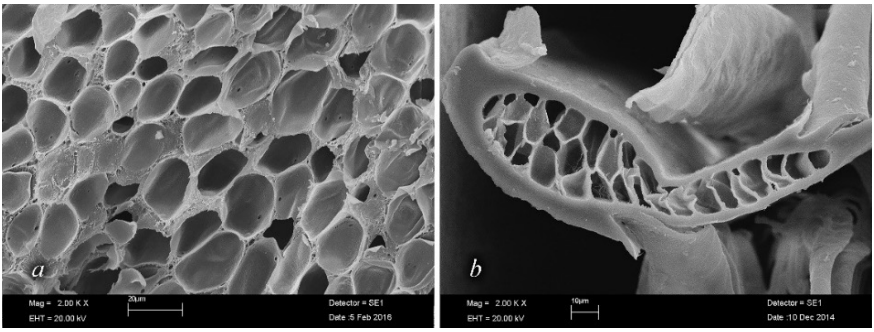

Figure 1. SEM images cross section of CFR (*a*) and CFF (*b*)

Chicken feather fibers are obtained by mechanical cutting the fibrous structure branched from the spine of the feather. This time the feather rachis is formed as the by-product, which constitutes about half of the feather weight.

In this study, it was aimed to develop materials for sound insulation from chicken feather material by taking advantage of the structural properties of that material. For this purpose, porous composite structures were developed by using different matrices from chicken feather rachis material and nonwoven structures were developed from fiber material. Each of these materials has a primary and secondary porous structure. It is envisaged that the complex structures to be obtained by combining them will exhibit higher sound insulation properties.

2.2. Material

2.2.1. Non-woven surface produced from the CFF

Nonwoven surfaces from the chicken feather fibers were produced in the Erciyes University Textile Engineering Department laboratories (Kayseri, Turkey). Feathers from the farm were washed, disinfected and dried, and then fiber was produced from these feathers. Non-woven surface samples were produced at different densities by thermal bonding using powder ethylene vinyl acetate (EVA) binding agent from the produced fibers. Some properties of this samples, coded as N1 and N2, are given in table 1 and the picture is given in Figure 2*a*.

Table 1. Some properties of nonwoven surface samples for experimental work

	Features and parameters	Samples	
		N1	N2
1	The binder polymer	EVA	EVA
2	Sample content	20gr CFF and 10gr EVA	10gr CFF and 5gr EVA
3	Average sample thickness 0,001m	12,30	11,00
4	Weigh of sample to surface, kg/m^2	1,1719	0,5859
5	Weigh of sample to volume kg/m^3	95,2744	53,2670
6	Porosity of sample	0,8866	0,9366
7	The air permeability of the sample, m/s	$2{,}9\cdot10^{-2}$	$11{,}3\cdot10^{-2}$

Figure 2. Samples produced out of CFF (*a*) and CFR (*b*)

Figure 3a shows the inner SEM image of the produced nonwoven surface sample. In this image, the binding polymer material particles can be observed as black stains.

2.2.2. Composite plates produced from CFR

Composite plates made of chicken feather rachis material were produced at Erciyes University Textile Engineering Department laboratories. The production of the fiber from the chicken feather is carried out on a special machine based on the separation of the fibers by mechanical cutting. During the process, the rachis is collected by separating into pieces. Granular composite structures were produced by hot pressing method by using a binder polymer (EVA) from rachis parts. Some features of these structures are given in Table 2 and the picture is given in Figure 2b. Figure 3b shows a SEM view of the inner section of the sample.

Table 2. Some properties of the composite samples for experimental studies

	Features and parameters	Samples	
		C1	C2
1	The binder polymer	EVA	EVA
2	Sample content	50gr CFR and 12,5gr EVA	33gr CFR and 8,25gr EVA
3	Average sample thickness, 0,005m	5	5
4	Weigh of sample to surface, kg/m2	2,4414	1,6113
5	Weigh of sample to volume kg/m3	488,2813	322,2656
6	Porosity of sample	0,3896	0,5972
7	The air permeability of the sample, m/s	$2{,}9 \cdot 10^{-2}$	$6{,}7 \cdot 10^{-2}$

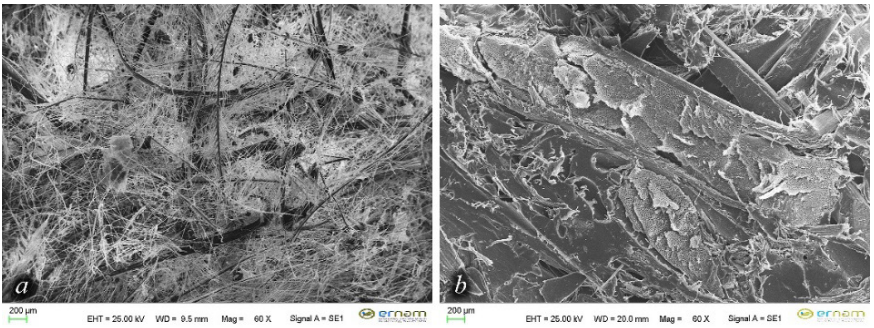

Figure 3. SEM image of the internal section of the nonwoven surface (*a*) and composite sample (*b*)

2.2.3. Traditional sound insulation materials

To compare sandwich construction samples made from chicken feather materials, samples were taken from traditional sound insulation materials and sound insulation parameters were measured. Some properties of these materials are given in table 3, and pictures are given in Figure 4.

Table 3. Some properties of the traditional sound insulation materials

Fabric Code	Fabric types	Features and Parameters			
		Content	Thickness, 0,001m	Density for surface, kg/m^2	Density for volume, kg/m^3
GW	Glass wool	Glass fiber	15,69	0,3010	19,1814
RW	Rock wool	Basalt	14,12	0,3919	27,7534
F	Felt	Textile waste	13,05	0,3745	28,6990

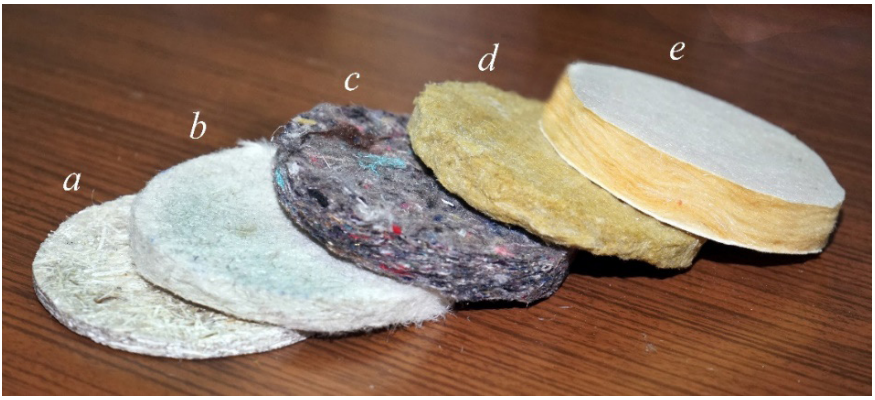

Figure 4. Examples of materials used in experiments
a – composite plate produced from CFR, *b* – nonwoven structure produced from CFF, *c* - felt made from F, *d* – nonwoven structure produced from RW, *e* – nonwoven structure produced from GW

2.3. Method

2.3.1. Production of sandwich structures

Sandwich structures are prepared as two different schemes which are *a* and *b* schemes. There is a nonwoven layer in the core of the samples prepared according to scheme *a* and there is a composite plate in the core of the samples prepared according to scheme *b* (Figure 5).

Examples of these structures are given in Figure 6.

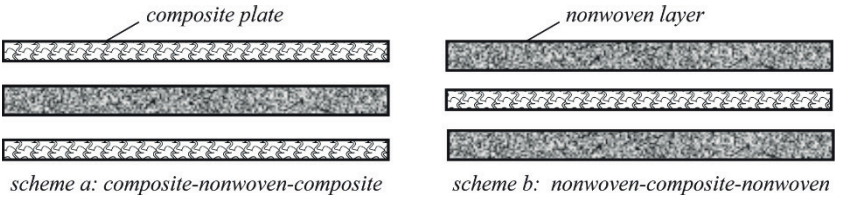

Figure 5. Schemes of preparing sandwich structures

In the experiments, two types of composite coded C1 and C2 and two types of nonwoven structures coded as N1 and N2 were used. These structures have different weight and density values. In order to see how the acoustic values of the sandwich structures produced from these materials with different weight and density values have been changed, a series of experiments have been performed and acoustic curves have been obtained.

Figure 6. Samples of sandwich structures produced on schemes *a* and *b*

2.3.2. Measurement of acoustic parameters

BSWA TECH branded impedance tube device was used to measure acoustic parameters such as sound absorption coefficient and loss of sound transmission of the samples of sandwich structures.

The test sample is placed on one end of the rigid and linear tube to measure the sound absorption coefficient. Planar waves are produced by a sound source. The sound pressure is measured from two points close to the sample. Two microphones are used for the test and the phase calibration is performed

between the microphones. The transfer function between these two microphone signals is measured. Using the transfer function, the sound absorption coefficient and the impedance of the sample are calculated. The available frequency range is determined by the diameter of the tube and the distance between the microphones. The device scheme for measuring the sound absorption coefficient is given in Figure 7.

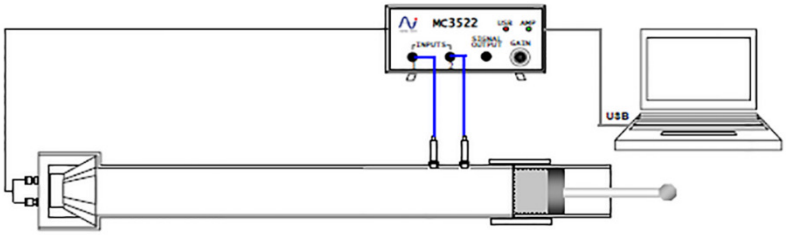

Figure 7. Sound absorption coefficient measurement

A modified impedance tube method with four microphones was applied for voice transmission loss test. For this measurement, the sample is prepared at the diameter of the impedance tube and placed at the end of the impedance tube. However, unlike the impedance tube measurement, there is a secondary tube after the sample (Figure 8)

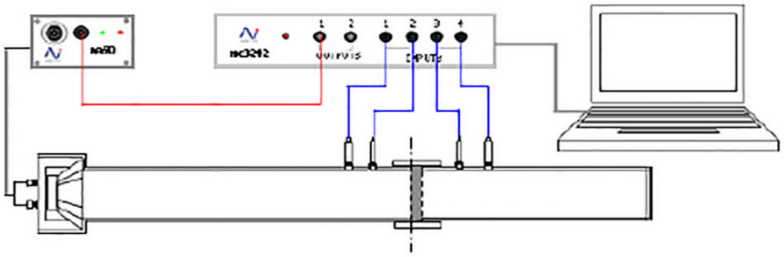

Figure 8. Sound transmission loss measurement

The planar waves from the audio source sent on the sample piece are measured on the first microphones as they were in the impedance tube measurement. Sound waves transmitted from the material to the secondary tube section are also received by the third and fourth microphones and the transfer functions between all the microphones are calculated separately.

In order to calculate loss of sound transmission, two different boundary conditions of the test fixture are measured. The opposite boundary conditions are chosen for the best measurement results. In the first condition the outlet of the secondary tube is closed with a hard lid and the sound waves are completely reflected back. In the second condition the outlet of the secondary tube is completely open and the sound waves propagate in space and do

not return back into the tube due to the reflection from a surface. The device scheme applied in measuring the loss of sound transmission is given in Figure 8.

Measurements were carried out according to the following standards.

1. ISO 10534-1: 1996 Acoustics-Determination of sound absorption coefficient and impedance in impedance tubes-Part1: Method using standing wave ratio
2. ISO 10534-2: 1998 Acoustics-Determination of sound absorption coefficient and impedance in impedance tubes-Part2: Transfer function method.

All samples were subjected to two different test procedures. In these tests, the sound absorption coefficient and the loss of sound transmission values of the samples were measured. Circular parts with a diameter of 10 cm and 3 cm from each sample were cut and prepared for the measurements.

3. TEST RESULTS

Figure 9 shows the graphs of the sound absorption coefficient, and the graphs of the change in the values of loss of sound transmission versus the frequency of sound, plotted from the results of measurements of composite and non-woven structures. The curves in these graphs are defined according to the code names in Table 1 and Table 2 of the composite and non-woven surface samples.

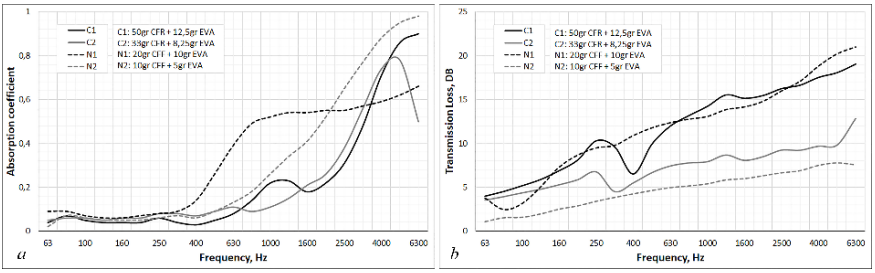

Figure 9. Acoustic curves of composite and nonwoven samples structures

Figure 10 shows acoustic curves of dual and triple combined structures formed from samples of C1 composite and N1 nonwovens made of chicken feather rachis and chicken feather fiber. These curves were plotted based on the measurement results of the change of the sound absorption coefficient and the loss of the sound transmission values according to the frequency of sound.

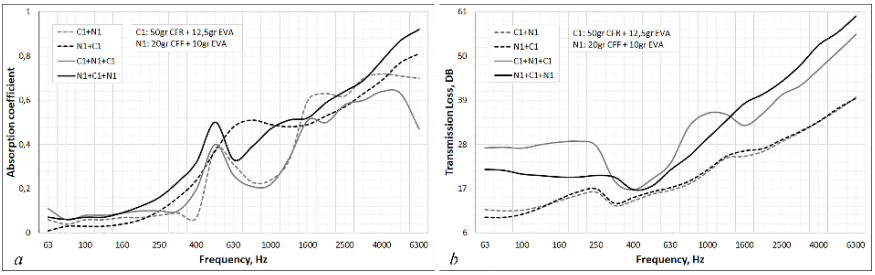

Figure 10. Acoustic curves of dual and triple combined structures with C1 and N1 content

Figure 11 shows acoustic curves for sandwich structures formed from N1 and N2 coded surface samples with C1 and C2 coded plates with different weight and density parameters produced from chicken feather rachis material.

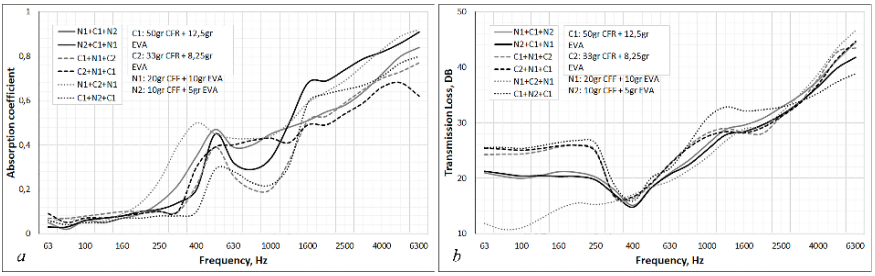

Figure 11. Acoustic curves of the sandwich structures with different contents

In Figure 12, acoustic curves of sandwich structures made of glass wool, stone wool and textile wastes, which are the traditional sound insulation materials, and chicken feather rachis material, are given.

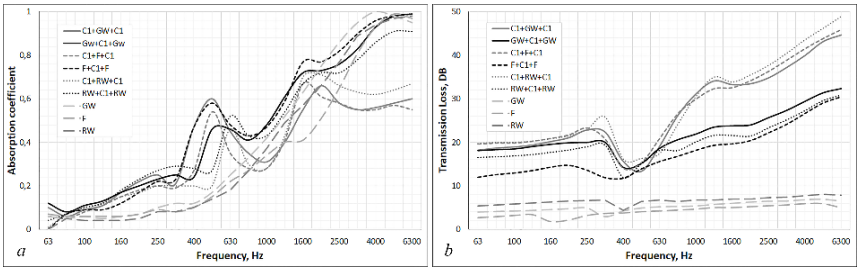

Figure 12. Acoustic curves of conventional sound insulation materials and sandwich structures made of CFR materials

4. DISCUSSION AND CONCLUSIONS

In Figure 9 we can see the graphs the variation of the sound absorption coefficient and loss of sound transmission values of the composite and non-woven samples according to the sound frequency. As can be seen from these

figures, the C1 code-named material has better acoustical properties than C2 material and N1 code-named material has better acoustical properties than N2.

On the other hand, the acoustical characteristics of the structures produced from the rachis and fiber material are selected from each other by general lines. Sound absorbing coefficient of structures made from rachis material shows only high values at high frequencies and low values at medium and low frequencies. On the other hand, the structures produced from fiber show moderate values even at medium frequencies. From this point of view, the N1 code-named material provides better absorption at medium frequencies than N2 (Fig, 9a). Apparently, this depends on the weight by volume (density) of the material being higher. When the sound transmission loss values of these samples are examined, it is seen that the values of C1 and N1 and the values of C2 and N2 structures are close to each other (Fig, 9b). We can say that an important part of the loss of sound transmission in nonwoven structure occurs because of the sound absorption and in composite construction it occurs because of the reflection of the sound.

When we put these two materials together and have two layered samples, we get the same sound transmission loss curves but it has better results than the single layered structures (Figure 10b, C1+N1 and N1+C1 structure curves). Apparently in the two-layer structures from the point of view of loss in the transmission of sound, the order of the arrangement of the composite and nonwoven layers does not matter. However, it is not possible to say the same about the sound absorption. There is a difference between the values of the sound absorption coefficients of these samples. This difference is not only due to the fact that the nonwoven structure has higher sound absorption ability than the composite structure but also it depends on the location of the layers. Here we can get such a result that in the case of two-layered materials, the layer with low density or high porosity must be in the front to obtain better sound absorption.

This situation is highly observed in three-layer sandwich structures. The sandwich structures subjected to the tests were produced in two schemes as shown above. Scheme 1: the layer made out of rachis is in the core; scheme 2: the layer made out of fiber is in the core (Figure 5 and Figure 6). As a result, there were significant differences between these structures, both in the sound absorption coefficients and in the loss of sound transmission (Figure 10 and Figure 12, the curves of C1+N1+C1 and N1+C1+N1 structures). Supporting the two layered structure with a third layer improves the acoustic parameters. Composite outer layers gave better results at lower frequencies and non-woven surfaces gave better results at higher frequencies in terms of loss of sound transmission. In addition, the sound absorption coefficient of the samples with non-woven surfaces in the outer layers has higher values on the whole scale. From this it should be understood that along with the thickness, weight, density and porosity of the layers in multilayer structures, the arrangement of the layers also affects some of the acoustic properties of this structure.

Serial experiments have been conducted to see how the acoustic values of sandwich structures made from materials with different weight and density values change. According to the sound frequency, the variation of the acoustic values of these structures is given in the graphs of Figure 10. According to these graphs, when the low-density nonwoven layer N2 is at the front in the sandwich structure which has composite at the core provides better sound absorption at higher frequencies but better at mid frequencies when it is at the back. The voice transmission loss curves of both of these variants are approximately the same.

In sandwich structures with a nonwoven layer at the core, when the low density C2 composite layer is at the front, it provides better sound absorption only at medium frequencies. Except for this, in terms of both sound absorption and loss of sound during transmission, no changes are observed.

In figure 11, nonwoven based structures in the core C2 with composite based structures in the core N2 appear to have no significant differences in acoustic properties when compared to the C1 and N1 structures in the core in Figure 10. However, it is observed that the N1+C1+N1 structure has slightly better values. This composite structure, which has a thickness of 3.5cm, provides sound insulation of 20-60DB at 63-6300Hz frequency range.

Materials such as glass wool, rock wool and felt, which are traditional sound insulation materials, have high sound absorption coefficient at high frequencies, but low sound absorption at medium and low frequencies. Loss of sound transmission for these materials has much lower values. It is seen that the materials obtained by supporting the porous composite materials produced from chicken feather rachis exhibit higher acoustic values than the unsupported materials (Figure 12). We can see that the sound absorption coefficient and sound transmission loss values at the middle and low frequencies of all three traditional insulation materials are significantly increased.

All of these show that the use of chicken feather materials, especially porous composite structures, as sound insulation material offers good perspectives.

ACKNOWLEDGEMENT

The study has been supported by TC Erciyes University Scientific Research Projects Coordination Unit with the project number FDK-2016-6847.

REFERENCES

1. Allard J.F. & Champoux Y. 1992. New empirical equations for sound propagation in rigid frame fibrous materials. *Journal of the Acoustical Society of America*, 91(6): 3346-3353

2. Allard J.F., Herzog P., Lafarge D., Tamura M. 1993. Recent topics concerning the acoustics of fibrous and porous materials. *Applied Acoustics*, 39(1-2): 3-21

3. Al Rahman L.A., Raja R.I., Rahman R.A. 2013. Experimental Study on Natural Fibers for Green Acoustic Absorption Materials. *American Journal of Applied Sciences*, 10(10): 1307-1314

4. Davern W.A. 1977. Perforated facings backed with porous materials as sound absorbers-an experimental study. *Applied Acoustics*, 10(2): 85-112

5. Del Rey R., Alba J., Sanchiz V. 2007. Proposal of an Empirical Model for Absorbent Acoustical Materials Based in Kenaf. Proceedings of the 19th International Congress on Acoustics. 2-7 September 2007, Madrid, Spain, s. 3361-3366

6. Delany M.E. & Bazley E.N. 1970. Acoustical properties of fibrous absorbent materials. *Applied Acoustics,* 3(2): 105-116

7. Dunn I.P. & Davern W.A. 1986. Calculation of acoustic impedance of multi-layer absorbers. *Applied Acoustics*, 19(5): 321-334

8. Ersoy S. & Kucuk H. 2009. Investigation of industrial tea-leaf-fibre waste material for its sound absorption properties. *Applied Acoustics*, 70(1): 215–220

9. Fatima S. & Mohanty A.R. 2011. Acoustical and fire-retardant properties of jute composite materials. *Applied Acoustics*, 72(2): 108–114

10. Fouladi M.H., Ayub M., M.J.M.Nor. 2011. Analysis of coir fiber acoustical characteristics. *Applied Acoustics*, 72(1): 35–42

11. Lee Y. & Joo C. 2003. Sound absorption properties of recycled polyester fibrous assembly absorbers. *Autex Research Journal*, 3(2): 78–84

12. Koizumi T., Tsujiuchi N., Adachi A. 2002. The development of sound absorbing materials using natural bamboo fibers. 2002 WIT Press, Ashurst Lodge, Southampton, SO40 7AA, UK

13. Kucuk M. & Korkmaz Y. 2012. The effect of physical parameters on sound absorption properties of natural fiber mixed nonwoven composites. *Textile Research Journal*, 82(20): 2043-2053

14. Lee E.Y. & Joo C.W. (2004). Sound Absorption Properties of Thermally Bonded Nonwovens Based on Composing Fibers and Production Parameters. *Journal of Applied Polymer Science*, 92(4): 2295–2302

15. Li T.T., Wang R., C.W. Lou, J.H. Lin. 2012. Acoustic absorption evaluation of high-modulus puncture resistance composites made by recycled selvages. *Textile Research Journal*, 82(6): 1597-1612

16. Lin J.H., Liao Y.C., Huang C.C., Lin C.C., Lin C.M., Lou C.W. 2010. Manufacturing process of sound absorption composite plank. *Advanced Materials Research*, 97–101: 1801–1804

17. Lin J.H., Lin C.C., Huang C.C., Lin C.W., Su K.H., Lou C.W. 2011. Manufacturing technique of sound-absorbent PET/TPU composites. *Advanced Materials Research*, 239-242: 1968-1971

18. Lin J.H., Huang C.C., Tai K.C., Lin C.C., Chuang Y.C., Lou C.W. 2011. Processing technique of fiber-based composite sound absorbent/thermal-insulating board. Advanced Materials Research, 287-290: 2677–2680

19. Liu X.J., Liu J.L., Xu B.J., Gao W.D. 2012. Acoustic analysis for a sound-absorbing structure with multi-layered porous material. *Journal of Vibration and Shock*, 31(5):106-110

20. Lou C.W., Lin J.H., Su K.H. 2005. Recycling polyester and polypropylene nonwoven selvages to produce functional sound absorption composites. *Textile Research Journal*, 75(5): 390–394

21. Narang P.P. 1995. Material parameter selection in polyester fibre insulation for sound transmission and absorption. *Applied Acoustics*, 45(4): 335–358

22. Yilmaz N.D., Pamela B.L., Powell N.B., Michielsen S. 2011. Effects of porosity, fiber

size, and layering sequence on sound absorption performance of needle-punched nonwovens. *Journal of Applied Polymer Science*, 121(5): 3056–3069

23. Patinha S., Cunha F., Fangueiro R., Rana S., Prego F. 2014. Acoustical Behavior of Hybrid Composite Sandwich Panels. *Key Engineering Materials*, 634: 455-464
24. Shahani F.; Soltani P., Zarrebini M. 2013. Sound Absorptıon Characterıstıcs Of Needled Nonwoven Fabrıcs. The International Istanbul Textile Congress 30 May-1 June 2013, Istanbul, Turkey.
25. Shahani F., Soltani P., Zarrebini M. 2014. The Analysis of Acoustic Characteristics and Sound Absorption Coefficient of Needle Punched Nonwoven Fabrics. *Journal of Engineered Fibers and Fabrics*, 9(2): 84-92
26. Shoshani Y. & Yakubov Y. 1999. A model for calculating the noise absorption capacity of nonwovens. *Textile Research Journal*, 69(7): 519–526
27. Shoshani Y. & Yakubov Y. 2000. Numerical assessment of maximal absorption coefficients for nonwovens. *Applied Acoustics*, 59(1): 77–87
28. Shoshani Y. & Yakubov Y. 2000. Generalization of Zwikker and Kosten theory for sound absorption in flexible porous media to the case of variable parameters. *Journal of Theoretical and Computational Acoustic*, 8(3): 415–441
29. Tai K.C., Chen P., Lin C.W., Lou C.W., Tan H.M., Lin J.H. 2010. Evaluation on the sound absorption and mechanical property of the multi-layer needle-punching nonwoven. *Advanced Materials Research*, 123–125: 475–478
30. Tascan M. & Vaughn E.A. 2008. Effects of Total Surface Area and Fabric Density on the Acoustical Behavior of Needlepunched Nonwoven Fabrics. *Textile Research Journal*, 78(4): 289-296
31. Tascan M., Vaughn E.A., Stevens K.A., Brown P.J. 2011. Effects of total surface area and fabric density on the acoustical behavior of traditional thermal-bonded highloft nonwoven fabrics. Journal of Textile Institute 102(9): 746–751
32. Thilagavathi G., Pradeep E., Kannaian T., Sasikala L. 2010. Development of Natural Fiber Nonwovens for Application as Car Interiors for Noise Control. *Journal of Industrial Textiles*, 39(3): 267-278
33. Voronina N. 1996. Improved empirical model of sound propagation through a fibrous material. *Applied Acoustics*, 48(2): 121-132
34. Wassilieff C. 1996. Sound Absorption of Wood-Based Materials. *Applied Acoustics*, 48(4): 339-356
35. Zulkifli R., Mohd Jailani M.N., Ismail A.R., Nuawi M.Z., Abdullah Sh., Mat Tahir M.F., Ab Rahman M.N. 2009. Comparison of acoustic properties between coir fiber and oil palm fiber. *European Journal of Scientific Research*, 33(1): 144–152
36. Zwikker C. & Kosten C.W. 1949. Sound absorbing materials. Oxford, UK: Elsevier, 1949
37. Martínez-Hernández A.L. & Velasco-Santos C. 2012. Keratin Fibers From Chicken Feathers: Structure and Advances in Polymer Composites. In Keratin: Structure, Properties and Applications. Pp: 149-211, Edited by Dullaart, R. & Mousquès, J. Nova Science Publishers, Inc. New York.

WIND ENERGY POTENTIAL OF THE TURKEY

Bayram KILIÇ, Emre ARABACI

INTRODUCTION

Wind energy is generated due to the different heating of the world surface by the solar radiation. Different heating of the ground surfaces causes the temperature, humidity and pressure of the air to be different, and these different pressure areas cause the air to move from high pressure zones to low pressure zones. This air movement is called the wind. Wind is an indirect product of solar energy. Approximately 2% of the solar energy reaching to the world is converted into wind energy.

The need for renewable energy resources and the use of these resources are increasing in parallel with the depletion of fossil fuel resources. Wind energy is an important part of renewable energy sources. Although there are some limits of wind energy potential, it is a free, reliable and sustainable energy source. Wind energy is the kinetic energy of the air flow forming the wind and the sun is caused by different heating of the ground surfaces. Wind power is one of the most growing renewable energy resources in the world today. Many countries are planning to meet 12% of the electricity demand in 2020 from wind energy. In the near future, there will be 10.6% of the total installed production power of Europe. The energy to be generated from wind power will correspond to the needs of approximately 34 million houses and 86 million inhabitants [1].

The most important advantages and disadvantages of wind energy are given below.

Advantages:

- • Non-release of gases with polluting effects
- • Having a clean energy source
- • Not exhausted
- • Easy installation and operation of wind plants compared to other facilities
- • High reliability
- • Be local

Disadvantages:

- • The amount of energy generation is not constant as there is no continuity of the wind
- • Large area coverage of wind turbines
- • Noise pollution formation
- • Low energy production compared to energy from fossil and nuclear fuels
- • High investment costs

WIND TERMINOLOGY

Wind speed: The amount of electrical energy a wind turbine can generate depends largely on the wind speed. For example; while the wind speed is doubled, the power to be produced increases eight times. The wind always shows changing wave characteristics in very small periods. The magnitude of the change depends on both air and surface conditions and obstacles. Wind speeds are reduced due to friction in the lower layers of the atmosphere. This situation causes the roughness of the land and the obstacles. The greater the roughness, the lower the wind. The water surface is the least affected surface.

Wind's daily change: In many places on earth, the day is windier than the nights. The main reason for this is that the temperature difference between sea surface and ground surface is more than daytime. This condition provides an important advantage because energy are produced and consumed more than daytime.

Wind acceleration (peak effect): High peaks are the most suitable places where turbines can be placed. When the turbine is placed on the hills, winds can be used coming from all directions. In addition, wind speeds on the hills are generally higher than the surrounding lands. Although the wind speed is high on smooth and rough hills, turbulence is a significant disadvantage.

Tunnel effect: Wind speed increases if air gets trapped between buildings and mountains. This is called a tunnel effect. This effect is mostly observed in buildings or narrow mountain passages. If the wind speed is 6 m/s in open terrain, it can reach 9 m/s due to natural tunnel effect. In such places, high efficiency can be achieved with wind turbine layout. However, due to high wind speed, turbulence may occur due to the roughness of the terrain. Turbulence can cause turbulence and deterioration in wind turbine.

Wind turbulence: Turbulence is a non-regular wind flow. Very hilly and rough terrain creates too much turbulence. Turbulence decreases the energy production efficiency in the wind turbine from wind and it is causes wear and damage in the turbine. One reason for the high towers is to avoid turbulence and generate more electricity. Turbulence in the seas is less common. Therefore, turbines installed in the sea have a longer life.

WIND ENERGY IN TURKEY

It is known that Turkey's energy resources are limited. In the near future, it is also important to note that these limited resources cannot meet the ever-increasing energy needs and that new resources should be used as soon as possible for energy production. The first requirement to benefit from wind energy is to determine the wind energy potential and wind characteristics of the region. It is important to make both academic studies and meteorological foundation in this subject. Coordinating the work done to date and accelerating the works to be done in larger areas, Turkey 'will affect in a positive sense to take advantage of wind energy.

Turkey has a very serious potential for wind energy. The estimated potential is about 60.000 MW. The wind power plants, which were first built in 1998, had a total installed capacity of 8.7 MW. Until 2005, this table was quite stable and did not receive enough attention. However, in 2005, when the parliament addressed the issue, the law, which introduced renewable energy sources in electricity generation, passed through the general assembly of the assembly. Between 2005 and 2009, there was an increase of 500 MW. In 2010, the renewable energy resources law, which will be able to pave the way for these investments and direct investors to this field, has entered into force. Investments have gained momentum in the last 2-3 years and have exceeded 2.000 MW as of July 2012. Turkey's total installed capacity of 56 471 MW. The share of the wind is around 3.5%. 114 projects are licensed by the Energy Market Regulatory Authority (EPDK) and 94 projects are awaiting license. The target until 2023 is to reach 20,000 MW in wind power capacity.

Potential determination studies for wind power plants built by public and private sector show that the potential in Turkey is quite enough. According to the records of Turkish State Meteorological Service, the average wind speed was 8.5 m/s in the direct wind measurements. The reason for this is that the wind can vary greatly in short intervals and small areas depending on both meteorological and topographic structure. As seen in Table 1, Turkey has the largest wind potential (10 m altitude) in the Marmara region [2].

Table 1. Wind Energy Potential of Turkey

Region Name	Average Wind Power Density (W/m^2)
The Mediterranean	21.36
Central Anatolia	20.14
Aegean	23.47
Black Sea	21.31
Eastern Anatolia	13.19
Southeastern Anatolia	29.33
The Marmara	51.91

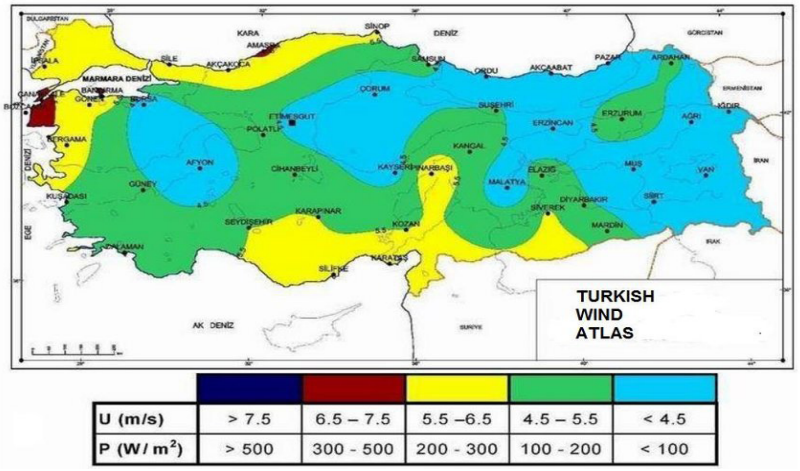

Figure 1. Wind Atlas Turkey [3]

WIND ENERGY ANALYSIS

The following equations can be used for wind energy applications. When wind energy is considered as kinetic energy, the flux (E) is equal to the mass of the moving air and the square of the velocity.

$$E = \frac{1}{2} m.V^2 \tag{1}$$

It is almost impossible to measure the mass of moving air in the above formula. Therefore we can find the volume from in terms of aero-dynamic volume. So we get a mass volume.

$$E = \frac{1}{2} \rho .v.V^2 \tag{2}$$

If we refer to the volume v , A gives the vertical control section and L gives the horizontal distance. Here is written and the following formula is obtained.

$$E = \frac{1}{2} \rho .A.t.V^3 \tag{3}$$

In practice, wind energy is obtained per vertical unit area as follows.

$$E_U = \frac{1}{2} \rho .V^3 \tag{4}$$

The density of the air is considered to be 1.263 kg/cm^3 at sea level.

$$E = a.V^{b} \tag{5}$$

Where a=0.62, b=3 for the parameters a and b. Wind energy is expressed in terms of average speed;

$$E = \frac{1}{2}\rho\,(\overline{V}^{3} + 3\overline{V}\sigma_{e}^{2}) \tag{6}$$

$$V = \overline{V} + \varepsilon \tag{7}$$

$\overline{V}$ =average speed, ε=instability, σ_e=standard wind speed deviation

$$P_a = M(V_1 - V_2)\overline{V} \tag{8}$$

Here, *M* is the air from unit of time, V_1 and V_2 are wind speeds.

The kinetic energy change in the wind can be written as follows.

$$E_k = \frac{1}{2}M(V_1^2 - V_2^2) \tag{9}$$

As a result, we can write the wind power as follows [4-6].

$$P = \rho.A.\overline{V}(V_1 - V_2)\overline{V} \tag{10}$$

Further

$$P = \rho.A.\overline{V}^{2}(V_1 - V_2) = \rho.A(\frac{V_1 + V_2}{2})^{2}(V_1 - V_2) \tag{11}$$

or

$$P = \rho.\frac{A.V_1^{3}}{4}[1+\alpha)(1-\alpha)] \tag{12}$$

$$\alpha = \frac{V_2}{V_1} \tag{13}$$

SAMPLE APPLICATION

This study was made to evaluate short of Turkey's wind energy potential. At the end of the evaluation, an application was made on the wind energy potential of Burdur province. The wind speed values of Burdur province are given in Table 2. The rotor diameter of the turbine to be used in the wind power plant is 48 m. The density of air in this location is 1.263 kg / m3. The electrical energy that can be produced in this plant is determined as follows.

Table 2. Wind Speed Values of Burdur Province

Month	Wind Speeds (m/s)
January	2.1
February	3.2
March	2.4
April	1.9
May	1.7
June	1.8
July	1.8
August	1.7
September	1.9
October	2.7
November	2.6
December	3.3

$$A \quad \frac{.D^2}{4} \quad \frac{3.14.(48^2)}{4} \quad 1808.64m^2$$

P_{jan}	$1.263x1808.64x(2.1^3)x\frac{8}{27} \quad 6268kW$
P_{feb}	$1.263x1808.64x(3.2^3)x\frac{8}{27} \quad 22178kW$
P_{mar}	$1.263x1808.64x(2.4^3)x\frac{8}{27} \quad 9356kW$
P_{apr}	$1.263x1808.64x(1.9^3)x\frac{8}{27} \quad 4642kW$
P_{may}	$1.263x1808.64x(1.7^3)x\frac{8}{27} \quad 3325kW$

P_{jun}	$1.263x1808.64x(1.8^3)x\frac{8}{27}$	$3947kW$
P_{jul}	$1.263x1808.64x(1.8^3)x\frac{8}{27}$	$3947kW$
P_{aug}	$1.263x1808.64x(1.7^3)x\frac{8}{27}$	$3325kW$
P_{sep}	$1.263x1808.64x(1.9^3)x\frac{8}{27}$	$4642kW$
P_{oct}	$1.263x1808.64x(2.7^3)x\frac{8}{27}$	$13322kW$
P_{nov}	$1.263x1808.64x(2.6^3)x\frac{8}{27}$	$11895kW$
P_{dec}	$1.263x1808.64x(3.3^3)x\frac{8}{27}$	$24323kW$

Table 3. Estimated Production Values of Wind Energy in Burdur Province

Month	**Wind Speeds (m/s)**	**Energy Production (kW)**
January	2.1	6268
February	3.2	22178
March	2.4	9356
April	1.9	4642
May	1.7	3325
June	1.8	3947
July	1.8	3947
August	1.7	3325
September	1.9	4642
October	2.7	13322
November	2.6	11895
December	3.3	24323

Table 3 shows that the highest energy value obtained from wind in Burdur province is 24323 kW in December. It is estimated that there will be mini-

mum energy production with 3325 kW in May and August. The annual total energy production value calculated for a single selected turbine is 99275 kW.

CONCLUSIONS

As a result, the evaluation of this resource has an important place in terms of both humanity and our country. The state should be directed to domestic and foreign investors through laws and various incentive mechanisms. Co-ordination between relevant governments agencies should be aimed at increasing the installed capacity in wind energy through various cooperations in the sector, at the same time, the steps to be taken in domestic turbine production should be accelerated. It is necessary to provide the necessary investments in order to achieve the determined targets. One of the ways to reach an independent and stronger position in energy is through wind power.

A brief summary is made of Turkey's wind energy potential. In addition, an application was made on the wind energy potential of Burdur province. In this study, the amount of energy produced was determined by a wind turbine in Burdur province. The study shows that the amount of energy can be obtained from a single wind turbine is 99275 kW. Therefore, in case of adequate investment, the potential of wind energy in Burdur province is highly promising.

REFERENCES

1. [1] Kılıç, B. Evaluating of Renewable Energy Potential in Turkey. International Journal of Renewable Energy Research, 4, 259-264, 2011.
2. [2] Kılıç, B., Şencan, A., İpek, O. Evaluating of Solar and Wind Energy in Isparta and İzmir. The Second International Conference on Nuclear and Renewable Energy Resources, Ankara, 928, 2010.
3. [3] http://www.mgm.gov.tr/ (Erişim Tarihi:22.02.2017)
4. [4] Kaygusuz, K., Sar, A. Renewable energy potential and utilization in Turkey. Energy Conversion and Management, 44, 459-478, 2003.
5. [5] Turkish Industrialists' and Businessmen's Association (TUSIAD).Turkey's energy strategy on the brink of the 21st century: An overview, M.O. İstanbul, Turkey, 1998.
6. [6] Duran, Ş.A., Dincer, İ., Rosen, M.A. Thermodynamic analysis of wind energy. Int. J. Energy Res. 30, 553-566, 2006.

CHAPTER 13

COD REMOVAL FROM GREY WATER USING NF270 MEMBRANE

Duygu KAVAK[1]

1.Introduction

Grey water is defined as wastewater from bathtub, shower, hand basins, washing machines, dishwashers and kitchen sinks (Fountoulakis et al., 2016). Grey waters can be classified in two groups: less polluted grey water and very dirty grey water. Few dirty grey water include wastewater from the shower, bath and washbasin. Very dirty grey water include wastewater from the kitchen and washing machine (Üstün and Tırpancı, 2015). Grey water constitutes the largest percentage (75%) of domestic wastewater (Thirugnanasambandham et al., 2014). Pollutants in grey water are caused by personal care products, detergents and body contamination. Discharging untreated grey water into the receiving environment causes harmful effects on living organisms and humans. For this reason, there is an increasing interest in the treatment of grey water in many parts of the world. Methods applied for grey water treatments include physical, chemical, and biological systems (Li et al., 2009; Hocaoglu and Orhon, 2013). There are advantages and disadvantages of these methods.

Membrane technology, which is known to be environmental friendly, has ease of construction and control, low consumption of energy, no requirement of chemical substances to be added and is feasible for recovery of valuable metals. Among pressure-driven membrane processes, NF has been found to be very effective for wastewater treatment (Couto et al., 2017; Licínio et al., 2015).

Thin film composite (TFC) membranes are considered as efficient for treatment of wastewater (Ismail, et al. 2015). TFC membrane which is used in this study consists of a dense ultrathin barrier layer, typically 0.2 mm thick on top of a microporous polysulfone supported by interfacial polymerization with different chemical compositions (Kuzu and Kavak, 2018; Scott, 1995; Menne, et al., 2016; Xia, et al. 2018). The superior properties of these membranes are that they operate at higher flux and lower pressure, have greater chemical stability so they are not biodegradable and have higher salt rejection (Scott, 1995; El-Arnaouty, et al., 2018).

Chemical oxygen demand (COD) is one of the most important parameters used in determining the pollution degree of domestic and industrial waste-

1 Department of Chemical Engineering, Faculty of Engineering and Architecture, Eskişehir Osmangazi University

water. The membrane processes provided the highest COD removal from waste water (Madaeni, and Mansourpanah, 2006).

In this study, chemical oxygen demand (COD) removal from washing machine grey water by cross-flow nanofiltration method using thin film composite NF270 polymeric membrane was investigated. In order to determine the effect of feed temperature and membrane pressure on COD removal, grey water was passed through NF270 membrane at different membrane pressures (10 and 15 bar) and feed temperatures (25 and 35^{o}C).

2.Material and Methods

Grey water is taken from a laundry company in Eskişehir, Turkey. The characteristics of grey water are shown in Table 1.

Table 1. Properties of raw grey water

Parameter	**Value**
COD, mg/L	3880
Max. Absorbance, nm	328
Ph	9.68
Conductivity, µS/cm	853

Polyamide thin film composite NF270 commercial nanofiltration membrane was used in the experiments. NF270 commercial thin film composite nanofiltration membrane was obtained from DOW FILMTEC™. Table 2 shows the properties of the NF270 membrane **(**http://www.sterlitech.com/membrane-process–development/flat-sheet-membranes).

Table 2. Specific properties of the NF270 membrane

Properties	NF270 membrane
Type	Organic matter removal, water softening
pH	2-11
Flux (GFD)/psi	72.0-98.0/130
$MgSO_4$ Rejection	%99.2
Pore size/MWCO	~200-400 Da
Polymer	Polyamide-TFC

Cross-flow nanofiltration system was used in the experimental study. A schematic representation of the system is given in Figure 1. This system is formed by a membrane module, a hydraulic hand pump, a feed tank, a high pressure pump, an analytical balance for the measurement of flux, a computer, a thermostat, a flowmeter, and other necessary fittings The effective area of the membrane in the system is 150 cm^2. Temperature is controlled by Wise-Circu heater in the system. This heater is used to keep the waste water in the supply tank at the desired temperature levels (Kavak 2017a; Kavak 2017b).

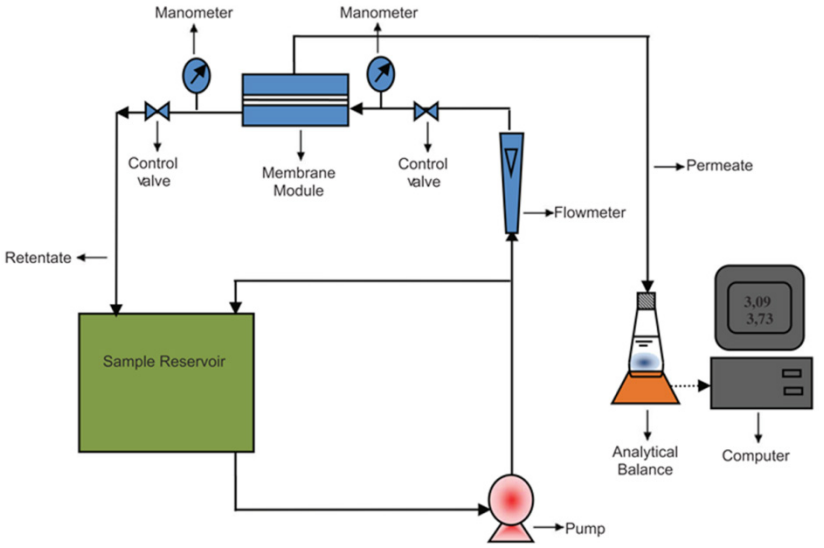

Figure 1. Schematic diagram of the cross-flow NF experimental set-up.

COD test kits were used to determine the chemical oxygen demand from grey water. Test kits were opened and a 2 ml waste water sample as added. The kits placed on the Hach LT 200 thermoreactor were stored at 148°C for 2 hours. After 2 hours the kits were removed from the thermoreactor and allowed to cool to room temperature. COD was analyzed using the Hach Lange DR 3900 UV-vis spectrophotometer. COD removal (%R) was calculated as Eq. (1)

where C_p (mg/L) and C_f (mg/L) represent the COD concentrations in the permeate and in the feed solution, respectively.

3. Results and Discussion

COD removal is given in Fig. 2. It was observed that COD removal did not change significantly with increasing temperature and pressure. According to Fig. 2, the maximum COD removal was obtained as 96.70% at 25˚C and 10 bar.

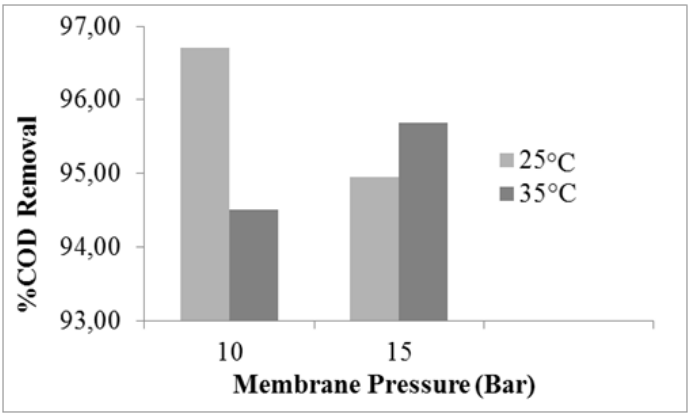

Fig. 2. COD removal of grey water (feed temperature: 25ºC and 35ºC, membrane pressure: 10 and 15 bar).

COD and pH values of permate after filtration are shown in Table 3.

Table 3. COD and pH values of the permeate

Parameters	COD (mg/L)	pH
10 bar, 25°C	128	9.96
10 bar, 35°C	213	9.71
15 bar, 25°C	196	9.56
15bar, 35°C	167	9.69

According to the Water Pollution and Control Regulation in Turkey, COD value should be below 180 mg/L for 2 hour composite sample (http://www.mevzuat.gov.tr/). The COD concentration after filtration was found as 128mg/L at 25°C and 10 bar pressure conditions. Similarly, the COD concentration after filtration was found as 167mg/L at 35°C and 15 bar pressure conditions. Under these conditions, the COD discharge limit is lowered.

4. Conclusions

In this study, COD removal from grey water by cross-flow nanofiltration method using NF270 membrane was investigated. As a result of the experiments, COD removal efficiencies were observed to be quite high (>94.50%). Increasing pressure and temperature did not affect COD removal significantly. The maximum COD removal was obtained as 96.70% at 25˚C and 10 bar. pH values were at the range of 9.56-9.96 at 25˚C and 35˚C.

After the experiments, COD concentrations remaining in permate are found to be lower than the discharge values defined for domestic wastewater by Water Pollution and Control Regulation in Turkey. According to the experimental results, NF 270 membrane is efficient for COD removal from grey water.

Acknowledgements

In this study, devices and tools bought by Eskişehir Osmangazi University Research Foundation were used (Project Number: 201215031).

5. References

1. Couto C. F., Marques L. S., Amaral S. M. C. and Moravia W. G., Coupling of nanofiltration with microfiltration and membrane bioreactor for textile effluent reclamation, Separation
2. Science and Technology (2017), 52(13), 2150–2160.
3. El-Arnaouty, M., Ghaffar, A. A., Eid, M., Aboulfotouh, M. E., Taher, N., & Soliman, E.-S. (2018). Nano-modification of polyamide thin film composite reverse osmosis membranes by radiation grafting. Journal of Radiation Research and Applied Sciences, 11(3), (2018) 204-216.
4. Fountoulakis M.S. Markakis N. Petousi I. Manios T., Single house on-site grey water treatment using a submergedmembrane bioreactor for toilet flushing Science of the Total Environment 551–552 (2016) 706–711.
5. Hocaoglu S. M. Orhon D. Particle Size Distribution Analysis of Chemical Oxygen Demand Fractions with Different Biodegradation Characteristics in Black Water and Gray Water Clean – Soil, Air, Water (2013), 41 (11), 1044–1051.http://www.mevzuat.gov.tr/ (Erişim Tarihi: 06.11.2018) http://www.sterlitech.com/membrane-process–development/flat-sheet-membranes (Erişim tarihi: 04.11.2018)
6. Ismail, A., Padaki, M., Hilal, N., Matsuura, T., & Lau, W. Thin film composite membrane—Recent development and future potential, Desalination 356, (2015) 140-148.
7. Kavak D. Treatment of dye solutions by DL nanofiltration membrane, Desalination and Water Treatment 69(1) (2017a) 116-122.
8. Kavak D. Removal of Iron, Copper and Zinc Mixtures from Aqueous Solutions by Cross Flow nanofiltration, Fresenius Environmental Bulletin, 26(1a) (2017b) 1101-1107.
9. Kuzu E. K., Kavak D. Investigation Of The Use Of Thin Film Polymeric Composite DK Membrane For COD Removal From Textile Industrial Waste Water, IV. International Ege Composite Materials Symposium Proceedings Book (2018) 459-467.
10. Li F. Wichmann K. Otterpohl R. Review of the technological approaches for grey water treatment and reuses, Science of the Total Environment 407 (2009) 3439–3449.
11. Licínio M. Gando-Ferreira Joana C. Marques and Margarida J. Quina, Integration of ion-exchange and nanofiltration processes for recovering Cr(III) salts from synthetic tannery wastewater, Environmental Technology 36(18) (2015) 2340–2348.

12. Madaeni, S., and Mansourpanah, Y. Screening membranes for COD removal from dilute wastewater, Desalination (197), (2006) 23-32.

13. Menne, D., Üzüm, C., Koppelmann, A., Wong, J. E., Foeken, C. V., Borre, F., Dähne L. Laakso T.. Pihlajamäki A., Wessling M. Regenerable polymer/ceramic hybrid nanofiltration membrane based on polyelectrolyte assembly by layer-by-layer technique, Journal of Membrane Science (520), (2016) 924-932.

14. Scott, K. (1995). Handbook of Industrial Membranes. Oxford, UK: Elsevier Advanced Technology, p.904.

15. Thirugnanasambandham K. Sivakumar V. Prakash Maran J. S. Kandasamy, Chitosan based grey water treatment—A statistical design approach Chitosan based grey water treatment—A statistical design approach, Carbohydrate Polymers 99 (2014) 593– 600.

16. Üstün, G. and E. Tırpancı A. Gri Suyun Arıtımı ve Yeniden Kullanımı.Uludağ Üniversitesi Mühendislik Fakültesi Dergisi, 20(2), (2015) 119-139.

17. Xia, L., Ren, J., Weyd, M., & McCutcheon, J. R.. Ceramic-supported thin film composite membrane for organic solvent nanofiltration. Journal of Membrane Science, (2018), 563 857-863.

CHAPTER 14

ENVIRONMENTAL AND ECONOMICAL ANALYSIS OF CO_2 EMISSIONS FROM MOTOR VEHICLES

Emre ARABACI, Bayram KILIÇ

INTRODUCTION

The number of vehicles in all over the world is increasing every year. While the number of vehicles in the world was approximately 0.93 billion in 2006, this number increased by 35% to 1.35 billion after a decade. 71% of these vehicles are passenger vehicles. According to this trend, it is estimated that the number of vehicles will be over 2 billion for the year 2030 (Figure 1) (Number of vehicles-World, 2018).

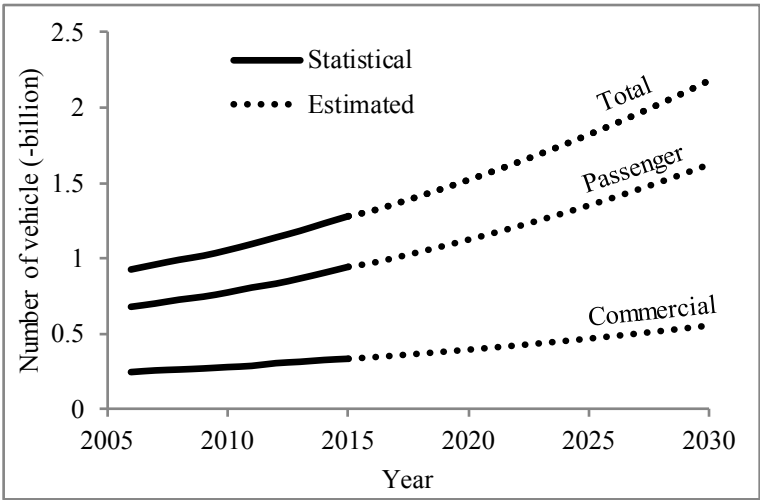

Figure 1. Trends in the number of vehicles in the world (Number of vehicles-World, 2018)

Every year, the number of vehicles in the world increases by approximately 3.6%. However, until the 1950s, emissions from motor vehicles in the world were less than they were today (Pulkrabek, 2014). The concept of "air pollution" has emerged as a result of the pollutant emissions caused by the increase in world population, industrial plants, power plants and number of vehicles (Halderman, 2015).

The main factor in the formation of air pollution is combustion. Nowadays, petroleum-based fuels are frequently used because of their advantages such as logistics, distribution and storage. In most of today's vehicles, internal combustion engines using petroleum-based fuels are used as energy sources and such vehicles are called "motor vehicles" (Kelen, 2014). Especially the

vehicles used in urban areas are the primary source of air pollutants for the region. When used at low speeds, motor vehicles generate more pollutant emissions (Hao, 2017). Due to the short distance and frequently changing load and speed demands, and consequently the use of variable gear positions, there is a significant increase in fuel emissions as well as exhaust emissions. The change of vehicle speed and load demands on intercity roads is quite low compared to the urban area. Also, considering the environmental structure, motor vehicle emissions on intercity roads are partially disposable. Due to the large number of buildings in the urban areas, lack of green areas, heavy traffic and slowly traffic, motor vehicle emissions are very high and cannot be disposed of most of the time.

There is a logarithmic relationship between the population and the number of vehicles. While the vehicle density was 10 people/vehicle in 2006, it became 8 people/vehicle in 2016. The vehicle density for 2030 is estimated as 5 people/vehicle (Figure 2).

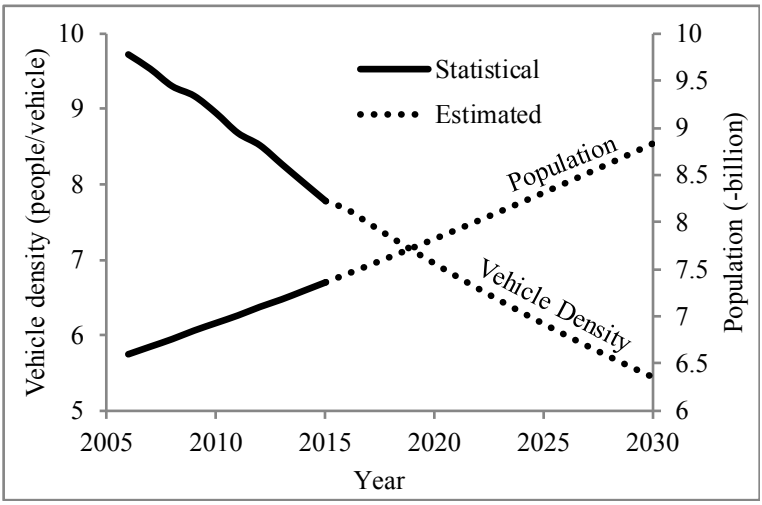

Figure 2. World population and vehicle density (World Population, 2018).

With the development of technology, new emission control strategies are designed (Uyumaz, 2017). The main reason for the development of these strategies is the mandatory requirements of vehicle emission standards for reducing vehicle exhaust emissions as a requirement of international environmental protocols such as Montreal and Kyoto (Environmental Protocols of Turkey, 2018).

As for everything in nature, there is also a lifetime (or life cycle) for motor vehicles. An effective emission standard only affects the aftermath. It is in theoretically and practically impossible to use an emission reduction system or a new emission standard on all vehicles currently in use. Compared to the total number of vehicles, the number of new vehicles registered for traffic every year is very low (Mitropoulos, 2015). For example, in 2015, there are 947 million motor vehicles in the world, while the number of new motor vehi-

cles produced and registered in the world in the same year is only 90 million (Global Vehicle Production, 2018). However, considering that the number of vehicles in the previous year is 907 million, it is seen that only one of the two vehicles produced replaces the old one. In other words, when compared to the number of vehicles, the emission control technology used in new motor vehicles for 2015 was only 5% on all motor vehicles' emissions. Assuming a system that reduces emissions by 10% to a very optimistic approach is used in vehicles, this effect is seen as 5% of 10% (=0.5%). Another issue that has been ignored is the fact that the annual frequency of use of motor vehicles (km/year) is increasing every year, although there is no complete statistical information. The fuel consumption and exhaust emissions are also increasing due to the use of vehicles on a yearly basis. The situation of the use of vehicles at very low speeds (urban traffic) or at high speeds (intercity traffic) is another issue that is ignored. It is also possible to apply usage restrictive and monetary and punitive regulations such as emission-based taxation (Alberini, 2018).

Thanks to the combustion occurring in motor vehicles, exhaust emissions, which are composed of incomplete and complete combustion products at different concentrations, are released to the environment in a controlled manner (Pulkrabek, 2004). The concentration of the mixture (a rich or a poor mixture depending on the air/fuel ratio) is generally a condition that changes with the engine speed and load, which directly affects the exhaust emissions concentrations of motor vehicles (Figure 3). In addition, because of the use of carbon-based fuels in motor vehicles, emissions are expressed as CO_2 equivalent. In a combustion event, CO_2 is a complete combustion product. CO_2 is released into the atmosphere during the breathing process, which is routinely performed by humans and other creatures to survive. In this respect, the emission of human is CO_2.

CO_2 is called greenhouse gas because of its ability to absorb heat from the air. The effects of emissions from motor vehicles are more clearly observed if they are expressed in terms of CO_2 equivalent rather than individually expressed. However, considering that CO_2 is a complete combustion product, it can be said that there is a strong correlation between CO_2 and fuel consumption (Akın, 2006).

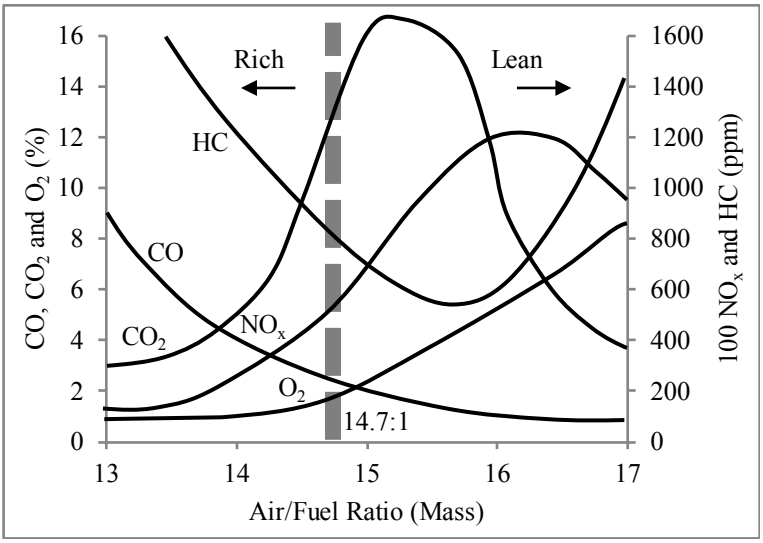

Figure 3. Motor vehicles emissions (Halderman, 2015)

The pollutants the vehicles have spread to the atmosphere in the simplest definition. The emission standards of motor vehicles vary by country and the vehicles are evaluated according to the standards of the countries in which they are used. However, vehicle emission standards are applied with more stringent rules every year. In all emission standards, the limits of harmful gases that generate pollutant emissions from motor vehicles are determined. However, as a general approach, emissions from motor vehicles are again expressed as CO_2 equivalents.

THE MEANING OF CO_2 EMISSIONS IN MOTOR VEHICLES

Carbon-containing fuels are generally used in motor vehicles. With the burning of this fuel, various gases are released. It is desirable that complete combustion occurs in all combustion processes. As an example, the combustion of iso-octane (C_8H_{18}) fuel with theoretical air (21% O_2 and 79% N_2) is as stoichiometric as follows (Arabacı, 2014).

C_8 H_18+12.5(O_2+3.76N_2)→8CO_2+9H_2 O+47N_2

According to this combustion equation, 15.05 kg of air (3.51 kg O_2 and 11.54 kg N_2) are required for 1 kg C_8H_{18}. As a result of full combustion, 3.09 kg CO_2, 1.42 kg H_2O and 11.54 kg N_2 are formed. In case of partial or incomplete combustion, gases such as CO_2 and NO_x are also released. For example, the combustion equation of LPG ($C_{3.7}H_{9.4}$) fuel determined in the approximate stoichiometric ratio in a single cylinder engine is as follows (Arabacı, 2014).

C_3.7 H_9.4+6.09(O_2+3.76N_2)
→3.32CO_2+0.38CO+4.70H_2 O+0.22O_2+22.88N_2

The emission values measured by emission devices and the limitations on emission standards are considered to be only legal requirements. Carbon-contining fuels can be referred to as CO_2 equivalent. Although new emission standards are regulated for vehicles over the years, the classification of CO_2 emissions, which is an indicator of fuel consumption, does not change. Low CO_2 emissions means low fuel consumption.

The emission classification may vary depending on the emission standards adopted by countries. The emission class shown in Table 1 is A, B1, B2, ..., F4, F5, G. Nowadays, countries may prefer to apply extra taxation or tax reduction according to the emission values of vehicles. For this reason, Table 1 is revised and CO_2, HC, CO, NO_2 and PM values can be classified and tax or tax deductions can be arranged (Table 2). In such arrangements, the desire to disseminate electric vehicles is an important factor.

Table 1. CO_2 emission classification (Classification of Vehicle Emissions, 2018)

Emission Class	CO_2 Limit (g/km)				
	1	2	3	4	5
A			<100		
B	101	106	111	116	121
	105	110	115	120	125
C	126	131	136	141	146
	130	135	140	145	150
D	151	156	161	166	171
	155	160	165	170	175
E	176	181	186	191	196
	180	185	190	195	200
F	201	206	211	216	221
	205	210	215	220	225
G			>225		

Table 2. Tax based emission classification (Emission Tax, 2018)

Emission Class	Emissions					(-)degression (+)extra tax ($)
	PM (mg/km) and others (g/km)					
	CO_2	HC	CO	NO_x	PM	
A1	<90	<0.02	>0.15	>0.007	=0	-20000
A2	91	0.021	0.151	0.0071	0.01	-10000
	125	0.036	0.19	0.013	0.3	
B	126	0.0361	0.191	0.0131	0.31	0
	160	0.052	0.27	0.024	0.50	
C1	161	0.0521	0.271	0.0241	0.51	+10000
	185	0.075	0.350	0.03	2.0	
C2	>185	>0.075	>0.350	>0.03	>2.01	+20000

The "vehicle emission label" is prepared for the vehicles produced, showing the fuel consumption and emission values. The CO_2 emission value used in this emission label is calculated based on the combined fuel consumption. Therefore, the CO_2 emission value used in these label is also an average value. The fuel consumption of vehicles and emission values related to this fuel consumption are determined by driving cycles such as NEDC and WLTP, which are arranged as simulation of real driving conditions (Barlow, 2009). Driving cycles are the concentrated state of actual driving conditions. These driving cycles can be designed depending on the distance or depending on the time. Combined fuel consumption and emission values can be determined in all driving cycles in the urban (low speed and stop-and-go), intercity (high speed and low speed) and their average.

The CO_2 emission of a vehicle can be calculated by the following equation (Teixeria, 2018).

$$E\_(CO\_2) = \frac{(A.c\_fuel)}{100} \quad (3)$$

Here, , and A represent the amount of CO_2 emission (g/km), fuel consumption (L/100km) and CO_2 multiplier for fuel, respectively. For example, the fuel CO_2 factor is 2640 g/L, 2392 g/L, 1665 g/L and 2252 g/L for diesel, gasoline, LPG and CNG, respectively. These values are the calculated values for full combustion at the stoichiometric ratio of fuels. This value can be calculated in different ways as shown in Eq. 4 (Teixeria, 2018).

$$E\_(CO\_2) = \frac{(A.c\_fuel)}{100} \quad (4)$$

Here, and represent the mass C ratio (%) and fuel density (kg/L) in the fuel, respectively. Eq. 3 or Eq. 4 can be used frequently to calculate the amount of emissions.

CONTROL STRATEGIES OF THE VEHICLE EMISSIONS

Nowadays, many strategies are applied to reduce emissions from motor vehicles and keep them under control within certain limits. The first systems that come into the mind are, but are not limited to, catalytic converter, particle filter and EGR (Halderman, 2015).

As is known, emissions from motor vehicles are caused by combustion and the concentration of pollutant gases after combustion varies according to the quality of the combustion process (Halderman, 2015). The emission control in the engines starts with the temperature measurement and the temperature values contain a lot of information. Engine coolant temperature, intake air temperature, fuel temperature and oil temperature measurement contain a lot of information about combustion. It is impossible to achieve emission control with only temperature data. Sensors such as the throttle position sensor, manifold absolute pressure sensor, mass flow sensor and oxygen sensor are also sensors that control the combustion directly or indirectly. Through the parameters obtained from all these sensors, it is desired to operate at optimum level in terms of performance, economy and environment under different operating conditions of the engine (Uyumaz, 2017).

There are also emissions that are not caused by combustion in motor vehicles. Evaporative emission control system is used to prevent the formation of hydrocarbons due to fuel evaporation. This system has carbon canister for holding fuel vapor. NOx emissions are generated especially in diesel engines with the effect of high combustion temperatures. In order to prevent these NOx emissions, the combustion temperature must be kept under control. NOx emissions are converted to nitric acid (HNO_3) when combined with water vapor when thrown into the atmosphere (Jiang, 2016). For this reason, some of the exhaust gases are taken into the cylinder and the combustion characteristic is deteriorated in a controlled way and the combustion temperature is kept at the desired level. This system is an exhaust gas recirculation (EGR) system and as a general definition it is to connect intake and exhaust manifolds. The EGR system is not required when the engine is idling and the engine is cold (Xie, 2017).

Piston rings cannot always guarantee excellent sealing. Exhaust gas can escape from the piston to the crankcase between the piston and the cylinder. Discharging these hydrocarbons into the atmosphere again causes air pollution. To avoid this situation, a positive crankcase ventilation (PCV) system has been developed and the gases accumulated in the crankcase (especially unburned HCs) are fed back to the intake system and burnt. Similarly, the secondary air injection (SAI) system provides the air required for the oxidation process in the exhaust manifold or in the catalytic converter (Halderman, 2015).

Catalytic converters ensure that the products formed after combustion become non-hazardous products by means of a certain heat treatment and are removed from the exhaust system. The efficiency of the catalytic converter depends on the fuel to the stoichiometric ratio of the air/fuel ratio. In order for the catalytic converter to operate efficiently, it is necessary to continuously measure the excess air through the oxygen sensor. Catalytic converters generally convert CO, HC and NOx emissions into H_2O and CO_2 (Michel, 2017).

ENVIRONMENTAL ANALYSIS OF CO_2 EMISSIONS

Because of the nature of life, breathing biological organisms release CO_2 from the air and release CO_2 into the atmosphere. Generally, it consumes 7-8 liters of air in 1 minute (Carbondioxide from Humans, 2018). When a simple calculation, a person consumes 10 liters of air per day. Considering that the amount of O_2 in the air is 21%, the amount of O_2 consumed in 1 day is 2.1 liters (2.8 kg). Assuming that the average room is 12 m^2 and its height is 2.5 m, the total volume of the room is 30 m^3. Assuming that the volume occupied by 20%, there are 24 m^3 of air (=5 m^3 of O_2) in the room. Assuming 8 hours a day in the same room and no fresh air intake into the room, the amount of oxygen in the room is reduced by 14% after 8 hours. At the end of 2 days, it will be impossible to breathe because the amount of oxygen in this room will drop below 16%. It is about 3.8 kg/day when the CO_2 emission of an adult person is 1 day.

In general, the CO_2 emissions of a passenger vehicle can be considered to be approximately 130 g/km and the average fuel consumption of this vehicle is 5.6 L/100 km. According to this emission value, when a vehicle moves 30 km, it releases CO_2 into the atmosphere as an adult man releases to the atmosphere in one day. With the assumption that this vehicle is used only 30 km/day between home and work, it can be said that human source the CO_2 emissions produced by humankind have doubled.

Even though this picture looks very frightening, the photosynthesis event, which balances this situation, relieves the world a little. Because it is known that a tree produces 114 kg of O_2 per year (Carbon and Tree, 2018). In other words, a tree eliminates 156 kg of CO_2 per year. In this regard, about 9 trees are needed to eliminate the CO_2 emissions of a human. Assuming that a vehicle is used for 15000 km/year, the amount of CO_2 emissions is about 2000 kg/year. This means that about 12 trees are needed for this vehicle. These values are ideal values and CO_2 emissions are much higher than these values.

An urban bus produces about 5 times more CO_2 emissions than a regular passenger car. However, on the other hand, the passenger car carries about 10 times more passengers. This value can be up to 80 times when it is taken into consideration that the automobiles used alone and the buses carrying the passengers are taken into account. The most optimistic table and CO_2 emissions from compulsory transport, such as work-home, school-house, are reduced by half when using public transport. By using urban electric transport such as subway, the CO_2 emission value resulting from compulsory transport can be approached to zero.

The amount of CO_2 emissions for vehicles varies with the amount of fuel consumed. In this regard, the CO_2 equivalent of each liter of fuel sold is approximately known. For example, in Turkey, the daily average of 40 million liters of fuel (gasoline+diesel fuel) sales are realized (Fuel Consumption, 2018). Considering these values, only the environmental threat arising from motor vehicles becomes clearer.

ECONOMICAL ANALYSIS OF CO_2 EMISSIONS

Vehicle preferences are generally carried out either in terms of economy or performance. In terms of economy, fuel consumption is low and CO_2 emissions are low. In terms of performance, the situation is the opposite. However, the only parameter here is not the CO_2 emission value. As is known, CO_2 emissions in vehicles are expressed as g/km. Therefore, it is necessary to determine the economic value of CO_2 emissions from a vehicle as follows.

$$F_{CO2} = \frac{E_{CO2}).x_{y}.t}{1000} \qquad (5)$$

Here (g/km) is a value calculated with Eq. 3 or Eq. 4 and is the emission value in kilometers. (km) is the annual usage of the vehicle and t ($/kg) is the unit cost of CO_2 emissions. Accordingly, is a monetary value ($). Here, the t value may vary according to the countries. However, there are three basic approaches for determining the t value. The first of these approaches is the calculation of the cost of CO_2, which should be theoretically incinerated for one kg of CO_2. For this, coal or other types of fuel can be taken as reference. For example, the t value for a petroleum-based fuel, which is theoretically stated by the formula $C_\alpha H_\beta$ (as theoretically expressed as C_8H_{18}), can be calculated as follows.

$$t = \frac{M_{C\alpha H\beta} . P_{C\alpha H\beta}}{\alpha . M_{CO2}} \qquad (6)$$

The t values for gasoline and diesel are calculated as 0.14 $/kg and 0.16 $/kg, respectively. Note that the unit cost for diesel fuel is higher (about 15%) than gasoline. The second approach in determining the t value is that countries determine a value based on their economic and development status, environmental conditions, and planting speed. In such countries, CO_2 emissions are an important factor in vehicle taxation. However, in some countries there are also gradual tax arrangements depending on the use of vehicles. The t value is increasing every day. For example, while the t value for 2002 was 0.025 $/kg, this value was about 0.15 $/kg in 2015 (Luckow, 2015). The third approach for the t value is the calculation of CO_2 emissions as a value that must be spent on disposal of the unit amount.

In all three approaches, an economic value of CO_2 emissions can be determined. The most preferred approach is the first approach. According to this approach, the annual CO_2 emission cost of a vehicle with a CO_2 emissions of 130 g/km is estimated to be 15000 km, and this figure is $292. This cost is approximately $6.4 billion for Turkey, where 22 million vehicles as of 2017,

is located. The value of Turkey is emerging as a cost of $80 per person when divided by the population.

CONCLUSIONS

Nowadays, when the total number of vehicles is increasing rapidly, a number of measures should be taken for CO_2 emissions from vehicles. The increase in the number of vehicles along with the population also increases the intensity of CO_2 emissions. Despite all the studies, statistics, researches and technological developments, the importance of this issue is still not understood by people. Looking at television commercials, the CO_2 emissions of vehicles are nothing more than small-letter writings that only pass quickly under the screen. For this reason, it should be considered as an issue that should be considered more and more with each passing day to minimize CO_2 emissions from vehicles.

Nowadays, although there are exceptional cases in the automotive industry, the design, environment, economy and performance. All of the methods offered for vehicle emissions control technologies are environmental design products. However, the human factor is of great importance as a vehicle emission control. The use of the motor vehicles we need to reduce the fuel consumption as well as the total emission of the environment. In addition, the comparison of the emission values between the two models when purchasing a motor vehicle will again indirectly create a total emission reduction effect. Today, interest in electric vehicles is increasing. However, hybrid electric vehicles may be an alternative choice in the widespread use of electric vehicles.

It is impossible to ignore the economic impact of CO2 emissions. When the CO_2 emission values of the vehicles are evaluated economically, they emerge as fuel consumption. In this regard, it can be said that keeping CO_2 emissions under control will provide an economic recovery.

It has been learned by all mankind that the environmental and economic impacts of CO_2 emissions from motor vehicles should be considered. As the excess of CO_2 emissions is a negative expression both environmentally and economically, countries need to take some measures to reduce CO_2 emissions on a legal basis. These measures may include taxation according to CO_2 emissions, incentives for hybrid electric and electric vehicles, the necessity of afforestation according to CO_2 emission value and frequency of vehicle use, and various requirements according to the fuel purchased on individual basis.

REFERENCES

1. AKIN, G. (2017). “Global Warming, Causes and Results” (Turkish). Journal of the Faculty of Languages and History-Geography, 46(2).

2. ALBERINI, A., et al. (2018). “The impact of emissions-based taxes on the retirement of used and inefficient vehicles: The case of Switzerland.” Journal of Environmental Economics and Management 88: 234-258.

3. ARABACI, E. (2014) "Conversion of a four stroke spark ignition engine to six stroke engine with exhaust heat recovery and investigating of the engine performance and exhaust emission characteristics (Turkish)" Gazi University, Graduate School of Natural and Applied Sciences, PhD Thesis.

4. BARLOW, T.J., Latham, S., McCrae, I.S., Boulter, P.G. (2009) A reference book of driving cycles for use in the measurement of road vehicle emissions" TRL publishing.

5. CarbonandTree(07.03.2018)Accessed:http://www.arborenvironmentalalliance.com/carbon-tree-facts.asp

6. Carbondioxide from Humans (07.03.2018) Accessed: https://micpohling.wordpress.com/2007/03/27/math-how-much-co2-is-emitted-by-human-on-earth-annually/

7. Classification of Vehicle Emissions (07.03.2018). Accessed: https://www.fleetnews.co.uk/cars/Car-CO2-and-fuel-economy-figures?CarType=&Manufacturer=ford&Model=fiesta&CO2To=&EquaMpgFrom=&SortBy=EquaCO2&SortDesc=false&FuelType=petrol

8. Emission Tax (07.03.2018). Accessed: https://www.lta.gov.sg/apps/news/page.aspx?c=2&id=08685840-d664-4713-9ccb-96dcd8936d08

9. Environmental Protocols of Turkey. (07.03.2018). Accessed: http://izindenetim.cevreorman.gov.tr/izin/AnaSayfa/birimler/uluslarasiKuruluslar/uluslararasiSozlesmeProtokolAnls/TurkiyeninTarafOlduguUluslararasiCevreProtok.aspx?sflang=tr

10. Fuel Consumption (07.03.2018). Accessed: http://www.enerjiatlasi.com/akaryakit-tuketimi/

11. Global Vehicle Production (07.03.2018). Accessed: https://www.statista.com/statistics/200002/international-car-sales-since-1990/

12. HALDERMAN, J. D. (2015). Automotive Fuel and Emissions Control Systems, Pearson Education.

13. HAO, L., et al. (2017). "Modeling and predicting low-speed vehicle emissions as a function of driving kinematics." Journal of Environmental Sciences 55: 109-117.

14. JIANG, J. and D. Li (2016). "Theoretical analysis and experimental confirmation of exhaust temperature control for diesel vehicle NOx emissions reduction." Applied Energy 174: 232-244.

15. KELEN, F. (2014)." Effects of Motor Vehicle Emissions on Human Health and Environment." Journal of The Institute of Natural & Applied Sciences 19:80-87. 5.

16. LUCKOW P., E. Stanton, B. Biewald, S. Fields, J. Fisher, F. Ackerman. (2014). CO2 Price Report. Synapse Energy Economics.

17. MICHEL, P., et al. (2017). "Optimizing fuel consumption and pollutant emissions of gasoline-HEV with catalytic converter." Control Engineering Practice 61: 198-205.

18. MITROPOULOS, L. K. and P. D. Prevedouros (2015). "Life cycle emissions and cost model for urban light duty vehicles." Transportation Research Part D: Transport and Environment 41: 147-159.

19. Number of vehicles-World. (07.03.2018) Accessed: https://www.statista.com/statistics/281134/number-of-vehicles-in-use-worldwide/

20. PULKRABEK, W. W. (2004). Engineering fundamentals of the internal combustion engine, Pearson Prentice Hall.

21. TALBI, B. (2017). "CO2 emissions reduction in road transport sector in Tunisia." Renewable and sustainable energy reviews 69: 232-238.

22. TEIXEIRA, A. C. R. and J. R. Sodré (2018). "Impacts of replacement of engine powered vehicles by electric vehicles on energy consumption and CO2 emissions." Transportation Research Part D: Transport and Environment 59: 375-384.

23. UYUMAZ, A., Boz,. F., Yılmaz,. E., Solmaz, H., Polat, S. (2017) " Developments in the Reduction Methods of Vehicle Exhaust Emissions (Turkish)" The Journal of Graduate School of Natural and Applied Sciences of Mehmet Akif Ersoy University, Special Issue1: 15-24.

24. World Population. (07.03.2018). Accessed: https://www.statista.com/statistics/805044/total-population-worldwide/

25. XIE, F., et al. (2017). "Effect of external hot EGR dilution on combustion, performance and particulate emissions of a GDI engine." Energy conversion and Management 142: 69-81.

CHAPTER 15

TREATMENT OF FURNITURE INDUSTRY EFFLUENT USING NF90 MEMBRANE

Duygu KAVAK[1]

1.Introduction

Chemicals or wastes generated during industrial processes cause environmental pollution. This pollution negatively affects the living. One of these industries causing pollution is the furniture industry which is an industry branch that provides intermediate products to many sectors. Some of the human living spaces that furniture industry is concerned in are home, office, vehicle and garden. The sector interacts with construction, ship, metal, plastic and glass industries and supports twenty subsectors. The number of companies manufacturing fabrication in the industry is increasing day by day. The main production consists of living room, kitchen, bathroom, office, bedroom garden furniture as well as hospital, hotel furniture, furniture parts and various accessory furniture.

Home and office furniture is 85% in total production and the remaining 15% furniture is estimated as motor vehicle furniture, airborne vehicles furniture, stores furniture and their parts. A total of 29.053 companies are operating in the wood products sector in our country. The number of companies related to the production of timber and parquet is 3.469. Companies that produce lumber and parquet constitutes 12% of wood products sector. In our country, there are 27 coating plants with a capacity of 98 million m^2/year. There are 43 plywood factories with a capacity of 240.000 m^3/year. Average coating capacity is 3.5 million m^2/year and average plywood capacity is 5.600 m^3/year (http://webdosya.csb.gov.tr/csb/dokumanlar/cygm0049.pdf).

The wastes from the sector can be examined under 3 main classes as process-specific wastes, wastes from the side processes and non-process wastes. Wastewater provided by materials and varnishing units in furniture industry are dyestuff and COD. Dyes are given in color and toxicity in wastewaters. When mixed, paints are discharged into wastewater, they create color, disrupt the aesthetic appearance and decrease the light permeability of the water and negatively affect the photosynthesis. At the same time, toxicity of dyes and by-products to nature, mutagenic and carcinogenic effects on humans make it necessary to be treated (http://webdosya.csb.gov.tr/csb/dokumanlar/cygm0065.pdf). Wastewater can cause some problems when they are discharged directly into the receiving environment without any treatment. The most important of these problems are that the dyes show toxic effects and cause bioaccumulation in nature. Since the dyes are chemically and photolytically stable, they are persistent in the natural environment. For all these reasons, discharge to the environment without purification causes ecotoxic risk and also causes aesthetic problems.

1 Department of Chemical Engineering, Faculty of Engineering and Architecture, Eskişehir Osmangazi University

Membrane technology, particularly nanofiltration (NF), is very attractive for wastewater treatment due to its effectiveness in removing organic and multivalent metals. It can operate at relatively low pressures and provide good permeability flow rates. Furthermore, the separation is carried out without phase change and without the use of chemical or thermal energy, so the process becomes energy efficient (Licínio et al., 2015). Pressure-driven membrane processes are called microfiltration (MF), ultrafiltration (UF), nanofiltration (NF) and reverse osmos (RO). NF and RO processes highly reduces TDS, salinity, hardness, nitrates, cyanides, fluorides,arsenic, heavy metals, color and organic compounds, e.g., totalorganic carbon (TOC), biological oxygen demand (BOD), chemical oxygen demand (COD) and pesticides, besides the elimination ofbacteria, viruses, turbidity and TSS from surface water, groundwater, and seawater (Sert et al., 2016).

Taking into account this lacking of information, this work intends to study the cross-flow nanofiltration for furniture industry wastewater samples. The retention of target solutes and the permeate flux are some of the most evaluated parameters for the efficient operation separation process by membranes. Then, the performance of the systems was evaluated in terms of removal of COD, color, and conductivity, as well as the performance of the permeate flux during the filtration time.

2.Material and Methods

In this study, color, conductivity and chemical oxygen demand (COD) removal from furniture industry wastewater were investigated by nanofiltration method. The effects of filtration pressure (2, 6 and 10 bar) and wastewater temperature (25°C and 35°C) on permeate flux and removal efficiencies are investigated. Raw wastewater from the Bursa Furniture factory was used in the experiments. The values of raw wastewater, COD, pH and conductivity before the treatments are shown in Table 1.

Table 1. Properties of raw furniture industry waste water

Parameter	**Value**
COD, mg/L	1940
Max. Absorbance, nm	566
pH	7.28
Conductivity, µS/cm	208

COD and color were analyzed using the Hach Lange DR 3900 UV-vis spectrophotometer at the λmax value of 566 nm. NF90 commercial nanofiltration membrane used in the experiments was obtained from DOW FILMTEC. Table 2 shows the specific properties of the NF90 membrane **(**http://www.sterlitech.com/membrane-process–development/flat-sheet-membranes).

Table 2. Specific properties of the NF90 membrane

Properties	**NF90 membrane**
Feed	Industrial/Commercial
Type	Low energy, Low Pressure
pH	2-11
Flux (GFD)/psi	46.0-60.0/130
$MgSO_4$ Rejection	%99,0
Pore size/MWCO	~200-400 Da
Polymer	Polyamide-TFC

Sterlitech-SEPA CF cross flow nanofiltration system was used in the experimental study. A schematic representation of the system is given in Figure 1.

This system consists of a membrane module, feed tank, pressure pump, scales, flowmeter, computer, thermostat and necessary fasteners. The effective area of the membrane in the system is 150 cm^2. Temperature control is provided by WiseCircu heater in the system. This heater is used to keep the waste water in the supply tank at the desired temperature levels. During the filtration time, the retained and permeate streams returned to the feeding volume for maintaining the homogeneity of samples.

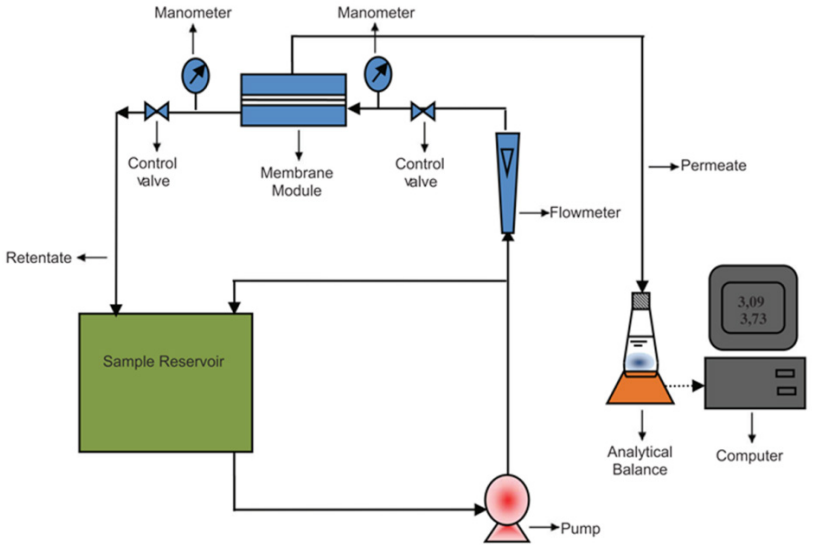

Figure 1. Schematic diagram of the cross-flow NF experimental set-up.

The performance of the membranes was evaluated in terms of permeate flux (J, L/m^2h) given by the ratio between the volumetric flow rate (Q, L/h) and membrane's filtration area (A, m^2), (Eq. (1)) (Bortoluzzi et al., 2017).

$$J = \frac{Q}{A} \quad (1)$$

Species removal or retention efficiency (E_F, %) was calculated as Eq. (2) based on the concentrations of a determined species in the permeate (C_P, mg/L) and in the feeding (C_F, mg/L) (Airton, 2017).

$$E_F = \frac{C_F - C_P}{C_F} \times 100 \quad (2)$$

3. Results and Discussion

3.1. Permeate flux results

The fluxes of NF90 membrane as a function of pressure are shown in Fig. 2. As presented in this figure, pressures of 2 to 10 bars were applied.

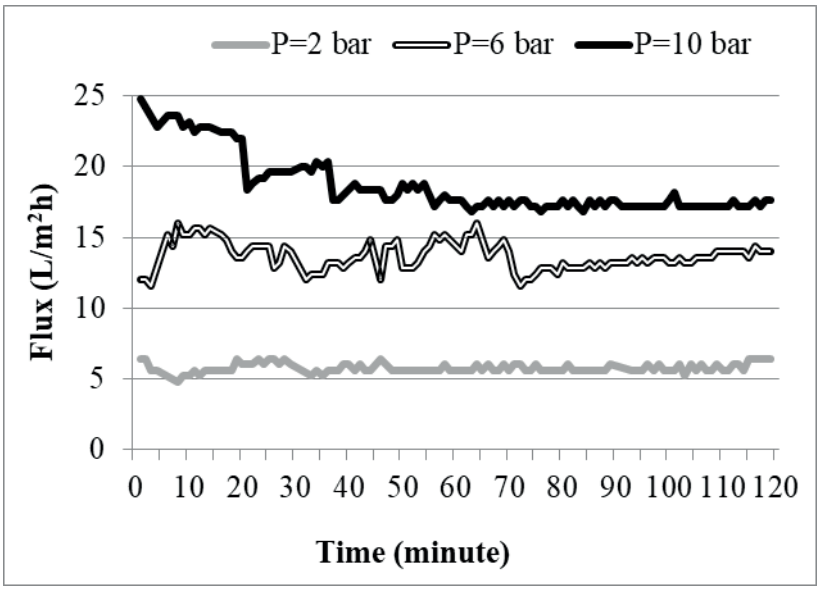

Figure 2. Effect of pressure on permeate fluxes of NF90 membrane (feed temperature: 25ºC, filtration pressure: 2,6,10 bar)

The permeate flux increased with increasing pressure. For example, the permeate flux increases from 6.40 to 17.60 L/m^{2}h as membrane pressure increases from 2 to 10 bar at 25ºC. Similarly, the permeate flux increases from 6.40 to 19.80 L/m^{2}h as membrane pressure increases from 2 to 10 bar at 35ºC. This is a result of the driving forces increasing with the increased operating pressure and overcoming the resistance of the membrane (Kavak, 2017a; Kavak, 2017b). The maximum permeate flux value of NF90 was obtained as 19.8 L/m^{2}h at 10 bar and 35ºC. It can be seen from the figure that

the water fluxes decrease with filtration time at 10 bar. The decline of flux is mainly due to the deposition and adsorption of foulants on the membrane surface (Wei et al., 2013; Banerjee and De, 2010).

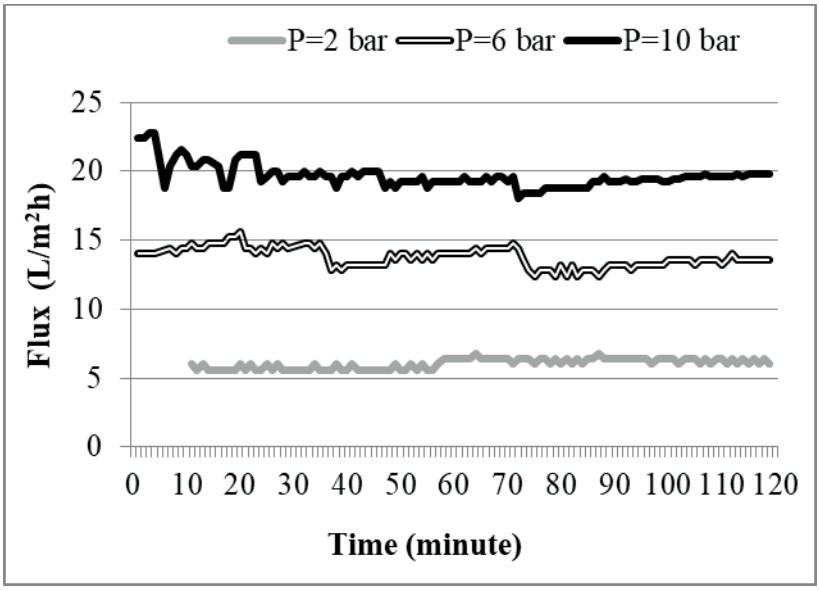

Figure 3. Effect of pressure on permeate fluxes of NF90 membrane (feed temperature: 35ºC, filtration pressure: 2,6,10 bar)

3.2. Color removal results

The color removal performance of the NF90 membrane is shown in Fig.4 and Fig.5. Very high percentage of color rejections were observed at all pressure and temperature values. Color removal percentages were obtained as 100%, 99.11% and 99.71% for 2, 6 and 10 pressure and 25ºC temperature, respectively (Figure 4).

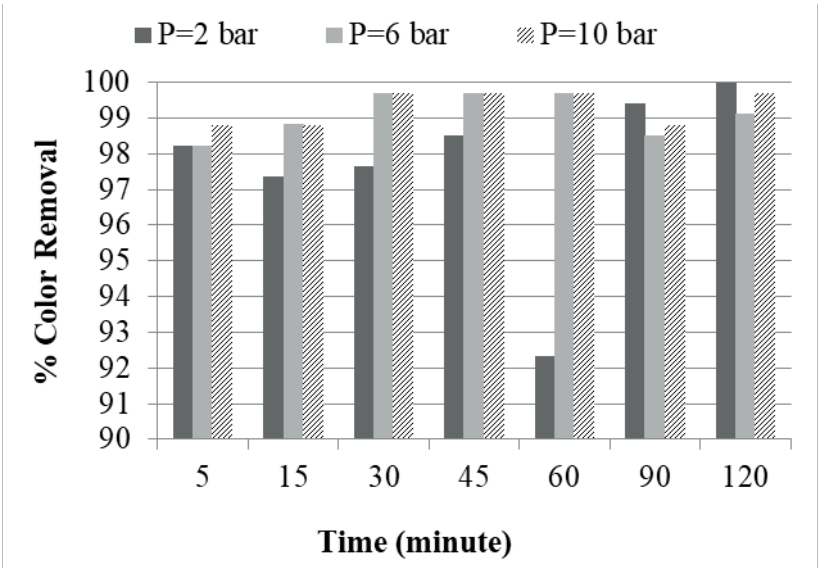

Figure 4. Effect of pressure on the color removal of furniture industry wastewater (feed temperature: 25ºC, filtration pressure: 2,6,10 bar).

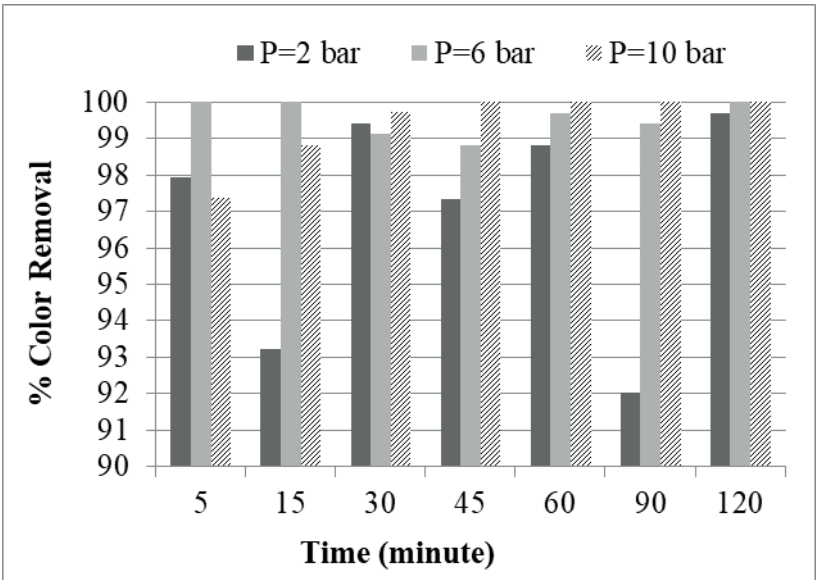

Fig. 5. Effect of pressure on the color removal of furniture industry wastewater (feed temperature: 35ºC, filtration pressure: 2,6,10 bar).

According to Figure 5, color removal percentages were obtained as 99.71%, 100.00% and 100.00 for 2, 6 and 10 pressure and 35ºC temperature, respectively. As can be seen from Fig. 4 and Fig.5, increasing pressure and temperature does not affect color rejection significantly.

3.3. Conductivity and pH results

The conductivity and pH values of the raw furniture wastewater were 208 µS; 7.28 repectively. Table 3 shows the conductivity and pH of the permeate obtained as a result of the experiments. After the treatment process by NF90 membrane, permate conductivity decreased from 208 mg/L to 14.77 mg/L at 25˚C and 10 bar. According to Table 3, the maximum conductivity removal was obtained as 93.00% at 25˚C and 10 bar. pH values were at the range of 6.39-7.50 at 25˚C and 35˚C. When the feed temperature was increased from 25˚C to 35˚C, some increase in pH values was observed.

Table 3. Conductivity and pH values of the permeate

Parameters	Conductivity (µS/cm)	Conductivity Removal (%)	pH
2 bar, 25ºC	23.80	88.80	6.39
6 bar, 25ºC	17.67	91.50	6.59
10 bar, 25ºC	14.77	93.00	6.73
2 bar, 35ºC	28.50	86.30	7.17
6 bar, 35ºC	20.00	90.38	7.35
10 bar, 35ºC	18.61	91.00	7.50

3.4. COD removal results

COD removal is given in Fig. 6. It can be seen that the COD removal at 35˚C for NF90 membrane is higher than 25˚C for all pressure values. These results indicate that 35˚C is more suitable for COD removal from furniture wastewater. It was observed that COD removal increased with increasing temperature and pressure. According to Fig. 6, the maximum COD removal was obtained as 92.16% at 25˚C and 10 bar.

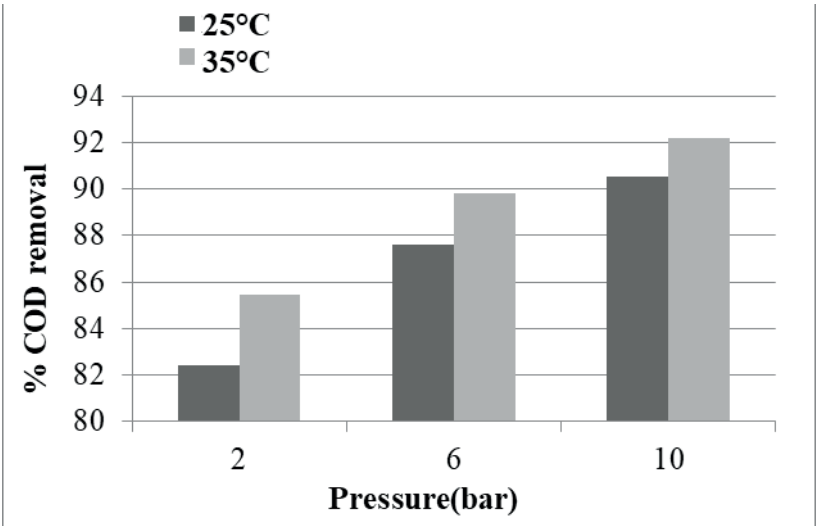

Fig. 6. COD removal of furniture industry wastewater (feed temperature: 25ºC, 35ºC,

filtration pressure: 2, 6, 10 bar).

4. Conclusions

In this study, performance of a NF90 membrane has been studied to treatment of furniture industry wastewater by cross-flow nanofiltration at different operating conditions. Effects of different factors including operating pressure and feed temperature were investigated. The following conclusions can be drawn from this study:

- It is always important to increase the working pressure to increase the permeate flux. The permeate flux increased with increasing pressure. The maximum permeate flux was obtained as 19.8 L/m^2h at 10 bar and 35ºC after 120 min of nanofiltration.
- Increasing pressure and temperature did not affect color rejection significantly. As a result of the color removal experiments, color removal efficiencies were observed to be quite high (>99%).
- NF90 membrane usage decraseded permeate conductivity from 208 mg/L to 14.77 mg/L at 25˚C and 10 bar. The maximum conductivity removal was obtained as 93.00% at 25˚C and 10 bar.
- When the feed temperature was increased from 25˚C to 35˚C, some increase in pH values was observed. pH values were at the range of 6.39-7.50 at 25˚C and 35˚C.
- When the test results for COD removal were examined, it was found that COD removal increased with the increase of temperature and pressure. COD removal at 35˚C for DK membrane is higher than 25˚C for all pressure values. The maximum COD removal was obtained as 92.16% at 25˚C and 10 bar.
- According to the experimental results, NF system is efficient for treating furniture industry wastewater.

Acknowledgements

In this study, devices and tools bought by Eskişehir Osmangazi University Research Foundation were used (Project Number: 201215031).

5. References

1. Airton C. Bortoluzzi Julio A. Faitão Marco Di Luccio, Rogério M. Dallago Juliana Steffens Giovani L. Zabot Marcus and V. Tres, Dairy wastewater treatment using integrated membrane systems, Journal of Environmental Chemical Engineering 5 (2017) 4819–4827.

2. Banerjee P. and De S. Steady state modeling of concentration polarization including adsorption during nanofltration of dye solution, Seperation and Purification Technology 71 (2010) 128–135.

3. http://webdosya.csb.gov.tr/csb/dokumanlar/cygm0049.pdf (Erişim tarihi: 01.10.2018)

4. http://webdosya.csb.gov.tr/csb/dokumanlar/cygm0065.pdf (Erişim tarihi: 02.11.2018)

5. http://www.sterlitech.com/membrane-process–development/flat-sheet-membranes (Erişim tarihi: 04.11.2018)

6. Kavak D. Treatment of dye solutions by DL nanofiltration membrane, Desalination and Water Treatment 69(1) (2017a) 116-122.

7. Kavak D. Removal of Iron, Copper and Zinc Mixtures from Aqueous Solutions by Cross Flow nanofiltration, Fresenius Environmental Bulletin, 26(1a) (2017b) 1101-1107.

8. Licínio M. Gando-Ferreira Joana C. Marques and Margarida J. Quina, Integration of ion-exchange and nanofiltration processes for recovering Cr(III) salts from synthetic tannery wastewater, Environmental Technology 36(18) (2015) 2340–2348.

9. Sert G. Bunani S. Kabay N. Egemen Ö. Arda M. Pek T.Ö. and Yüksel M., Investigation of mini pilot scale MBR-NF and MBR-RO integratedsystems performance—Preliminary field tests Journal of Water Process Engineering 12 (2016) 72–77.

10. Wei X. Kong X. Wang S. Xiang H. Wang J. and Chen J. Removal of heavy metals from electroplating wastewater by thin-film composite nanofiltration hollow-fiber membranes, Industrial Engineering Chemistry Research 52 (2013) 17583–17590.

DC-DC CONVERTERS AND SIMULINK APPLICATIONS

Hilmi ZENK

Introduction

In most industrial applications, the constant voltage DC source has to be converted to a variable voltage DC source. A DC chopper, also known as DC/DC converters, converts DC directly into DC. A converter can also be considered the equivalent DC circuit of an AC transformer with a continuously switchable winding ratio. As the transformer can increase or decrease the AC voltage, the DC/DC converter can also increase or decrease the voltage value of a DC source. Converters are often used for motor attraction control in electric cars, sea hoists, fork lift trucks, and mine-pit tractors. The advantages of soft speed control, high efficiency and dynamic response are the preferred reasons for DC/DC converters. It is also used for the active braking of motors to return energy into the material. This feature protects the energy in the transfer systems with frequent interruptions. The conversion of power from DC to DC is made by switching type power converters.

Converters consist of reactive elements and switches. Operation principle is done by adjusting the transmission and cutting times of the switches used in circuit. If the frequency of the voltage supplying the load is large, it is possible to continuously transfer DC power to the load. The satisfactory operation of such converters depends on the appropriate configuration of the reactive elements and the appropriate switching methods.

Switch mode DC/DC converters are non-linear and time-varying systems. The appropriate protective properties of the converter application are indicated together with the design criteria. DC/DC converters can be classified as follows.

1. Buck Converter (Step-Down)
2. Boost Converter (Step-Up)
3. Buck-Boost Converter (Step (Down / Up)
4. Cúk Converter
5. Zeta Converters
6. Sepic Converters

7. Interleaved Buck Converter

8. Push-Pull Converters

9. Flyback Converter

Reducing and amplifying converters are basic converters[1]. Reducer-amplifier and CUK converters are composed of basic converters. Full-bridge converters are derived from reducer converters. The converter variants are defined as switch mode DC power supplies and DC motor control applications[2], depending on their specific application. In this section the converters are analyzed in steady state and the coil and capacitor losses are neglected.

1. Buck Converters

Figure 1.1 shows a simplified diagram of the reducer type transducer structure. The L inductor and the C capacity are used to filter the output voltage. In the circuit, the output load is indicated by R resistance. The diode D is generally referred to as the free passage diode. The current of the inductor in the buck converter is continuous or discontinuous [3].

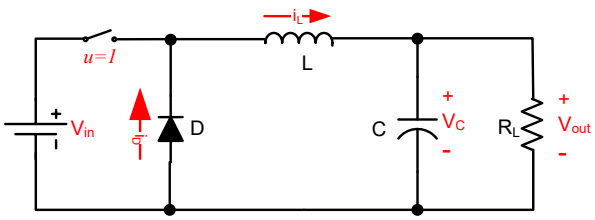

Figure 1.1 Buck (step-down) converter circuit

Continuous current Mode; Two different conditions of the reducing power stage are taken into account. First, the semiconductor power switch is in Q transmission and the D_1 diode is in section. In discontinuous current mode, Q_1 and D_1 message vain. In Figure 1.2, these two conditions are shown by adding a simplified linear circuit instead of a switch. The state at which the semiconductor switch is in transmission is expressed by the time D × Ts = T_{ON}, where D is the transmission time in the Ts period determined by the control circuit. The cutting time is expressed by the T_{OFF} symbol.

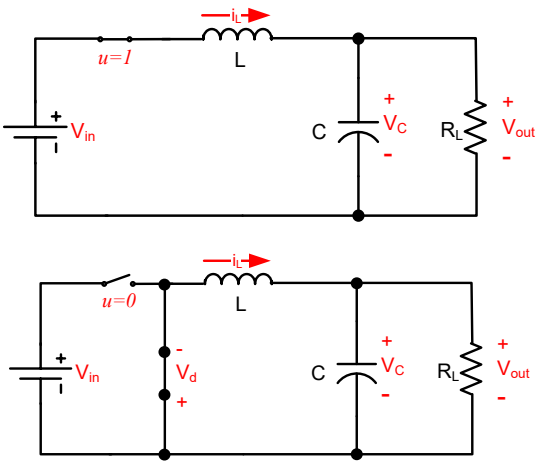

a) b)

Figure 1.2. Buck converter operating modes, a) switch on status, b) switch off status

The changes in the inductance voltage and current with the key operation modes given in Figure 1.2 can be obtained using equations (1.1) and (1.2). Change in inductor current for transmission status, can be calculated by equation (1.3) and (1.4).

$$v_L = L\frac{V_{in}}{dt} \tag{1.1}$$

$$\Delta I_L = \frac{V_L}{L}\Delta T \tag{1.2}$$

$$\Delta I_{L\max} = \frac{V_{in} - (V_L) - V_0}{L} T_{on} \tag{1.3}$$

$$\Delta I_{L\min} = \frac{V_{in} + (V_D + V_L)}{L} T_{off} \tag{1.4}$$

$$V_0 = DV_{in} \tag{1.5}$$

In steady-state operating conditions, the output voltage of the buck converter can be found as shown in equation (1.5) using the amount of inductor current, the amount of increase in the transmission and the reduction in the cut. Figure 1.3 MATLAB / Simulink environment, a Buck converter circuit is prepared.

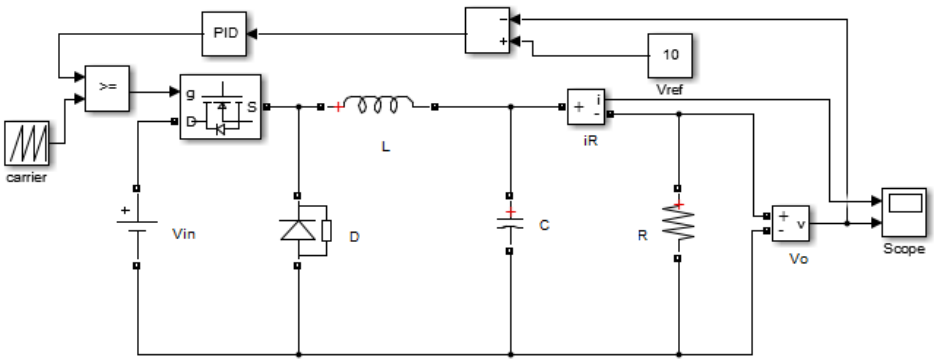

Figure 1.3. Buck converter circuit MATLAB/Simulink equivalent

2. Boost Converters

An ideal amplifier type transducer structure consists of semiconductor switch, diode, coil and capacity elements as shown in Figure 2.1.

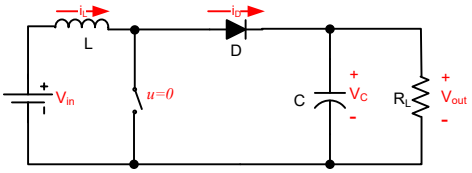

Figure 2.1. Boost (step-up) type DC converter structure

The control mechanism of the circuit shown in Figure 2.2.a is carried out according to the transmission of the semiconductor power switch to transmission and cutting. When the key is moved to the transmission, the current passing through the coil increases and the energy on the coil starts to be stored. As soon as the switch is taken to the cut, the charge current passing through the coil starts to flow through the D diode to the capacity C and to the load. The coil discharges its energy and the direction of the polarity of the voltage on the coil is the same as the polarity of the voltage source and is connected to the load via diode D. This increases the output voltage level. Thus the D diode goes to the section and the circuit is divided into two different parts as seen in Figure 2.2.a. The output voltage remains constant as long as the switching circuit of the time circuit of the RC circuit is too large.

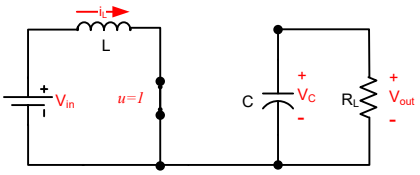

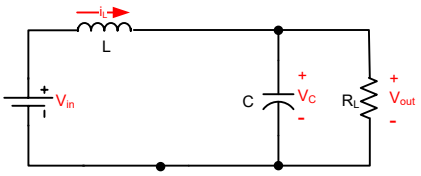

a) b)

Figure 2.2. Boost converter operating modes, a) switch on status, b) switch off status

The circuit indicating the cutting state of the semiconductor switch is shown in Figure 2.2.b. In this case the load is fed through the source. When the switch is in transmission, the equivalent circuit is as shown in Figure 2.2.a. The voltage supply feeds the coil and the rate of rise of the coil current varies as in equation (2.1) depending on the Vs source and L value. If the voltage source is constant, the ascent rate of the coil current is positive and constant. Thus, the coil does not saturation. This is the following in equation (2.2) The semiconductor switch remains in transmission over the DT range in a switching period and the DT range can be expressed as unt. In the case of the transmission of the switch, the net increase in the coil current is equation (2.3).

$$v_s = L\frac{di_L}{dt} \tag{2.1}$$

$$\frac{\Delta I_L}{\Delta t} = \frac{V_L}{L} \tag{2.2}$$

$$\Delta I_L = \frac{V_s}{L} DT \tag{2.3}$$

The equivalent circuit when the switch is in cut is shown in Figure 2.b it happens. In this case, the voltage on the coil is given in equation (2.4). Where the output voltage is higher than the source voltage ($V_o > V_s$) the direction of the voltage on the coil and the flow of the flow is expressed in equation (2.5). When the key is taken to the cut, the gap (1-D) is expressed by T, and the flow through the coil is obtained in the equation (2.6). Since the net change of the current in a period is zero, the sum of the equation (2.3) and the equation (2.6) is zero. Accordingly, the expression in equation (2.7) is obtained. By simplification of this expression, the expression in equation (2.8) is obtained.

$$v_{in} = v_s - v_0 \tag{2.4}$$

$$\frac{d_{iL}}{dt} = \frac{v_s - v_0}{L} \tag{2.5}$$

$$\Delta I_L = \frac{v_s - v_0}{L}(1-D)T \tag{2.6}$$

$$\frac{v_s}{L}DT = \frac{v_s - v_0}{L}(1-D)T = 0 \tag{2.7}$$

$$v_0 = \frac{v_s}{1-D} \tag{2.7}$$

Figure 1.3 MATLAB / Simulink environment, a Boost converter circuit is prepared.

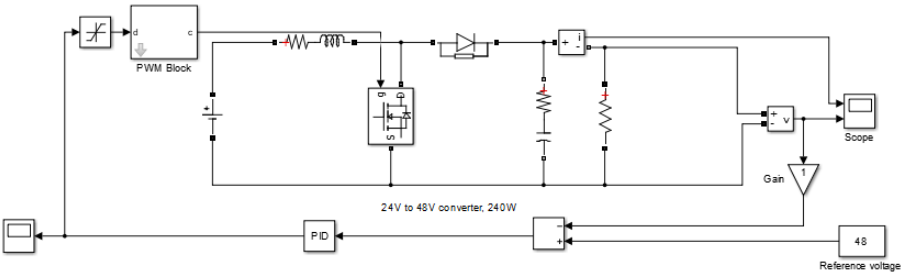

Figure 2.3. Boost converter circuit MATLAB/Simulink equivalent.

3. Buck-Boost Converter

Buck-boost converters are commonly used in the regulation of DC power sources where the output is desired to be negative polarity relative to the common terminal of the input voltage, and where the output voltage may be less or more than the input voltage. This type of converter is achieved by connecting two converters of the drop and boost type. Output-to-input voltage conversion ratio in steady state; is the product of the conversion rates of the connected converters [5].

$$D\frac{1}{(1-D)} = \frac{V_{out}}{V_{in}} \tag{3.1}$$

Equation (3.1) determines the duty cycle of the output voltage in relation to the input voltage. Such a connection is shown in Figure 3.a. When the switch is closed, the coil is energized but the diode does not conduct. When the switch is turned on there is no stored energy in the bobbin. In the steady state analysis investigated here, the value of the output capacitor is fixed is considered to be too large to provide an output voltage.

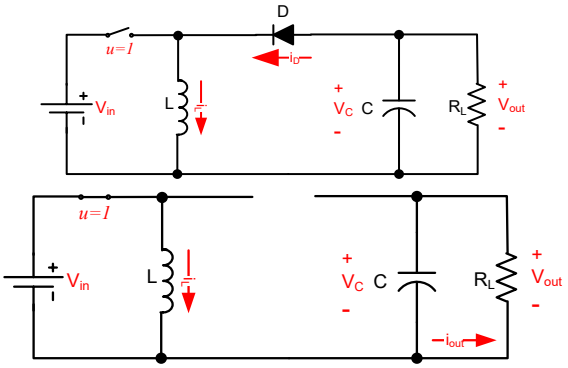

a) b)

Figure 3.1. a) Buck-Boost converter circuit diagram b) Converter when switched ON position

Figure 3.1.b and Figure 3.1.a shows the waveforms for continuous current continuous conduction mode of the inductance current. By equalizing the integral of the inductance voltage over a time period;

$$V_{in}DT_S + (-V_{out})(1-D)T_S = 0 \tag{3.2}$$

$$D\frac{1}{(1-D)}(P_{in} = P_{out}) = \frac{I_{out}}{I_{in}} \tag{3.3}$$

Figure 3.3 MATLAB/Simulink environment, Buck-Boost converter circuit is prepared.

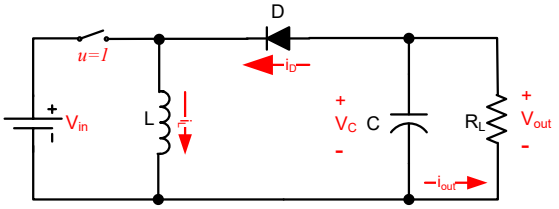

Figure 3.2. Circuit diagram of Buck-Boost converter when switched OFF position

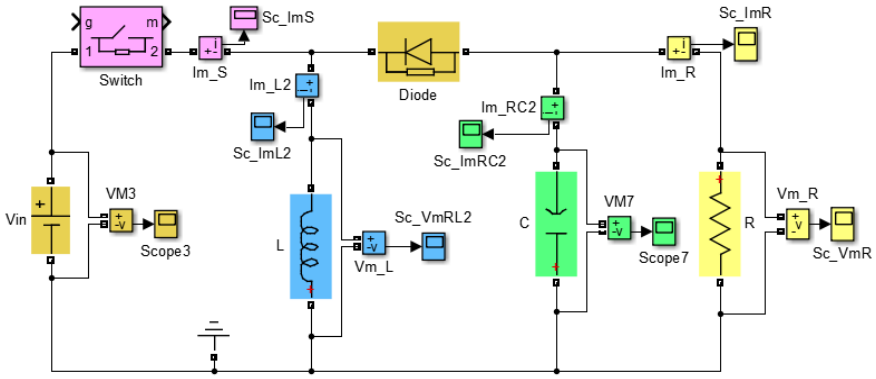

Figure 3.3. Buck-Boost converter circuit MATLAB / Simulink equivalent.

4. Cúk Converters

Cúk converter circuit connection shown in Figure 4.1 Converter circuit, the power switch is ideal, coils and capacitors losses and the DC is not an ideal voltage source V_{in} is the input source is assumed to be zero internal resistance.

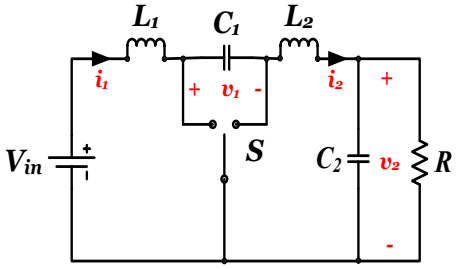

Figure 4.1. Ideally switch using Cúk converter

Due to the lack of real systems, this switch ideal diode circuit in Figure 4.2, a switching MOSFET and the problem is resolved in a way close to the ideal.

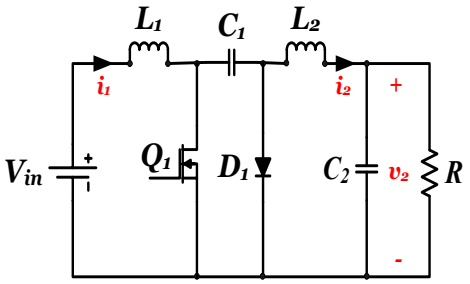

Figure 4.2. Complete Cúk converter circuit

.

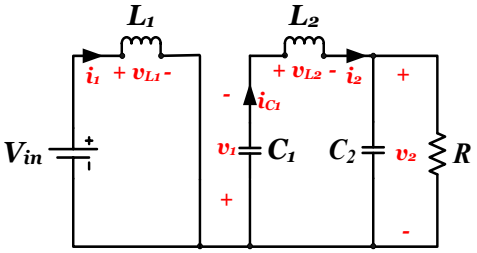

Figure 4.3. MOSFET switch to the "ON" position.

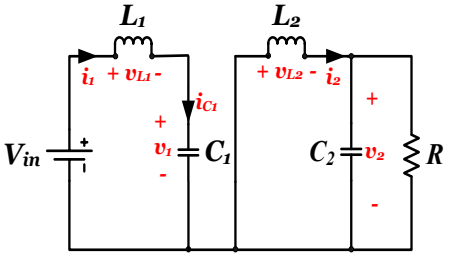

Figure 4.4. MOSFET switch to the "OFF" position, but C_1 connected D_1.

Figure 4.3 shows the MOSFET switch status of the new circuit to the case where transmission. In this case, completing the circuit of the DC source L_1, capacitor C_1 will discharge by transferring energy to the output. Figure 4.4 MOSFET switch position at the same time you are at the state of the diode circuit is new to the case where transmission. In this case, connect input capacitor C_1 starts charging. Circuit of Figure 4.3 is applied to the laws of Kirchhoff's voltage and current flows from the inductor and the capacitor voltage is equal to (4.1), (4.2), (4.3) and (4.4) are obtained.

$$v_{L1} = V_{in} \tag{4.1}$$

$$v_{L2} = -v_1 - v_2 \tag{4.2}$$

$$i_{C1} = i_2 \tag{4.3}$$

$$i_{C2} = i_2 - \frac{v_2}{R} \tag{4.4}$$

Figure 4.4 circuit is applied to the laws of Kirchhoff's voltage and current flows from the inductor and the capacitor voltage is equal to (4.5), (4.6), (4.7) and (4.8) are obtained.

$$v_{L1} = V_{in} - v_1 \tag{4.5}$$

$$v_{L2} = -v_2 \tag{4.6}$$

$$i_{C1} = i_1 \tag{4.7}$$

$$i_{C2} = i_2 - \frac{v_2}{R} \tag{4.8}$$

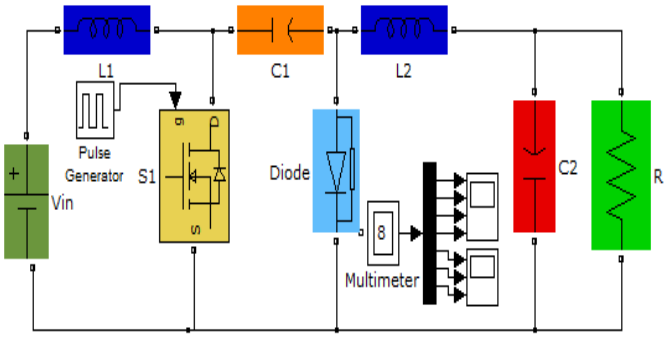

Figure 4.5. Cúk converter circuit MATLAB/Simulink equivalent.

Figure 4.5 MATLAB / Simulink environment, a Cúk converter circuit is prepared. All the elements of the circuit in Figure 4.6, the time rate of flow and stress observed. 10V MOSFET source voltage of the switch corresponds to the case where the working rate of 75%, the output voltage is about 26V. In Figure 7, the voltage of about 2.5 V at the level of 25% of the working rate. As a result, Cúk converter switch duty cycle is greater than 50% of the output voltage increases, decreases when less than 50%.

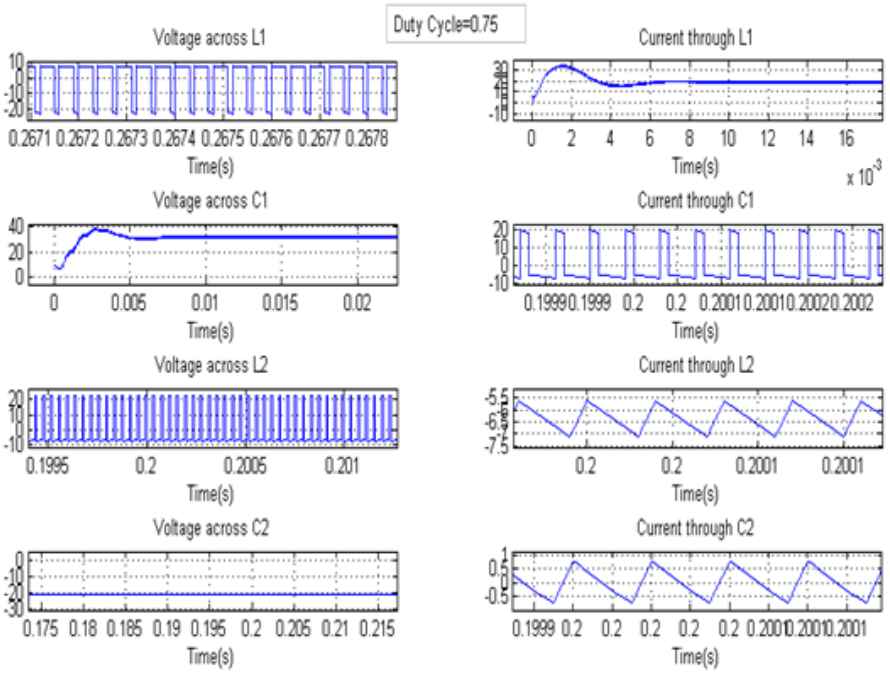

Figure 4.6. Cúk converter signals, D=%75.

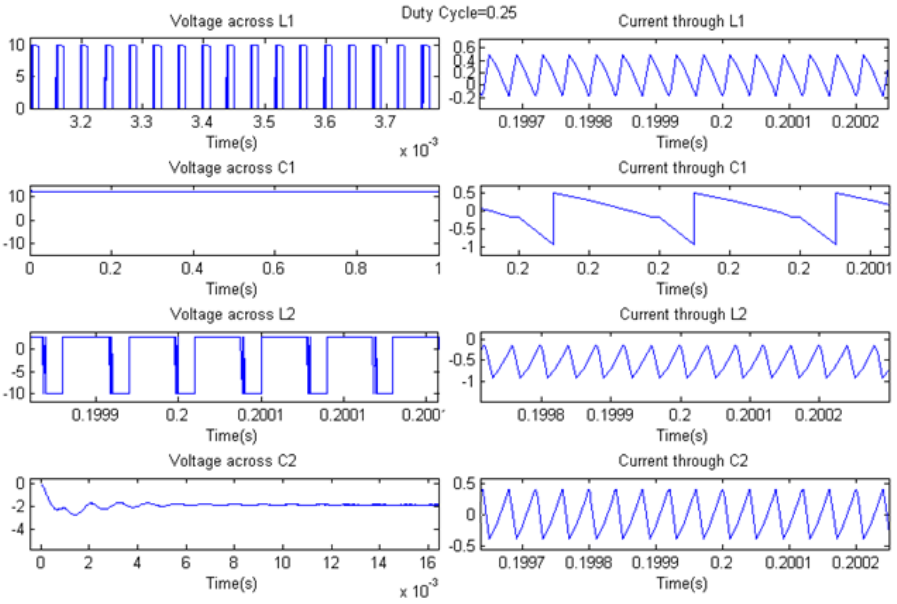

Figure 4.7. Cúk converter signals, D=%25.

5. Zeta Converters

The Zeta converter can be represented by a fourth order nonlinear system, as is the case for Cúk and SEPIC converters. The reason being is that it includes two capacitors and two inductors as dynamic storage elements. The Zeta converter can both amplify and reduce, without polarity inversions, the value of the input source voltage Vin. We briefly summarize next the most important features involved in the modeling of the Zeta converter [6-13].

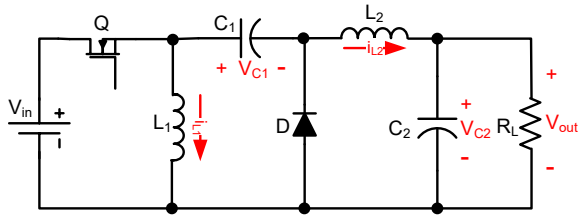

Figure 5.1. A Zeta converter using a MOSFET semiconductor realization of the switches.

Figure 5.1. depicts a semiconductor realization of a Zeta DC-to-DC power converter. The ideal switch based realization of the Zeta converter is depicted in Figure 5.2.

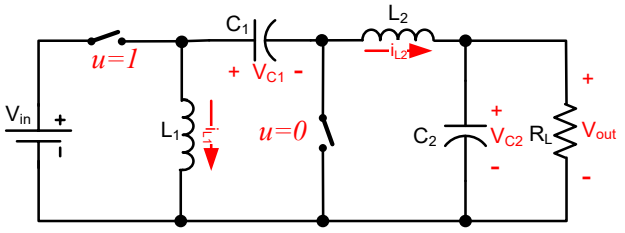

Figure 5.2. The Zeta converter with ideal switches.

The Zeta converter exhibits two different modes of operation. The first mode is obtained when the transistor is ON and instantaneously, the diode D is inversely polarized generating an equivalent circuit shown in Figure 5.3. During this period, the current through the inductor L1 and L2 are drawn from the voltage source Vin. This mode is the charging mode. The second mode of operation starts when the transistor is OFF and the diode D is directly polarized generating the equivalent circuit shown in Figure 5.4. This stage or mode of operation is known as the discharging mode since all the energy stored in L2 is now transferred to the load R.

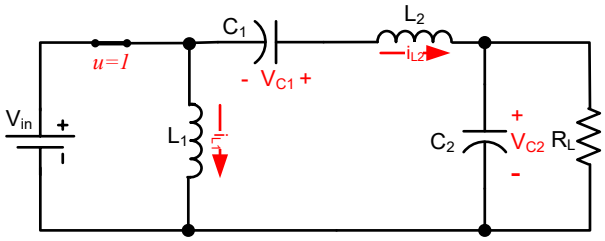

Figure 5.3. MOSFET switch position function value u = 1.

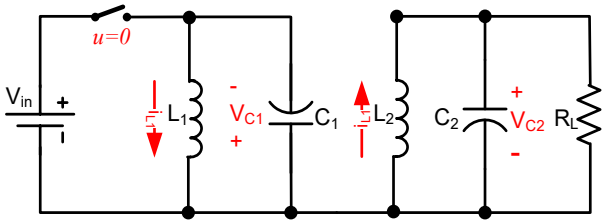

Figure 5.4. MOSFET switch position function value u = 0.

The dynamical model of the Zeta converter is found to be,

$$L_1 \frac{\partial i_{L1}}{\partial t} = -(1-u)v_{C1} + uV_{in} \tag{5.1}$$

$$L_2 \frac{\partial i_{L2}}{\partial t} = uv_{C1} - v_{C2} + uV_{in} \tag{5.2}$$

$$C_1 \frac{\partial v_{C1}}{\partial t} = (1-u)i_{L1} + ui_{L2} \tag{5.3}$$

$$C_2 \frac{\partial v_{C2}}{\partial t} = i_{L2} + \frac{v_{C2}}{R} \tag{5.4}$$

After the required change of state and time variables one obtains the following normalized model for the converter,

$$\dot{x}_1 = -(1-u)x_2 + u \tag{5.5}$$

$$\dot{x}_2 = (1-u)i_1 + ui_1 \tag{5.6}$$

$$\alpha_1 \dot{x}_3 = ux_2 - x_4 + u \tag{5.7}$$

$$\alpha_2 \dot{x}_4 = x_3 - \frac{x_4}{Q} \tag{5.8}$$

$$\alpha_1 = \frac{L_2}{L_1} \tag{5.9}$$

$$\alpha_2 = \frac{C_2}{C_1} \tag{5.10}$$

$$Q = R\sqrt{C_1/L_1} \tag{5.11}$$

The equilibrium equations are given by,

$$\begin{bmatrix} 0 & -(1-u) & 0 & 0 \\ (1-u) & 0 & -u & 0 \\ 0 & u & 0 & -1 \\ 0 & 0 & 1 & \frac{-1}{Q} \end{bmatrix} \begin{bmatrix} \bar{x}_1 \\ \bar{x}_2 \\ \bar{x}_3 \\ \bar{x}_4 \end{bmatrix} + \begin{bmatrix} -u \\ 0 \\ -u \\ 0 \end{bmatrix} \tag{5.12}$$

The average normalized equilibrium point, parameterized in terms of u_{av} =u is found to be given by,

$$\bar{x}_1 = \frac{1}{Q}\frac{u^2}{(1-u)^2} \tag{5.13}$$

$$\bar{x}_2 = \frac{u}{1-u} \tag{5.14}$$

$$\bar{x}_3 = \frac{1}{Q}\frac{u}{(1-u)} \tag{5.15}$$

$$\bar{x}_4 = \frac{u}{(1-u)} \tag{5.16}$$

A parameterization in terms of the desired output equilibrium voltage x_4 is found by elimination of the parameter U, yielding,

$$\bar{x}_1 = \frac{\bar{x}_4^2}{Q} \tag{5.17}$$

$$\bar{x}_2 = \bar{x}_4 \tag{5.18}$$

$$\bar{x}_3 = \frac{\bar{x}_4^2}{Q} \tag{5.19}$$

$$\bar{x}_4 = \frac{\bar{x}_4}{\bar{x}_4 + 1} \tag{5.20}$$

The static transfer function is hence given by,

$$T(u) = \bar{x}_4 = \frac{u}{(1-u)} \tag{5.21}$$

which confirms the basic features of the Zeta converter as a possible scaling or amplifying converter.

6. SEPIC Converters

The single-ended primary inductance converter (SEPIC) is a DC/DC-converter topology that provides a positive regulated output voltage from an input voltage that varies from above to below the output voltage. It operates in continuous, discontinuous, or boundary conduction mode. SEPIC is controlled by the duty cycle of the control transistor. SEPICs are useful in applications in which a battery voltage can be above and below that of the regulator's intended output. As with other switched mode power supplies specifically DC-to-DC converters, the SEPIC exchanges energy between the capacitors and inductors in order to convert from one voltage to another. A simple circuit diagram of a SEPIC converter is shown in Figure 6.1, consisting of a coupling capacitor, C_1 and output capacitor, C_2; coupled inductors L_1 and L_2 and diode [14].

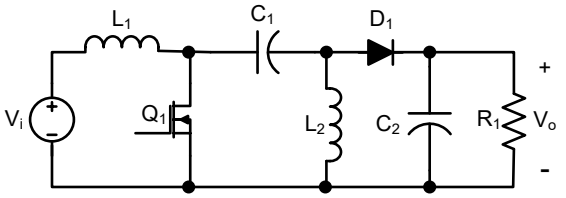

Figure 6.1. Simple circuit diagram of SEPIC converter

Figure 2 shows the circuit when the power switch is turned on. The first inductor, L_1, is charged from the input voltage source during this time. The second inductor takes energy from the first capacitor, and the output capacitor is left to provide the load current. No energy is supplied to the load capacitor during this time. Inductor current and capacitor voltage polarities are also marked.

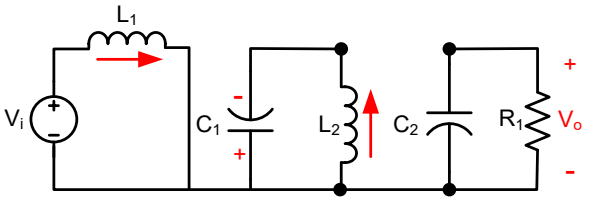

Figure 6.2. SEPIC converter when switched ON

When the power switch is turned off, the first inductor charges the capacitor C_1 and also provides current to the load, as shown in Figure 3. The second inductor is also connected to the load during this time. The output capacitor sees a pulse of current during the off time, making it inherently noisier than a buck converter [15].

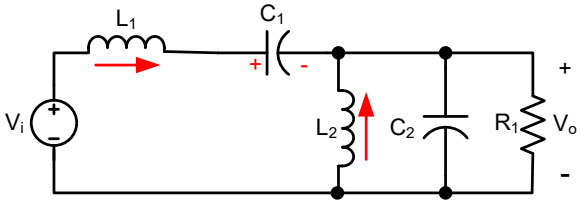

Figure 6.3. SEPIC converter when switched OFF

The formulae of duty cycles are given as follows:

$$D_{\max} = \frac{V_0 + V_D}{V_{i(\min)} + V_0 + V_D} \tag{6.1}$$

$$D_{\min} = \frac{V_0 + V_D}{V_{i(\max)} + V_0 + V_D} \tag{6.2}$$

For determining the inductance is to allow the peak-to-peak ripple current to be approximately 40% of the maximum input current at the minimum input voltage. The ripple current flowing in equal value inductors L_1 and L_2 is given by,

$$\Delta I_L = I_i \%40 = I_0 \frac{V_0 \%40}{V_{i_{\min}}} \tag{6.3}$$

The inductor value is calculated by,

$$L_1 = L_2 = L = \frac{V_{i_{\min}}}{\Delta I_L f_{sw}} D_{\max} \tag{6.4}$$

where f_{sw} is the switching frequency and D_{max} is the duty cycle at the minimum V input. The peak current in the inductor, to ensure the inductor does not saturate, is given by,

$$I_{L1peak} = I_0 \frac{V_0 + V_D}{V_{i_{\min}}} \left(1 + \frac{\%40}{2}\right) \tag{6.5}$$

$$I_{L2peak} = I_0 \frac{V_0 + V_D}{V_{i_{\min}}} \left(1 + \frac{\%40}{2}\right) \tag{6.6}$$

If L_1 and L_2 are wound on the same core, the value of inductance in the equation above is replaced by 2L due to mutual inductance. The inductor value is calculated by,

$$L_1^{'} = L_2^{'} = \frac{L}{2} = \frac{V_{i_{\min}}}{2\Delta I_L f_{sw}} D_{\max} \tag{6.7}$$

Power Switch Selection, the parameters governing the selection of the MOSFET are the minimum threshold voltage $V_{th(min)}$, the on resistance $R_{DS(ON)}$, gate-drain charge Q_{GD} and the maximum drain to source voltage, $V_{DS(max)}$. Logic level or sublogic-level threshold switch' should be used based on the gate drive voltage. The peak switch voltage is equal to $V_{in} + V_{out}$. The peak switch current is given by,

$$I_{Q1_{peak}} = I_{L_{2peak}} + I_{L_{2peak}} \tag{6.8}$$

The RMS current through the switch is given by,

$$I_{Q1_{rms}} = I_0 \sqrt{\frac{(V_0 + V_{i_{\min}} + V_0)(V_0 + V_D)}{V_{i_{\min}}^2}} \tag{6.9}$$

$$P_{Q1_{rms}} = I_{Q1_{rms}}^2 R_{DS_{ON}} D_{\max} + (V_{i_{\min}} + V_0) I_{Q1_{peak}} \frac{Q_{DO} f_{sw}}{I_G} \tag{6.10}$$

P_{Q1}, the total power dissipation for MOSFETs includes conduction loss (as shown in the first term of the above equation) and switching loss as shown in the second term. I_G is the gate drive current. The $R_{DS(ON)}$ value should be selected at maximum operating junction temperature and is typically given in the MOSFET data sheet. Ensure that the conduction losses plus the switching losses do not exceed the package ratings or exceed the overall thermal budget.

Input Capacitor Selection: The SEPIC has an inductor at the input. Hence, the input current waveform is continuous and triangular. The inductor ensures that the input capacitor sees fairly low ripple currents. The RMS current in the input capacitor is given by,

$$I_{C_{in_{rms}}} = \frac{\Delta I_L}{\sqrt{12}} \tag{6.11}$$

The input capacitor should be capable of handling the RMS current. Although the input capacitor is not so critical in a SEPIC application, a

equation (6.10) ìf or higher value, good quality capacitor would prevent impedance interactions with the input supply.

Output Capacitor Selection: When the power switch Q_1 is turned on the inductor is charging the output current is supplied by the output capacitor. The RMS current in the output capacitor is,

$$I_{C_{0_{rms}}} = I_0 \sqrt{\frac{V_0 + V_D}{V_{i_{\min}}}} \tag{6.12}$$

The ESR, ESL and the bulk capacitance of the output capacitor directly control the output ripple. Assume half of the ripple is caused by the ESR and the other half is caused by the amount of capacitance.

$$ESR \leq \frac{V_{ripple}\%50}{I_{L_{1peak}} + I_{L_{2}peak}} \tag{6.13}$$

$$C_0 = \frac{I_0 D}{\%50 V_{ripple} f_{sw}} \tag{6.14}$$

In surface mount applications, tantalum, polymer electrolytic and polymer tantalum or multi-layer ceramic capacitors are recommended at the output [6]. SEPIC Coupling Capacitor Selection: The selection of SEPIC capacitor, C_s, depends on the RMS current, which is given by,

$$I_{C_{0_{rms}}} = I_0 \sqrt{\frac{V_0 + V_D}{V_{i_{\min}}}} \tag{6.15}$$

The SEPIC capacitor must be rated for a large RMS current relative to the output power. The voltage rating of the SEPIC capacitor must be greater than the maximum input voltage. The peak-to-peak ripple voltage on Cs,

$$\Delta V_{cs} = \frac{I_0 D_{\max}}{C_s f_{sw}} \tag{6.16}$$

State Space Analysis of SEPIC converter for continuous conduction mode can be done in two modes of operation. For a given network has two states in CCM, S_1 on, S_2 off and S_1 off, S_2 on, the response of the network in each state may be time weighted and averaged. The state equations can be expressed in matrix form as,

$$\dot{X} = A_1 x + B_1 u \tag{6.17}$$

$$Y = C_1 x + D \tag{6.18}$$

where X is the time derivative of the state variable vector, A_1 is the state matrix, x is the state variable vector, B_1 is the input matrix, u is the input and Y is the output. The state variables are taken as,

$$x_1 = i_{L_1} \tag{6.19}$$

$$x_2 = i_{L_2} \tag{6.20}$$

$$x_3 = i_{C_1} \tag{6.21}$$

$$x_4 = i_{C_2} \tag{6.22}$$

Mode 1: Switch S: ON (0< t < DT)

$$A_1 = \begin{bmatrix} 0 & 0 & 0 & 0 \\ 0 & 0 & \frac{1}{L_2} & 0 \\ 0 & -\frac{1}{C_1} & 0 & 0 \\ 0 & 0 & 0 & -\frac{1}{RC_2} \end{bmatrix} B_1 = \begin{bmatrix} \frac{1}{L_1} \\ 0 \\ 0 \\ 0 \end{bmatrix} \tag{6.23}$$

Mode 2: Switch S: OFF (DT < t < (1-D)T)

$$A_2 = \begin{bmatrix} 0 & 0 & -\frac{1}{L_1} & -\frac{1}{L_1} \\ 0 & 0 & 0 & -\frac{1}{L_2} \\ -\frac{1}{C_1} & 0 & 0 & 0 \\ \frac{1}{C_2} & \frac{1}{C_2} & 0 & -\frac{1}{RC_2} \end{bmatrix} B_1 = \begin{bmatrix} \frac{1}{L_1} \\ 0 \\ 0 \\ 0 \end{bmatrix} \tag{6.24}$$

The state space averaged equation is given as,

$$X = [A_1 d + A_2(1-d)]x + [B_1 d + B_2(1-d)]u \tag{6.25}$$

Therefore, the large signal model is expressed as,

$$\begin{bmatrix} i_{L_1} \\ i_{L_2} \\ \dot{v}_{C_1} \\ \dot{v}_{C_2} \end{bmatrix} = \begin{bmatrix} 0 & 0 & \frac{d-1}{L_1} & \frac{d-1}{L_1} \\ 0 & 0 & \frac{d}{L_2} & \frac{d-1}{L_2} \\ \frac{1-d}{C_1} & \frac{-d}{C_1} & 0 & 0 \\ \frac{1-d}{C_2} & \frac{1-d}{C_2} & 0 & \frac{-1}{RC_2} \end{bmatrix} \begin{bmatrix} i_{L_1} \\ i_{L_2} \\ v_{C_1} \\ v_{C_2} \end{bmatrix} + \begin{bmatrix} \frac{1}{L_1} \\ 0 \\ 0 \\ 0 \end{bmatrix} [u] \tag{6.26}$$

7. Interleaved Buck Converter

The circuit diagram of IBC is given as shown in Figure 1. This is equivalent to a parallel combination of two sets of switches, diodes and inductors connected to a common filter capacitor and load [16]. The

switches are operated out of phase. Assume the converter operates with duty ratio less than 50% and in continuous conduction mode [17].

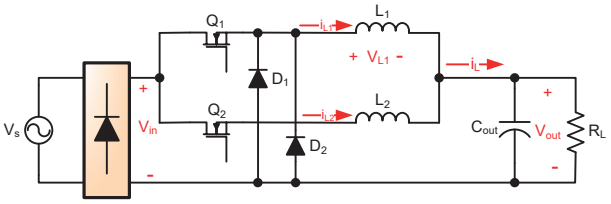

Figure 7.1. Simple circuit diagram of 2 phase IBC

A two phase IBC will operate in four different modes and is explained as follows.

A. IBC Mode-1

In Operation mode-1 switch Q_1 is turned on by giving a gate pulse. At the same time switch Q_2 is off. Current flows through the switch Q_1, inductor L_1 and load, making current through L_1 to increase as long as Q_1 is turned on. During this time current in L_2 decreases linearly. The equivalent circuit is as in Figure 2. The variations of i_{L1} and i_{L2} during T are given by,

$$\Delta i_{L!} = \left(\frac{V_{in} + V_{out}}{L_1} \right) T_1 \tag{7.1}$$

$$\Delta i_{L2} = \left(\frac{-V_{out}}{L_2} \right) T_1 \tag{7.2}$$

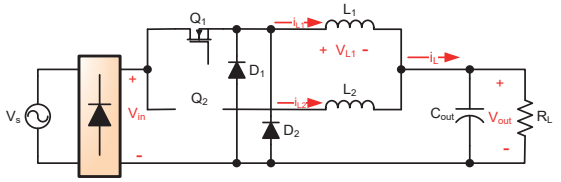

Figure 7.2. *Equivalent Circuit of IBC in Mode 1*

B. IBC Mode-2

Since IBC operates with a duty cycle less than 0.5, in this mode both the switches are OFF. Diodes D_1 and D_2 are the conducting devices. The equivalent circuit is illustrated in Figure 3.The energies stored in L_1 and L_2 are released to the load through the forward biased diodes. So i_{L1} and i_{L2} are decreased linearly. Thus the variations in i_{L1} and i_{L2}during T_2 are given by,

$$\Delta i_{L!} = \left(\frac{-V_{out}}{L_1} \right) T_2 \tag{7.3}$$

$$\Delta i_{L2} = \left(\frac{-V_{out}}{L_2} \right) T_2 \tag{7.4}$$

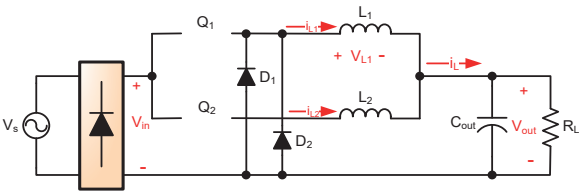

Figure 7.3. *Equivalent Circuit of IBC in Mode 2*

C. *IBC Mode-3*

During T_3 Q_2 is turned On and Q_1 turned off. The equivalent circuit is illustrated in Figure 7.4. The turning on of Q_2 charges the inductor L_2 and since Q_1 is off inductor L_1 is discharged to the load. The variations in i_{L1} and i_{L2} during T_3 are given by,

$$\Delta i_{L!} = \left(\frac{-V_{out}}{L_1} \right) T_3 \tag{7.5}$$

$$\Delta i_{L2} = \left(\frac{V_{in} - V_{out}}{L_2} \right) T_3 \tag{7.6}$$

Equation (7.5) shows i_{L1} linearly decreasing during T_3 since the slope is negative and a constant.

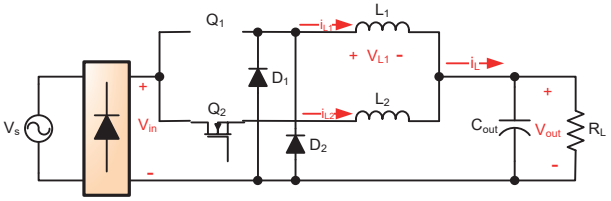

Figure 7.4. *Equivalent Circuit of IBC in Mode 3*

D. *IBC Mode-4*

The operating mode is same as mode 2. The variations in i_{L1} and i_{L2} during T_4 are given as in equation (7.3) and (7.4).

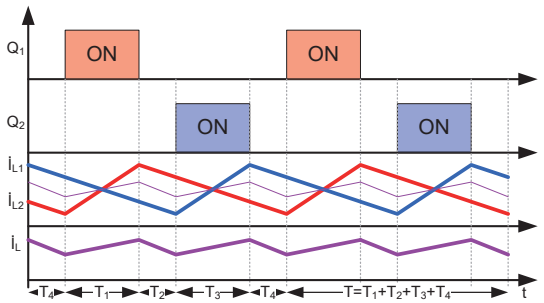

Figure 7.5. *Inductor Current Waveforms*

8. Push-Pull Converters

The Figure 8.1 represents the electronic schema of the proposed boost voltage converter using the push pull structure. The operation of push-pull converter: When Q_1 switches ON, current flows through the upper half of the T_1 transformer primary and the magnetic field in T_1 expands. The expanding magnetic field in T1 induces a voltage across the T_1 secondary; the polarity is such that D_2 is forward-biased and D_1 is reverse-biased. D_2 conducts and charges the output capacitor C_1 via L_1. L_1 and C_1 form an LC filter network. When Q_1 turns OFF, the magnetic field in T_1 collapses and after a period of dead time (dependent on the duty cycle of the PWM drive signal), Q_2 conducts, current flows through the lower half of T_1's primary, and the magnetic field in T1expands. At this point, the direction of the magnetic flux is opposite to that produced when Q_1 conducted. The expanding magnetic field induces a voltage across the T_1 secondary; the polarity is such that D_1 is forward- biased and D_2 is reverse-biased. D_1 conducts and charges the output capacitor C_1 via L_1. After a period of dead time, Q_1 conducts and the cycle repeats.

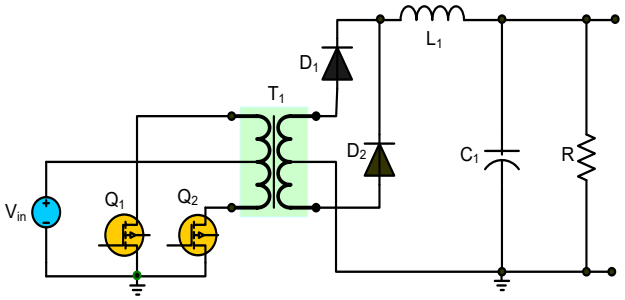

Figure 8.1. Proposed DC/DC Push-pull converter

There are two important considerations with the push-pull converter:

• Both transistors must not conduct together, as this would effectively short circuit the supply. This means that the conduction time of each transistor must not exceed half of the total period (D < 0.5) for one complete cycle, otherwise conduction will overlap.

• The magnetic behavior of the circuit must be uniform; otherwise, the transformer may saturate, and this would cause destruction of Q_1 and Q_2.

This behavior requires that the individual conduction times of Q_1 and Q_2 must be exactly equal and the two halves of the center-tapped transformer primary must be magnetically identical. These criteria must be satisfied by the control and drive circuit and the transformer. The output voltage equals that of equation (8.1).

$$V_{out} = 2DV_{in}\frac{N_2}{N_1} \tag{8.1}$$

Where: D is the duty cycle of the transistor, Q_1 and Q_2, 0<D<0.5

Push-Pull Control Loop

The push-pull converter is controlled with a voltage mode control scheme. The PWM module is configured for Push-Pull mode with an independent time-base. The DC Link voltage is measured by the voltage sensors and sent to DSP control. This value is subtracted from the voltage reference in software to obtain the voltage error. The voltage error is then fed into a control algorithm that produces a duty cycle value based on the voltage error, previous error, and control history. The output of the control algorithm is also clamped to minimum and maximum duty cycle values for hardware protection. The voltage mode control algorithm must be executed at a fast rate in order to achieve the best transient response. Therefore, the control algorithm is executed in the ADC interrupt service routine, which is also assigned the highest priority in the UPS code [18]. A block diagram of the push-pull converter control scheme is shown in Figure 8.2.

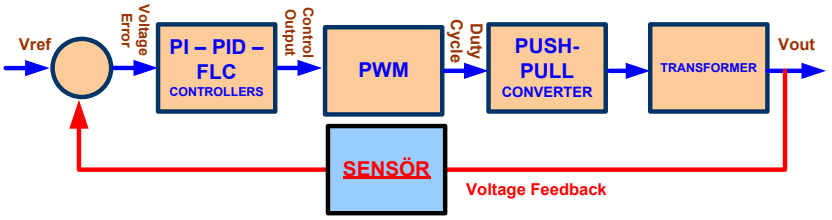

Figure 8.2. A Block diagram of Push-pull voltage control loop

Simulation of the Full System

Figure 8.3. PI in the system, in turn, is connected to the PID and FLC. These controllers, variable speed error between the reference and the output signal audited by the push-pull converter is PMDC motor actual speed with PWM method determines the position of the MOSFET switch. Push-pull converter, determines the output voltage of the switch position. This voltage determines the speed of the motor.

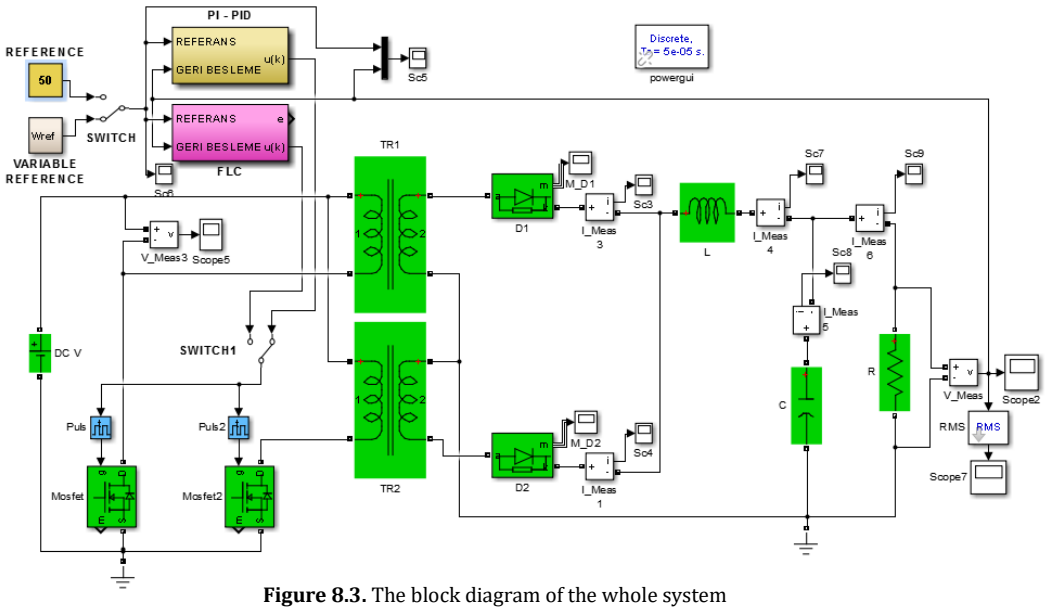

Figure 8.3. The block diagram of the whole system

9. Flyback Converter

Figure 9.1 shows the circuit shape of the flyback converter, which is one of the insulated converter types. In flyback transducers, the polarity of the windings is such that current does not flow from one another to the other [19]. Therefore, a transformer movement is not realized. Accordingly, the V_{in} voltage is applied to the primary winding when the S switch is in communication. Due to the inverse polarization of the secondary winding relative to the primary winding, the D diode is also polarized and therefore no current flows from the secondary. The load current is supplied by capacitor C (Figure 9.2.a). Increased primary current due to constant voltage at L_p tips will be linear [20]. When the switch Q is cut, the energy stored in the air gap and the magnetic core is transmitted to the load via the coil L_s. (Figure 9.2.b). Since there is a constant voltage at the ends of L_s, the current decreases linearly. The energy stored in the air range is obtained from the primary inductance and the primary current according to Equation (9.1);

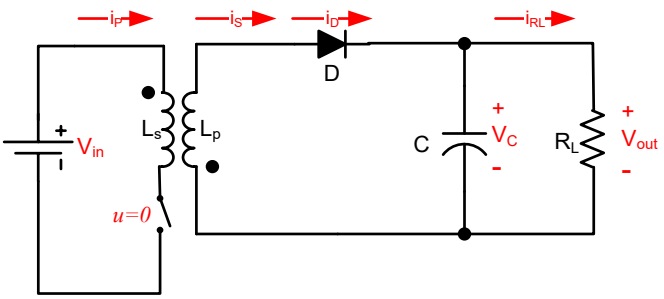

Figure 9.1. The block diagram of the Flyback converter

$$V_{Lp} = \frac{L_P I_P^2}{2} \tag{9.1}$$

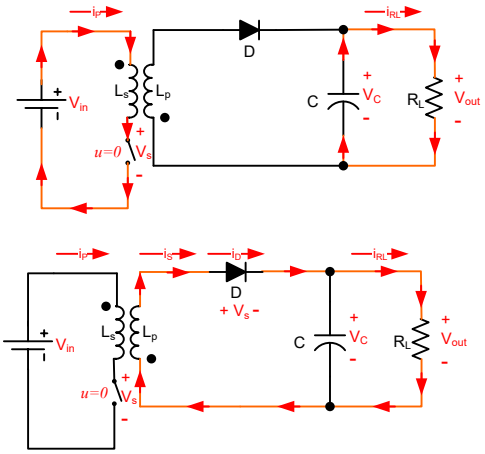

a) b)

Figure 1.2. Flyback converter operating modes, a) switch on status, b) switch off status

As with other transducers, there are continuous, discontinuous and boundary operating conditions in flyback transducers [21]. In the case of a discontinuous state, the secondary current drops to zero and the switch remains at zero for a certain time before the next transmission state is reached. The sum of T_{on} and T_{off} times is about 80% of the period. The remaining 20% is called dead time (td) [22]. In the case of continuous, there is no *TD*. The secondary current does not drop to zero until the next transmission state.Since the average voltage drop on the transformer winding inductances in steady state will be zero. In the equation, V_{in}: Input voltage, V_{out}: Output voltage, T_{on}: Transmission time of the semiconductor, T_{off}: Breakdown time of the semiconductor, V_d: Transmission voltage drop of

the diode, V_s: Voltage drop in the conduction state of the semiconductor, a: Winding ratio between transformer windings, definitions.

$$V_{in} - V_s)T_{on} = (V_{out} + V_d)\frac{L_P I_P^2}{2} T_{off} a \tag{9.2}$$

$$T = T_{off} + T_{on} + T_d \tag{9.3}$$

$$T_{on} = \frac{(V_{out} + V_d)Ta}{(V_{in} + V_s) + (V_{out} + V_d)a} \tag{9.4}$$

Since the values outside the input voltage are constant in Equation (9.4), the maximum value of the switching time is obtained with the smallest input voltage.

$$T_{on_{\max}} = \frac{(V_{out} + V_d)Ta}{(V_{in_{\min}} + V_s) + (V_{out} + V_d)a} \tag{9.5}$$

The primary current will increase linearly as the switch has a constant voltage on the primary coil in the transmission state. The current reaches its maximum value, the largest transmission time reaches t_{onmax}. It should be noted that the largest transmission time is possible at the smallest input voltage. According to this, the maximum prime r current I_{pmax} value is given in equation (9.6).

$$I_{p_{\max}} = \frac{(V_{in_{\max}} + V_s)T_{on_{\max}}}{L_P} \tag{9.5}$$

Here, L_p is the primary inductance. This current value is stored in the primary winding (in the magnetic core and air gap) for transfer to the secondary winding;

$$P_{in} = \frac{L_P + I_{P\max}^2}{2T} \tag{9.6}$$

When equality (9.5) is replaced in equality (9.6), input power equality (9.7) is obtained.

$$P_{in} = \frac{[V_{in_{\min}} + T_{on\,mac}]}{2TL_P} \tag{9.7}$$

References

[1] Rashid, Muhammad H. Power Electronics: Circuits, Devices, and Application (for Anna University). Pearson Education India.

[2] Mohan, Ned, William P. Robbins, and Tore Undeland. "Power electronics: converters, applications and design." (1995).

[3] Ürgün, Satılmış, Tarık Erfidan, and Nasır Çoruh. "DA-DA Buck Dönüştürücü Tasarımı ve Gerçeklenmesi Design and Implementation of DC-DC Buck Converter."

[4] Çoruh, Nasır, Tarık Erfidan, and Satılmış Ürgün. "DA-DA Boost Dönüştürücü Tasarımı ve Gerçeklenmesi Design and Implementation of DC-DC Boost Converter."

[5] Rashid, M. H., ed. Power electronics handbook. Butterworth-Heinemann, 2017.

[6] Sira-Ramirez, Hebertt J., and Ramón Silva-Ortigoza. Control design techniques in power electronics devices. Springer Science & Business Media, 2006.

[7] Middlebrook, Richard D., and Slobodan Cuk. "A general unified approach to modelling switching-converter power stages." 1976 IEEE Power Electronics Specialists Conference. IEEE, 1976.

[8] Guo, Liping, John Y. Hung, and R. M. Nelms. "Comparative evaluation of linear PID and fuzzy control for a boost converter." Industrial Electronics Society, 2005. IECON 2005. 31st Annual Conference of IEEE. IEEE, 2005.

[9] Lin, B-R. "Analysis of fuzzy control method applied to DC-DC converter control." Applied Power Electronics Conference and Exposition, 1993. APEC'93. Conference Proceedings 1993., Eighth Annual. IEEE, 1993.

[10] Mattavelli, Paolo, et al. "General-purpose fuzzy controller for DC-DC converters." IEEE Transactions on Power Electronics 12.1 (1997): 79-86.

[11] Zenk, Hilmi, and Akpinar, A. Sefa. "Dynamic Performance Comparison of Cúk Converter with DC Motor Driving and Using PI, PID, Fuzzy Logic Types Controllers." Universal Journal of Electrical and Electronic Engineering 2.2 (2014): 90-96.

[12] Zenk, Hilmi, and Atilgan Altinkok. "Output Voltage Control of PI And Fuzzy Logic Based Zeta Converter." IOSR Journal of Electrical and Electronics Engineering (IOSR-JEEE) 12.6.3 (2017): 63-70.

[13] Calderón, Antonio J., Blas M. Vinagre, and Vicente Feliu. "Fractional order control strategies for power electronic buck converters." Signal Processing 86.10 (2006): 2803-2819.

[14] Zenk, Hilmi. "A Comparative Application of Performance of the SEPIC Converter Using PI, PID and Fuzzy Logic Controllers for PMDC Motor Speed Analysis." Journal of Multidisciplinary Engineering Science Studies (JMESS) 2.12 (2016): 1126-1231.

[15] Josephine, R. L., et al. "Simulation of incremental conductance mppt with direct control and fuzzy logic methods using SEPIC converter." Journal of Electrical Engineering 13.3 (2013): 91-99.

[16] Garinto, Dodi. "A novel multiphase multi-interleaving buck converters for future microprocessors." Power Electronics and Motion Control Conference, 2006. EPE-PEMC 2006. 12th International. IEEE, 2006.

[17] Joseph A., Francis J., —Design and Simulation of Two Phase Interleaved Buck Converter‖, International Journal of Advanced Research in Electrical, Electronics and Instrumentation Engineering, vol.4, Special Issue 1, 2015.

[18] Dzung, Phan Quoc, Nguyen Minh Huy, and Nguyen Hoai Phong. "Designing an uninterruptible power supply based on the high efficiency push–pull converter." SCIENCE & TECHNOLOGY16.K3-2013.

[19] Çoruh, N., et al. "Flyback Dönüştürücü Tasarımı ve Analizi." EMO yayınları, Kocaeli Üniversitesi Elektrik Mühendisliği Bölümü s 297.

[20] Zhang, Xiangjun, Hankui Liu, and Dianguo Xu. "Analysis and design of the flyback transformer." Industrial Electronics Society, 2003. IECON'03. The 29th Annual Conference of the IEEE. Vol. 1. IEEE, 2003.

[21] Xiangjun Zhang, Hankui Liu, Dianguo Xu, “Analysis and design of the flyback transformer”, IECON '03. The 29th Annual Conference of the IEEE Volume 1, 2-6 Nov. 2003 Page(s):715 – 719.

[22] Pressman A.I., "Switching Power Supply Design", Second Ed. McGraw-Hill, 1998, pp. 105-140.